Characterization of a novel *deafwaddler* mutant implicates a role for PMCA2 regulation in the interaction with cadherin 23 and resulting auditory phenotype

Claire J. Watson

A dissertation
submitted in partial fulfillment of the
requirements for the degree of

Doctor of Philosophy

University of Washington
2012

Reading Committee:
Bruce Tempel, Chair
William Catterall
William Zagotta

Program Authorized to Offer Degree:
Pharmacology

University of Washington

Abstract

Characterization of a novel *deafwaddler* mutant implicates a role for PMCA2 regulation in the interaction with cadherin 23 and resulting auditory phenotype

Claire J. Watson

Chair of the Supervisory Committee:
Professor Bruce L Tempel
Otolaryngology-Head and Neck Surgery, Pharmacology

The transport of calcium ions across a cell membrane is critical for cell signaling in eukaryotic organisms. Maintenance of a low intracellular concentration is necessary for recognition of the calcium signal and, conversely, high intracellular levels of calcium are toxic. In stereocilia bundles of auditory hair cells, the plasma membrane calcium ATPase 2 (PMCA2) is the primary mechanism for calcium extrusion. Calcium carries part of the transduction current into the stereocilia and plays a role in adaptation. Furthermore, extracellular calcium in the microdomain surrounding the stereocilia is required for rigidity of cadherin 23, a component of the stereocilia tip-link encoded by the *Cdh23* gene. Therefore, PMCA2 is a critical player in normal function of hair cells and subsequent auditory transduction.

The work described in this thesis deals primarily with understanding how variants in the *Atp2b2* gene, which encodes for PMCA2, and alterations in the PMCA2 pump affect auditory transduction. A novel PMCA2 null allele, *dfw*^{i5}, was characterized and used to highlight the

interaction of the *Atp2b2* and *Cdh23* genes. We demonstrate that only one affected copy of *Cdh23* is necessary to cause broad frequency hearing impairment in +/*dfw*^{j5} mice. These mice were also used to study the role of PMCA2 function in the maturation of auditory sensitivity. We show that three weeks of age is a critical time period in the development of auditory transduction where sensitivity improves in wild-type controls but worsens at most frequencies in +/*dfw*^{j5}. Frequency dependent recovery of sensitivity occurs by 5 weeks in +/*dfw*^{j5} and correlates to preferential expression of *α-Atp2b2* and an up-regulation in PMCA2 in these mice.

We also quantitatively compare PMCA2 function in auditory transduction using an allelic series of *deafwaddler* mice. Surprisingly, heterozygotes of two PMCA2 null alleles, *dfw*^{2J} and *dfw*^{j5}, have different auditory phenotypes which we attribute to differential mutant allele regulation. Higher levels of mutant *Atp2b2* in +/*dfw*^{j5} correlate to decreased auditory sensitivity. A key finding of this thesis is that the differential regulation of *dfw*^{j5} and *dfw*^{2J} alleles corresponds to ancestral haplotype at *Atp2b2*, and implicates PMCA2 regulation as a feature of age-related hearing loss in C57BL/6J.

Table of Contents

List of Figures

Figure Number Page

List of Tables

Table Number Page

List of Abbreviations

ABR	Auditory brainstem response
AHL	Age-related hearing loss
ANOVA	Analysis of variance
ATP	Adenosine triphosphate
B6	C57BL/6J inbred mouse strain
BALB/c	BALB/cByJ inbred mouse strain
bp	Base pairs
Ca^{2+}	Calcium
CBA	CBA/CaJ inbred mouse strain
cDNA	Complementary deoxyribonucleic acid
CF	Climbing fibre
CHO	Chinese hamster ovary
CNS	Central nervous system
dB	Decibels
DBA	DBA/2J inbred mouse strain
dfw	*Deafwaddler*
EJC	Exon junction complex
EM	Electron microscopy
ENU	N-ethyl-N-nitrosourea
ERG	Electroretinogram
gDNA	Genomic deoxyribonucleic acid
HET	Heterozygote
IHC	Inner hair cell
INL	Inner nuclear layer
JAX	Jackson Laboratory
K^{+}	Potassium
kb	Kilobase
kDa	Kilodalton

kHz	Kilohertz
KO	Knockout
lincRNA	Long intergenic non-coding ribonucleic acid
mdfw	Modifier of *deafwaddler*
MET	Mechanoelectric transducer
MFE	Minimum free energy
MGI	Mouse genome informatics
MUT	Mutant
mRNA	Messenger ribonucleic acid
N(x)	Backcross generation
NS	Not significant
OHC	Outer hair cell
P(x)	Post-natal (in days)
PCD	Purkinje cell degeneration
PCR	Polymerase chain reaction
PMCA	Plasma membrane calcium ATPase
PN	Purkinje neuron
PPF	Paired-pulse facilitation
qPCR	Quantitative polymerase chain reaction
RSD	Relative standard deviation
SEM	Standard error of the mean
SNP	Single-nucleotide polymorphism
SPL	Sound pressure level
VOR	Vestibular ocular reflex
WT	Wild-type

Acknowledgements

First, I would like to thank Bruce Tempel for his guidance, enthusiasm and support and for providing me with the resources to complete this research. I appreciate the additional guidance I received from my supervisory committee: William Catterall, David Perkel, William Zagotta and Ning Zheng. I would like to acknowledge the support from the Auditory Neuroscience and Speech and Hearing Science training grants which afforded me the opportunity to interact with many wonderful scientists and colleagues. Many thanks go out to Linda Robinson, Jin Li, Carol Robbins and Valerie Street for their assistance providing resources, insight and technical assistance during the 6 years I have spent in the Tempel lab. Thank you to Dale Cunningham and Wai Pang Chan for their invaluable assistance in the preparation of EM tissue and the use of the scanning electron microscope. Thank you to Edith Wang, Ning Zheng and Rebecca Minich for intriguing discussions about RNA secondary structure, stability and function. I would also like to thank the other graduate students in the Tempel lab for their camaraderie over the years, in particular Jessica Weatherstone and Braulio Peguero who have been around for at least 4 years my journey.

Lastly, I thank my family unconditionally for their constant love and emotional support. To my parents, Bob and Laurie Walker, you have inspired me throughout my life while letting me dictate my own path. I would not be who I am today without you. To my sister, Lea Ann Walker, everything I know I learned from you, and I feel so lucky to have such an exemplary big sister to look up to. And finally, to my husband, Tom Watson, you have encouraged me, challenged me, stood up for me, believed in me and allowed me to grow as a scientist and a person, for which I am forever grateful.

Dedication

To Mom, Dad, Lea Ann and Tom, for all of your support

Chapter 1

Introduction

Inherent to the survival of cells in living organisms is the task of communicating with and adapting to their environment. These surroundings can include neighboring cells as well as extracellular space. Mechanisms of cellular communication and adaptation can range from temperature sensitive changes in the plasma membrane, to the binding of ligands, or the movement of charge into and out of the cell. Movement of small ions across a cell membrane can serve a two-fold purpose; 1) to carry an ion current that will change the voltage potential of the plasma membrane, and 2) to act as a signaling source inside the cell. Calcium can fulfill both of these roles.

1.1. *A mechanism of calcium regulation: the PMCAs*

Calcium (Ca^{2+}) is a critical electrochemical charge carrier as well as second messenger. The concentration of calcium in the cytoplasm needs to be maintained at a low level to permit calcium flux into the cell upon channel opening. Low cytosolic levels also allow cells to be sensitive to small changes in calcium concentration and favor its use as a signaling molecule. Conversely, high concentrations of intracellular calcium can induce cytotoxicity and subsequent

cellular death. Removal of calcium following cell activity in addition to maintenance of low intracellular concentrations occurs via several mechanisms that include endogenous calcium buffers, extrusion into extracellular space and incorporation of calcium into intracellular compartments (Carafoli, 2002; Clapham, 2007; Mammano *et al.*, 2007; Beurg *et al.*, 2010). Movement calcium across a membrane requires ion exchangers or ion pumps, the latter which require utilization of energy from ATP.

One class of calcium pump is the plasma membrane Ca^{2+} ATPases (PMCAs) which are responsible for pumping calcium from the cytoplasm, across the plasma membrane, and into extracellular space. There are four PMCA isoforms, PMCA1-4, that can each vary by alternative splicing events at two sites, site A and site C (Strehler *et al.*, 1989; Heim *et al.*, 1992; Keeton *et al.*, 1993). Site A is located in the first intracellular loop and has been implicated in phospholipid interactions (Heim *et al.*, 1992) (Ficarella *et al.*, 2007) and targeting of PMCAs to the apical or basolateral membrane of polarized cells (Hill *et al.*, 2006; Antalffy *et al.*, 2012). Site C is near the C-terminus of the protein and affects the integrity of the calmodulin binding domain, thus regulating the ability of PMCAs to interact with the ubiquitous calcium binding protein and alter its pumping kinetics (Keeton *et al.*, 1993; Hilfiker *et al.*, 1994; Caride *et al.*, 2007). PMCA1 and PMCA4 are expressed ubiquitously while the distribution of PMCA2 and PMCA3 isoforms is more limited and these are commonly considered the isoforms of the CNS (Keeton *et al.*, 1993; Stauffer *et al.*, 1995).

1.2. *PMCA2 in mammalian tissues*

The remainder of this thesis will focus on one of the four PMCA isoforms, PMCA2, which is encoded by the *Atp2b2* gene (in mouse, or *ATP2B2* gene in humans). Of the four

PMCA isoforms, PMCA2 is the most efficient at pumping calcium followed closely by the other neuronal isoform, PMCA3 (Brini *et al.*, 2003). Peak amplitudes and decay constants of calcium transients in CHO cells expressing PMCA2 and 3 are smaller than cells expressing PMCA1 or 4 (Brini *et al.*, 2003) suggesting that the distribution of these isoforms in neuronal tissues may be a consequence of their efficient calcium clearance kinetics. In addition to the brain, PMCA2 mRNA has been detected in the heart, liver, kidney, spleen, mammary gland (and other reproductive tissues), the retina and the inner ear (Keeton *et al.*, 1993; Silverstein & Tempel, 2006). Outside of its role in auditory transduction (which is the focus of the next section), PMCA2 has been primarily implicated to play a role in mammalian cerebellar and retinal physiology.

PMCA2 is abundantly expressed in the developing rat retina by P14 and marked staining in the adult rat was seen in amacrine cells of the inner nuclear layer (INL) (Renteria *et al.*, 2005). It has also been localized to the inner retina of the mouse with PMCA2 detected in amacrine cells, rod bipolar cells, horizontal cells and ganglion cells (Krizaj *et al.*, 2002) and is notably absent from cones (Duncan *et al.*, 2006). The functional effect of PMCA2 on retinal physiology was detailed in a study by Duncan *et al*. in 2006 by comparing control mice to those lacking PMCA2 expression. PMCA2 null mice show no gross morphological defects suggesting that PMCA2 is not required for the normal development of the mouse retina. However, electroretinogram (ERG) recordings are significantly affected in PMCA2 null mice and implicate PMCA2 function in the transmission of normal signals from rod outer segments to rod bipolar cells.

The Purkinje neurons (PNs) of the cerebellum also express an abundance of PMCA2 (Stahl *et al.*, 1992). Morphological differences in the overall cellular structure of the cerebellum

of PMCA2 null mice reported to date have been minor (Kozel *et al.*, 1998; Empson *et al.*, 2010), although PNs themselves have stunted dendrites (Empson *et al.*, 2007) and sub-cellular changes in molecular composition have also been reported (Kurnellas *et al.*, 2007). Because PMCA2 is also expressed in the vestibular epithelia of the inner ear, the motor and vestibular components of the ataxia in PMCA2 mutant mice has been difficult to segregate. Recently, two studies have highlighted the contribution of PMCA2 to cerebellar physiology.

In 2007, Empson *et al*. describe the contribution of PMCA2 to short-term plasticity in PNs. They show that paired pulse facilitation (PPF) is significantly enhanced in PNs of PMCA2 null mice. A similar increase in PPF was seen in wild-type cells treated with a non-selective P-type ATPase inhibitor, carboxyeosin, while there was no change in PMCA2 null cells treated with carboxyeosin, suggesting that the increase in PPF in control cells is due to PMCA2 inhibition. Another study by Empson *et al*. in 2010 examines calcium handling in PNs of morphologically intact PMCA2 +/- mice. Here, PN calcium transients induced by climbing fibre (CF) stimulation were monitored. As expected, PMCA2 +/- mice have slowed calcium clearance from PNs. Additionally, basal calcium levels were higher in +/- PNs and the current response to CF stimulation in PNs was weaker in these mice. Depolarization induced stimulation of PNs affected PMCA2 +/- cells in a similar way. In line with the reduced response to CF stimulation, spontaneous firing of PNs was decreased in PMCA2 +/- confirming reduced excitability in these cells. To assess if the physiological changes in PMCA2 +/- PNs affect motor coordination (these mice have no overt ataxic phenotype), mice were challenged on a beam test where they recorded more hindlimb slips and took longer to cross the beam than controls. In conclusion, current studies suggest that PMCA2 activity is important for proper

functioning of PNs in the cerebellum by altering calcium handling in these cells and can affect motor function in mice.

1.3. *Mutants highlight the function of PMCA2 in the inner ear*

The most important contribution of PMCA2 to normal mammalian physiology is its role in the inner ear. PMCA2 is expressed in the stereocilia bundles of both auditory and vestibular hair cells, in addition to the spiral ganglion neurons that innervate these cells (Furuta *et al.*, 1998; Kozel *et al.*, 1998; Street *et al.*, 1998; Yamoah *et al.*, 1998; Dumont *et al.*, 2001; Wood *et al.*, 2004; McCullough *et al.*, 2007). To date, several murine and human genetic alterations in PMCA2 have been identified and used to provide the bulk of the literature describing the role of PMCA2 in the inner ear. The first naturally occurring mutation characterized in PMCA2 (or any PMCA) was the *deafwaddler*, $Atp2b2^{G283S}$, point mutation in the mouse (Street *et al.*, 1998). Also referred to as *dfw*, homozygous mutant mice are deaf and have a noticeable ataxic phenotype. Biochemical assays have estimated that the *dfw* mutation reduces Ca^{2+} transport by PMCA2 to 30% of control (Penheiter *et al.*, 2001). A null allele in PMCA2 was identified at the same time as *dfw*, and was termed dfw^{2J} (Street *et al.*, 1998). Homozygous dfw^{2J} mutants are also deaf and have an overt ataxia. Heterozygous mutants for these two alleles, in addition to a new null allele, dfw^{3J}, were characterized by McCullough and Tempel in 2004. The two null alleles were very similar to each other with heterozygotes reliably displaying high-frequency hearing loss. A targeted knockout of PMCA2 ($Atp2b2^{KO}$) was also generated around the same time as the *dfw* mutation was identified (Kozel *et al.*, 1998). The knockout was created by disrupting exon 19 and heterozygous and homozygous mutants demonstrate severe auditory deficits, but are hard to compare to other PMCA2 mutants because of the background

strain used to produce this line. The ataxia seen in the knockouts was similar to that described in other null mutants and the otoconia (calcium carbonate crystals) usually present in the vestibular organ were missing in these mice.

Aside from null mutations, mouse mutants affecting the pumping efficiency of PMCA2 have also been studied and warrant a comparison to the original *deafwaddler* mutant. The *Wriggle Mouse Sagami* (*wri*) mutant is thought to contain a point mutation of a critical residue in transmembrane domain 4 of PMCA2 (Takahashi & Kitamura, 1999). Again, while heterozygous mice are described to have progressive hearing loss it is hard to make a detailed comparison due to the genetic background of this strain (Takahashi, 1999). Two of the most recently characterized mouse mutants of PMCA2, termed *Oblivion* and *Tommy*, are missense point mutations in transmembrane 6 and the ATP binding pocket of PMCA2, respectively (Spiden *et al.*, 2008; Bortolozzi *et al.*, 2010). Homozygous *Oblivion* mutants are deaf and homozygous *Tommy* mutants are severely impaired (thresholds at or above 100 dB SPL at all frequencies). Additionally, heterozygous mice for each mutation have significant hearing loss. The loss in +/*Obl* mice progresses with age across all frequencies whereas +/*Tommy* mice have less impairment, especially at lower frequencies.

Both of these mutant pumps are correctly targeted to the cell membrane but have significantly reduced rates of calcium clearance compared to wild-type PMCA2. Calcium clearance rates in *dfw*, *Oblivion* and *Tommy* mutant pumps have all been examined by the same group and with the same method (Brini *et al.*, 1995) which was also used to assess the relative clearance efficiency of the PMCA isoforms (Brini *et al.*, 2003). Although they were not compared in the same study, clearance efficiency seems to roughly correspond to auditory phenotypes in the heterozygous mutants (while controls for each study have similar clearance

rates). Cells expressing the *dfw* (Ficarella *et al.*, 2007) and *Tommy* (Bortolozzi *et al.*, 2010) pumps have noticeably slowed calcium half-peak decay rates of 32.9 s and 39.4 s, respectively, compared to wild-type pumps (half-peak decay rates are 7.4 s and 6.8 s for these cells in respective studies). Cells expressing *Oblivion* mutant pumps have a 45.5 s half-peak decay rate (while it is 6.6 s for wild-type controls), seemingly reflecting the severity of the phenotype in this strain (Spiden *et al.*, 2008).

Alterations in PMCA2 which affect auditory function in humans have also been discovered. A human mutation similar, but not identical, to the *dfw* mutation is caused by a substitution of a glycine residue to a serine residue ten amino acids away from the homologous site of the *dfw* point mutation (Ficarella *et al.*, 2007). Another point mutation discovered in the human population is only four amino acids from the homologous residue for the *Tommy* mutation and lies in the ATP-binding pocket of PMCA2 (Schultz *et al.*, 2005). Both of these human point mutations occur only as heterozygous alleles in the population and hearing loss is only detected in individuals who possess an additional mutation in a known modifier gene. It is noteworthy that each of these mutations lies in close proximity to known mouse mutants (*dfw* and *Tommy*) which suggests that these portions of PMCA2 may be more able to tolerate functional alterations by mutations than other regions of the protein. A third human alteration in PMCA2 gene expression has been implicated in patients who have 3p-syndrome and also suffer from pronounced sensorineural hearing loss (McCullough *et al.*, 2007). These patients have the largest (most proximal) deletions of the distal end of chromosome 3 mapping to the 3p25.3 locus, and encompass all or part of the *ATP2B2* gene. In summary, it is clear from genetic studies in both mice and humans that PMCA2 is a critical protein for auditory

transduction and moreover, small changes in protein function or expression can have a pronounced effect on auditory phenotype.

1.4. *The genetics of hearing loss*

As a testament to the many molecular players and unique features of auditory transduction, many genes have been identified to cause hereditary human loss in humans (see www.hereditaryhearingloss.org for a current list). Similarly, over 18 inbred mouse strains available at the Jackson Labs (JAX) have hearing loss phenotypes and eight genetic loci have currently been identified to contribute to some of these phenotypes (Johnson *et al.*, 2006). Here we will focus on one of the two of the loci, *ahl*, for which the causal gene has been identified. The *ahl* locus was originally mapped to mouse Chromosome 10 (Chr. 10) as a major contributor to the hearing loss in the C57BL/6J strain (B6) (Johnson *et al.*, 1997; Zheng & Johnson, 2001). Subsequent mapping narrowed the region, and identification of two other modifying loci in the same region (*mdfw* and waltzer) indicated that the same gene might underlie these hearing loss phenotypes. The *Cdh23* gene was found to precipitate the waltzer phenotype (Di Palma *et al.*, 2001) and shortly thereafter a mutation in *Cdh23* was also shown to correspond with hearing loss phenotypes in *ahl* affected mice (Noben-Trauth *et al.*, 2003). The difference between the *ahl* and *mdfw* alleles has never been resolved, and hearing impairment caused by either locus can be attributed to the same alteration in the *Cdh23* gene (Noben-Trauth *et al.*, 2003). The *Cdh23* gene encodes a structural protein of the hair cell stereocilia called cadherin 23. In combination with another protein, protocadherin 15, cadherin 23 forms the tip-link of the stereocilia bundles by connecting the side of a taller stereocilia to the tip of the adjacent shorter stereocilia (Siemens *et al.*, 2004; Kazmierczak *et al.*, 2007). The tip link is important for the

structural integrity of the stereocilia bundle (Di Palma *et al.*, 2001). Additionally, tension on the tip-link is responsible for opening of the mechanoelectric transducer channels located at the tip of the lower stereocilia (Pickles *et al.*, 1984; Howard & Hudspeth, 1988; Assad *et al.*, 1991; Beurg *et al.*, 2009). Moreover, calcium is an important player in the maintenance of the tip-link. The recent crystal structure of two of the cadherin repeat domains in cadherin 23 reveals the location of calcium binding sites in the protein and implicates calcium binding as a critical factor in the structural rigidity of the protein (Sotomayor *et al.*, 2010).

The *ahl* locus has been largely attributed to cause age-related hearing loss in the B6 inbred mouse strain (Johnson *et al.*, 1997; Zheng & Johnson, 2001) but, although a linked mutation has been identified in *Cdh23* (Noben-Trauth *et al.*, 2003), a direct causal relationship has never been established. To this end, a congenic mouse was generated at JAX with a B6 genetic makeup at the *ahl* locus in an otherwise good-hearing CBA/CaJ (CBA) background (Kane *et al.*, 2012). This mouse is designated as CBA.B6^{ahl}, and the reverse congene, B6.CBA^{ahl+}, was also generated. Somewhat surprisingly, neither congenic mouse strain had the same degree of age-related hearing loss as B6, suggesting that the *ahl* allele is necessary, but not sufficient for the B6 phenotype, and also indicating another gene contributes to age-related hearing loss in B6.

Originally, the *mdfw* allele was discovered because it worsened the severity of a (then unidentified) PMCA2 allele, *dfw*^{2J} (Noben-Trauth *et al.*, 1997). The *dfw*^{2J} allele arose on a sub-strain of another inbred mouse, BALB/cByJ, which we now know is also affected by the *ahl* locus. In crosses to an *ahl* resistant strain, hearing loss in the +/*dfw*^{2J} mice was inconsistent, and indicated the presence of a modifier allele that was termed, *mdfw*, for modifier of *deafwaddler*. Since the identification of the causal *ahl* gene (and hence the *mdfw* gene), the interaction

between *deafwaddler* and cadherin 23 has been acknowledged (Noben-Trauth *et al.*, 2003; Johnson *et al.*, 2006; Spiden *et al.*, 2008) mainly due to the fact that mutations in human *CDH23* also interact with mutations in *ATP2B2* (Schultz *et al.*, 2005; Ficarella *et al.*, 2007). However, a closer examination of the interaction of the two genes has not been undertaken in mouse models, despite the wealth of resources available. Due to the relevance of the interaction to human hearing, a higher resolution analysis of the interaction between the genes is described in Chapter 2. Additionally, in Chapter 3, we report a difference in haplotype at the *Atp2b2* locus between CBA and B6 which correlates to reduced transcript expression in B6, implicating *Atp2b2* as a candidate gene that contributes to the hearing loss phenotype in this strain.

Chapter 2

The characterization of a novel PMCA2 mutant allele, *dfw^{i5}*

Summary

While PMCA2 is expressed in a several cell types, arguably the most important physiological role for PMCA2 is in auditory transduction. Several mouse mutations in PMCA2 have been characterized previously, each with varying effects on PMCA2 function. However, not until very recently has a mouse mutation in the nucleotide binding domain of PMCA2 been characterized (Bortolozzi *et al.*, 2010). Given that one of the two known human mutations in PMCA2 lies in the ATP-binding domain (Schultz *et al.*, 2005), we wondered if this region of the protein might be particularly sensitive to sequence variation and set out to characterize a new mutant allele, that we have designated *dfw^{i5}*. The *dfw^{i5}* mutation, *Atp2b2^{K580Stop}*, is a point mutation that results in the substitution of a lysine residue that is critical to coordinating the ATP molecule in the binding domain, directly into a predicted stop-codon. Western blots reveal that the *dfw^{i5}* is a null allele, with no detectable PMCA2 truncation products. Homozygous mutants are completely deaf and have a severe motor/vestibular deficiency while heterozygous mutants have no observable vestibular phenotype, but have substantial hearing loss at high

frequencies. While transferring the allele into the good hearing, CBA/CaJ background, we report a highly significant interaction with the *Cdh23*^{ahl} allele in these mice.

2.1. Introduction

PMCA2 is predominately expressed in the central nervous system of mammals and is the fastest pump of the PMCA family (Brini *et al.*, 2003). It has been shown to be expressed at high levels in the auditory and vestibular sensory epithelia of the inner ear, as well as in the Purkinje neurons of the cerebellum (Stauffer *et al.*, 1995; Street *et al.*, 1998; Burette *et al.*, 2003; Wood *et al.*, 2004; Empson *et al.*, 2007). Accordingly, PMCA2 mutants display motor, vestibular and auditory phenotypes that can range from mild to very severe (Kozel *et al.*, 1998; Street *et al.*, 1998; Takahashi & Kitamura, 1999; McCullough & Tempel, 2004; Spiden *et al.*, 2008; Bortolozzi *et al.*, 2010). Mice that lack PMCA2 as a result of a targeted deletion of exon 19 have and unsteady gait and difficulty remaining upright even at rest (Kozel *et al.*, 1998). PMCA2 is expressed in hair cells of the vestibular sensory epithelium and null mutants lack expression in these cells (Street *et al.*, 1998). Toluidine blue-stained sections of the saccule in PMCA2 knockout mice were shown to lack otoconia, which are dense calcium carbonate crystals that sit on a gelatinous membrane that encompasses the stereocilia bundle (Kozel *et al.*, 1998). The cerebellar morphology in the knockout mice was also slightly different from controls. In comparison, a Purkinje cell degeneration model, *pcd*, which results in a decrease in the expression of the *Nna1* gene (Fernandez-Gonzalez *et al.*, 2002), has progressive degeneration of these neurons but only a moderate ataxia phenotype in comparison to the PMCA2 knockout (Mullen *et al.*, 1976). The more severe phenotype in the PMCA2 knockout, coupled with only minor morphological differences when compared to the *pcd* model, implies

that this behavioral phenotype in PMCA2 mutant mice can be largely attributed to the vestibular system. For simplicity, this behavior in PMCA2 mutants will be referred to as a vestibular deficiency, although a motor component cannot be ruled out.

The hair cells of the organ of Corti are also highly dependent on PMCA2 activity. During mechanotransduction in auditory hair cells, Ca^{2+} enters through the mechanoelectric transducer (MET) channels at the tips of the stereocilia and must be removed quickly for continuous auditory transduction. MET channels are cation selective and currents are primarily carried by K^{+} and Ca^{2+} ions (Corey & Hudspeth, 1979; Ohmori, 1987). However, in addition to carrying part of the conduction charge, Ca^{2+} is essential for slow and fast adaptation in the stereocilia (Eatock, 2000; Fettiplace & Ricci, 2003), allowing these cells to respond to sustained stimuli. Because Ca^{2+} is so critical to auditory mechanotransduction, regulators of Ca^{2+} are equally important.

Free Ca^{2+} concentration in stereocilia bundles is thought to be regulated in part by endogenous calcium buffers, but Ca^{2+} flux in the stereocilia cannot be modeled appropriately without accounting for Ca^{2+} extrusion pumps (Lumpkin & Hudspeth, 1998). Moreover, Ca^{2+} pumps are a major source of ATP hydrolysis in the stereocilia (Shin *et al.*, 2007). PMCA2 has been identified as the Ca^{2+} extrusion pump of the stereocilia, and several mouse mutants have confirmed the dependence of auditory transduction on PMCA2 (Kozel *et al.*, 1998; Street *et al.*, 1998; Yamoah *et al.*, 1998; Takahashi & Kitamura, 1999; Dumont *et al.*, 2001; McCullough & Tempel, 2004; Spiden *et al.*, 2008; Bortolozzi *et al.*, 2010). While several mouse models have been identified and characterized, only a few known human PMCA2 mutations exist. Additionally, in humans carrying a mutated PMCA2 allele, auditory sensitivity is only affected when expressed in conjunction with another modifier allele (Schultz *et al.*, 2005). Of note, one

of the known human modifiers of PMCA2 is the *CDH23* gene. The mouse homolog, *Cdh23*, is also a known modifier of PMCA2 (Noben-Trauth *et al.*, 2003). The interaction between the *Cdh23*^{ahl} allele (herein referred to as *ahl*), has been reported in +/*dfw*^{2J} mice that are also homozygous for *ahl* and has been largely qualitative in nature. Due to the direct correlate to human hearing loss, a higher resolution analysis of the interaction in mouse is warranted. In this study, we set out to characterize the vestibular, anatomical and auditory phenotype of a novel PMCA2 mutant, *dfw*^{i5}, while also examining the modifier effect of the *ahl* allele in more detail.

2.2. Methods

Animals

The *Atp2b2*^{dfwi5} allele arose in a mutagenesis screen wherein DBA/2J mice were exposed to N-ethyl-N-nitrosourea (ENU) then crossed to C57BL/6J and screened for motor disorders at the Ernest Gallo Clinic and Research Center (Speca *et al.*, 2006). Originally identified as Line 70, the mutant was transferred from San Francisco to the Tempel Lab and renamed *dfw*^{i5} (kind gift of A. Peterson). Final auditory and molecular characterization was done using *dfw*^{i5} mice that had been transferred into CBA/CaJ for at least 10 generations, designated as incipient congenic CBACa.D2(B6)-*Atp2b2*^{dfwi5}. Mice used for rotarod and swim tests were from earlier generations, N3-N5, and those used for scanning EM anatomical characterization were from N6. Mice from generations N3-N6 were used to study the interaction of the *dfw*^{i5} and *Cdh23*^{753A} alleles, however the *Cdh23*^{753A} allele was only carried by some littermates in N3 and N4. Animals were maintained on a 12 hour light/dark cycle and kept in an environment with

minimal exposure to noise. All procedures were approved by the University of Washington Institutional Animal Care and Use Committee (IACUC).

Auditory Testing

All mice were tested for auditory sensitivity using auditory brainstem responses (ABRs) at five weeks of age across frequencies ranging from 5.6 kHz to 40 kHz. Mice were anesthetized with a mixture of ketamine (130 mg/kg) and xylazine (10 mg/kg) prior to auditory testing and put into a sound proof box on a heating pad and secured with a bite plate. The speaker output was calibrated at the beginning of each test day. A series of 350 tones at a given frequency and intensity were administered and brain responses were recorded with two electrodes placed subcutaneously at the forebrain and hindbrain. A reference electrode was placed on the animal's hindlimb and electrocardiogram recordings were monitored to ensure an appropriate level of anesthesia throughout the experiment. Tones were 3 ms long with a 1 ms rise/fall $\cos^2$ function (delivered with alternating polarity). Brainwaves were recorded for 15 ms following the initiation of each tone with 75 ms spacing between repetitions (13.3 Hz). ABRs are amplified (1000x) and filtered (0.3-3 kHz) by a pre-amplifier (P55; Grass-Telefactor, West Warwick, RI) and digitized. Threshold at a particular frequency was determined by visual detection as the lowest intensity sound (dB SPL) which evoked a recognizable and reproducible brainwave (at least 2 out of 3 trials), usually wave V.

Behavioral/Vestibular Testing

Mice were assessed for complex motor and vestibular function between P33-P37 using rotarod tests and between P39-P43 using swim tests. For rotarod testing, mice were placed on a

rod and allowed to equilibrate to the apparatus. Training sessions required that each animal tested was able to remain on a stationary rod for 30 s and on a rotating rod for 90 s at 5 rpm, and were given two opportunities to do so. Mice that were unable to pass training did not participate in test trials. Mice were rested for 30 minutes before testing on Day 1 and then performed six trials with an initial speed of 0.0 rpm and an acceleration speed of 0.2 rpm/s. Six more trials were performed on Day 2 using the same parameters as on Day 1. For swim testing, mice were placed into a warm (30 ^{o}C) water bath and swimming style and vigor were scored on a 3-point scale as previously reported (Marshall & Berrios, 1979; Kiernan *et al.*, 1999). For style, 3.0 points were given for a mouse swimming with its head and back above water, 2.5 points with only the head above water, 2.0 points if the ears were wet, 1.5 points if their eyes were at water level, 1.0 points if only the nose was above water, 0.5 if the head was submerged, and 0.0 points for the whole body submerged. For vigor, 3.0 points were given if all four limbs were used while swimming, 2.5 points if only hindlimbs were used to swim, 2.0 points if the mouse sustained periods of floating, 1.5 points if the mouse floated for the majority (greater than 50%) of testing, 1.0 points for occasional limb movements, 0.5 points for occasional movement of only hindlimbs, and 0.0 points for no movement. The ability of each mouse tested to resurface after forced submersion was noted.

Expression Analysis

For both protein and RNA analysis, tissue was collected from mice between five and six weeks of age. For protein Western blots, fresh brain tissue was flash frozen on dry ice and stored at -80^{o}C until further use. Tissue was equilibrated for 30 minutes at -20^{o}C, homogenized in cold lysis buffer [20 mM NaF, 1 mM Na vanadate, 0.5% Triton X-100, 0.1% SDS, 1x Tris-

buffered saline (TBS) pH 7.4] with 10 µL/mL protease inhibitor cocktail added immediately prior to use (Sigma). Protein concentrations of each sample were determined using a bicinchoninic acid (BCA) Protein Assay (Pierce) and a NanoDrop Spectrophotometer ND-1000 (NanoDrop Technologies Inc.). Samples were prepared for Western blotting by diluting in an appropriate amount of lysis buffer and adding sample buffer [62.5 mM Tris-HCl pH 6.8, 5 mM EGTA, 25% glycerol, 2% SDS, 0.01% bromophenol blue, and 350 mM dithiothreitol (DTT, added fresh)] in a 1:1 ratio. Total brainstem protein (5 µg) from mice of each genotype was loaded into wells of a 4-20% gradient polyacrilamide RGEL (BioRad). Separated proteins were then transferred to a nitrocellulose membrane (BioRad) and blocked in 5% milk in 1xTBS + 0.1% Tween-20 for at least 30 minutes. The membrane was put in 5% milk in 1xTBS + 0.1% Tween-20 solution containing primary antibodies for β-actin (monoclonal, anti-mouse, Sigma) and PMCA2 (N-terminal, polyclonal, anti-rabbit, Affinity BioReagents) at a concentration of 1:15,000 and 1:7,500 respectively and then kept at 4^{o}C on a shaker overnight. Membranes were washed, then incubated for 1.5 hours at room temperature in 5% milk in 1xTBS + 0.1% Tween-20 containing secondary antibodies against mouse and rabbit IgG respectively (GE Healthcare), also at 1:15,000 and 1:7,500 dilutions, respectively. Again, membranes were washed and excess solution was drained from the membrane before incubating in the appropriate amount of enhanced chemiluminescence (ECL) detection solution (GE Healthcare) for 5 minutes at room temperature. Western blots were visualized immediately using a Fotodyne Luminary/FX instrument (Fotodyne Inc.) with chemiluminescent detection capabilities. The image shown in this section was inverted to look like a conventional blot developed using film.

For RNA expression analysis, fresh brainstem tissue was stored in RNA*later* (Qiagen), equilibrated for 24 hours at 4^{o}C to allow the solution to penetrate the tissue, and transferred

to -20^{o}C for later use. RNA was isolated using the RNeasy Plus Universal Mini Kit (Qiagen) according to the manufacturer's protocol. Homogenization was accomplished using a POLYTRON PT 1200 rotor-starter homogenizer. Total RNA from each sample (2 µg) was reverse-transcribed into complimentary DNA (cDNA) using SMARTScribe Reverse Transcriptase (Clontech) and random hexamer primers (Applied Biosystems). These samples were used for quantitative PCR (qPCR) analysis using SYBR green master mix (BioRad) and primers designed for Total-*Atp2b2* (PMCA2) and the reference genes *Actb* (*β*-actin) and *Sdha* (succinate dehydrogenase, subunit A). Forward and reverse primer sequences are as follows: Total-*Atp2b2*, 5'-ACTCCTGGGTCAGCATTCC-3' and 5'-TAGTAGCACGCGGCGGTCA-3'; *Actb*, 5'-CCACCATGTACCCAGGCATT-3' and 5'-ACAGTGAGGCCAGGATGGAG-3'; *Sdha*, 5'-GGGAACACTGGAGGAAGCAC-3' and 5'-TGGCACAGTCAGCCTCATTC-3'. qPCR reactions were done on a BioRad iCycler with iQ5 software. Data for each sample is an average of at least three runs where technical replicates had a relative standard deviation (RSD) of less than 3% for each primer set.

Scanning Electron Microscopy

Cochleae from 5-6 week old mice were dissected rapidly and placed in 0.1 M sodium cacodylate buffer containing 0.001% $CaCl_2$ (pH 7.4), the stapes removed and the oval window opened. A small hole was made at the apex of the cochlea, which was immediately perfused with the same buffer containing 4% glutaraldehyde by injecting fixative into the oval window. Cochleae were incubated at room temperature on a shaker for 1 hour in 4% glutaraldehyde-containing buffer, and then stored overnight at 4^{o}C in fresh fixative. The next day, cochleae were washed 3 times for 10 minutes each in 0.1 M sodium cacodylate buffer (pH 7.4) and then

placed in the same buffer containing 1% osmium tetroxide on a shaker for 30 minutes at 4°C in light-protected containers. Following three more washes, cochleae were stepped through 10 minute graded ethanol washes of 35%, 70%, 95% and 100% followed by a second wash in 100% ethanol. Cochleae were dried in an Autosamdri-814 critical point drier (Tousimis), mounted on specimen stubs using colloidal silver paste (Electron Microscopy Sciences) and stored in a vacuum-sealed desiccator. At least 24 hours later, when the silver paste was dry, cochleae were further dissected under a dissecting scope to expose the sensory epithelium beginning at the apex. After initial imaging sessions of the apical portion of each cochlea, further dissection was required to expose middle and basal portions of the epithelium. Prior to imaging, cochlea were sputter coated for 4 minutes at 10 mA using a Hummer VI-A sputtering system (Anatech LTD). Electron micrographs were collected from a JEOL JSM-840A scanning electron microscope (JEOL Ltd.) at 20 kV equipped with a JEOL DSG Plus digital scan imaging system (JEOL Ltd.). The relative location and distance from the apex of each image was noted. Hair cells counted for apical, middle, and basal turns fall between, 0.2-1.4 mm, 1.6-3.0 mm, and 3.4-4.8 mm of a total 5.1 mm from the apex and represent an average of 473 µm, 655 µm, and 615 µm of epithelium/cochlea imaged, respectively.

2.3. Results

2.3.1. *PMCA2 and Atp2b2 expression in dfw^{i5}*

Two previously described deafwaddler alleles (*dfw^{2J}* and *dfw^{3J}*) encode pre-mature stop-codons and result in null PMCA2 alleles (McCullough & Tempel, 2004). Although *dfw^{i5}* also encodes a pre-mature stop-codon, the nature of the mutation is different (*dfw^{2J}* and *dfw^{3J}* are deletions and *dfw^{i5}* is caused by a point mutation, Figure 2.1) making it feasible that the *dfw^{i5}*

allele is not recognized as aberrant and results in a truncated protein product. To determine the outcome of the *dfw*^{i5} mutation, protein blots using brainstem tissue from multiple mice of each genotype were assessed for PMCA2 expression and/or the presence of truncation products (Figure 2.2A). The expected size of a truncation product for *dfw*^{i5} is 67 kDa and the band should appear about mid-way between PMCA2 and β-actin staining. Using an N-terminal antibody to PMCA2, no visible truncation product (nor full-length protein) was detected in *dfw*^{i5}/*dfw*^{i5} mice. The absence of a truncation product was confirmed using variety of exposure times, antibody concentrations, total protein loading amounts and tissue types (including cochlea). Accordingly, *dfw*^{i5}, like *dfw*^{2J} and *dfw*^{3J}, appears to be a PMCA2-null allele. Reduced PMCA2 expression is also seen in +/*dfw*^{i5} mice compared to wild-type littermates (Figure 2.2A).

Next, we looked to see if transcript levels were also affected by the *dfw*^{i5} mutation. Total RNA from brainstem of 5 week old mice was converted to cDNA and total *Atp2b2* transcript levels were quantified by real-time PCR. Expression was the highest in wild-type controls, reduced in +/ *dfw*^{i5} and minimal in *dfw*^{i5}/*dfw*^{i5} (Figure 2.2B). The reduction of expression in mutant animals is notable considering that the primary transcript of *dfw*^{i5} is only one nucleotide different than the wild-type transcript. This suggests that there is a significant amount of cellular energy dedicated to processing the 296 kb long primary transcript and ensuring the integrity of the mature, 7 kb *Atp2b2* transcript.

2.3.2. *Behavioral characterization of dfw*^{i5}

Mice containing mutations in PMCA2 have been reported to display both auditory and vestibular deficits. To assess the degree to which the *dfw*^{i5} allele affects vestibular function, we

compared these mice to the previously described *dfw* and *dfw*^{2J} alleles. Biochemical assays have estimated that the *dfw* mutation reduces Ca^{2+} transport by PMCA2 to 30% of control (Penheiter *et al.*, 2001). The result of the *dfw*^{2J} frameshift mutation is a null PMCA2 allele (McCullough & Tempel, 2004) which presumably contributes no calcium ATPase activity. Homozygous mutants for *dfw* and *dfw*^{2J} alleles have an obvious vestibular phenotype, with that of *dfw*^{2J}/*dfw*^{2J} being the most severe.

Homozygous *dfw*^{i5} mutant animals also have a profound balance defect similar to that of *dfw*^{2J}/*dfw*^{2J}. The phenotype is manifested by difficulty remaining upright, circling and head-tossing in addition to an inability to perform simple motor tasks such as the rotarod behavioral test. Homozygous mutants from each strain were also severely affected in a swim test where *dfw*^{2J}/*dfw*^{2J} and *dfw*^{i5}/*dfw*^{i5} mice were unable to stay afloat for even a few seconds (data not shown). However, heterozygous mice for each strain were able to perform equally well as wild-type littermates in both rotarod (Figure 2.3A) and swim (Figure 2.3B) tests. This differs from previously published data indicating that +/*dfw*^{2J} animals had a shorter latency to fall when compared to wild-type littermates in a rotarod test (McCullough & Tempel, 2004). The disparity between these results may be due to the age in which the mice were tested. Mice tested in this study were P33.4 ± 0.5 and P33.5 ± 0.5 for wild-type and heterozygous individuals, respectively, while mice tested previously were younger (about 7 days) and lighter (at least 2 grams on average). It is possible that younger mice may not be able to compensate for a vestibular deficiency or that this behavioral phenotype is only apparent during an earlier developmental stage. Additionally, the ability to remain on the rotating rod may be affected by the weight and size of the animal being tested.

2.3.3. *Cochlear Scanning EM of dfw^{i5}*

Scanning electron microscopy (EM) of whole cochlea from 5-6 week old +/+, +/dfw^{i5} and dfw^{i5}/dfw^{i5} mice was performed to examine anatomical abnormalities in the auditory sensory epithelium of +/dfw^{i5} and dfw^{i5}/dfw^{i5} mice (Figure 2.4). Images shown are representative of the apex, middle and basal cochlear turns for each genotype. Wild-type cochlea display organized stereocilia bundles of both inner and outer hair cells (IHCs and OHCs, respectively) throughout the organ of Corti in the inner ear (Figure 2.4A, 2.4E and 2.4I). The +/dfw^{i5} mice have stereocilia bundles ranging from generally normal (albeit slightly compressed) to disorganized and fused stereocilia (Figure 2.4B, 2.4F and 2.4J). The dfw^{i5}/dfw^{i5} mice have disorganized, fused, and often stubby stereocilia bundles which appear more abnormal towards the basal, high frequency area of the cochlea (Figure 2.4C, 2.4G and 2.4K). Moreover, missing stereocilia bundles (indicating dead or missing hair cells) were virtually non-existent in wild-type cochleae while the frequency of missing hair cells was quite dramatic in regions of dfw^{i5}/dfw^{i5} cochleae, especially in the base where hair cells were sparsely distributed if they were present at all. A patch of stereocilia bundles is shown from the base of dfw^{i5}/dfw^{i5} (Figure 2.4K) to reflect the abnormal morphology, although this is not representative of the number of hair cells at this location in the cochlea (see Figure 2.4L). Cochleae of +/dfw^{i5} mice showed an intermediate phenotype with occasional missing hair cells in the apex and middle cochlear turns and increasing hair cell loss towards the base (Figure 2.4D, 2.4J and 2.4L). A one-way ANOVA between genotypes for each cell type (IHC or OHC) indicated a significant effect of genotype for apical, middle and basal IHCs ($p<0.0005$, $p<0.003$ and $p<0.0001$, respectively), as well as OHCs of the middle and basal turns ($p<0.05$ and $p<0.002$, respectively). An unpaired, non-directional t-test showed significant differences between genotypes indicated in Figure 2.4D,

2.4H and 2.4L. It is important to note that cells with abnormal stereocilia were counted despite the negative effect this would likely have on auditory transduction. Therefore, the averages presented should be considered a conservative estimate of functional loss. Additionally, smaller hair cells (which may not function normally) frequently seen in the middle and base of +/*dfw*^{i5} cochleae may contribute to the increased numbers of hair cells per 50 μm and the large variability in hair cell counts for these regions of the cochlea (Figure 2.4H and 2.4L).

2.3.4. *Auditory characterization of +/dfw*^{i5}

Since homozygous mutants for the *dfw*^{i5} allele are profoundly deaf, we were particularly interested in characterizing the degree of hearing loss in heterozygous mutants. Auditory sensitivity was examined in wild-type and +/*dfw*^{i5} mice using auditory brainstem response (ABR) thresholds at 5 weeks of age at 5.6, 8, 11.3, 16, 22.6, 32 and 40 kHz (Figure 2.5). This age was chosen because auditory responses via ABR are mature and any age-related hearing loss in these adolescent mice should be negligible. Wild-type mice hear relatively well across this entire frequency range, with the lowest thresholds (or best sensitivity) at 11.3 and 16 kHz. The +/*dfw*^{i5} mice have statistically significant hearing loss at 5.6, 22.6, 32 and 40 kHz relative to controls with the most severe loss at the highest frequencies. It is notable that the best sensitivity in +/*dfw*^{i5} is also at 11.3 and 16 kHz, where thresholds are indistinguishable from controls, suggesting that auditory hair cells at this location in the cochlea are able to tolerate a significant reduction in PMCA2 activity.

2.3.5. *dfw^{i5} and its interaction with ahl*

The *dfw^{i5}* mutation originally arose on the DBA/2J (DBA) allele in a mixed strain DBA and C57BL/6J (B6) background. While backcrossing several generations into the good-hearing CBA/CaJ (CBA) background, auditory evaluation of +/*dfw^{i5}* individuals at five weeks of age showed a strong interaction with the original age-related hearing loss locus (*ahl*). The *ahl* allele is associated with a single-nucleotide polymorphism (SNP) that alters splicing in the *Cdh23* gene encoding cadherin 23 (Noben-Trauth *et al.*, 2003), a structural protein required to form tip-links in the stereocilia of auditory hair cells (Siemens *et al.*, 2004; Kazmierczak *et al.*, 2007). It is present in both DBA and B6 strains and has been associated with early onset age-related or progressive hearing loss in these strains (Johnson *et al.*, 2000). Homozygosity at *ahl* has been shown to reduce auditory sensitivity in mice with hypofunctional PMCA2 alleles (Noben-Trauth *et al.*, 1997; Noben-Trauth *et al.*, 2003). However, the extent of this interaction has not been fully defined for mice heterozygous at the *ahl* locus, nor across a broad range of frequencies. Recent studies have shown that isolated homozygosity at the *ahl* locus in an otherwise CBA background cannot fully recapitulate the hearing loss seen in B6 (Kane *et al.*, 2012). This indicates that other genes contribute to hearing loss in this strain, and highlights the importance of understanding the interaction between *ahl* and *Atp2b2* with better resolution.
A particular SNP in the *Cdh23* gene at the *ahl* locus, *Cdh23^{G753A}* (Noben-Trauth *et al.*, 2003), was used to screen for the presence or absence of these alleles in +/*dfw^{i5}* individuals in generations N3 to N6. Segregating +/*dfw^{i5}* individuals based on their genotype at the *ahl* locus showed a strong effect on auditory phenotype, with the most significant losses in sensitivity occurring at lower frequencies (Figure 2.6). At N3, only one mouse was homozygous at the *ahl* locus and had the most severe hearing loss of any animal (Figure 2.6, closed squares). The

+/*dfw*^{i5} mice that were also heterozygous for the *ahl* allele were severely affected across all frequencies (Figure 2.6, half-filled squares), and those mice that were negative for the *ahl* allele (CBA-like at this locus) have significant hearing loss at mid- and high-frequencies (Figure 2.6, open squares), most closely resembling the +/*dfw*^{i5} phenotype at N10 (see Figure 2.5 for comparison).

Another locus, *ahl8,* has also been associated with early-onset hearing loss in DBA and is caused by a SNP in the *Fscn2* gene (Shin *et al.*, 2010). To check if this hearing loss locus may also contribute to the +/*dfw*^{i5} phenotype, all animals from the N3 generation which were subjected to ABR testing (a total of 12 mice) were screened for the SNP. All of these mice were negative confirming that the *ahl8* allele was not carried into our line and does not affect the phenotype of mice used in this study.

2.3.6. *Progression of the +/dfw^{i5} auditory phenotype by backcross generation*

Auditory function is highly sensitive to genetic manipulation, with over 120 identified loci involved in non-syndromic hearing loss in humans (www.hereditaryhearingloss.org). Furthermore, there are currently eight unique age-related hearing loss loci known to contribute to hearing loss phenotypes in common inbred mouse strains (Johnson *et al.*, 2006). As discussed in the previous section, the *ahl* locus is known to interact with mutations in the *Atp2b2* gene, and is present in both DBA and B6 inbred strains. Since our original mouse carrying the *dfw*^{i5} allele was on a mixed DBA/B6 background, it was necessary to eliminate the known hearing loss loci carried by these inbred strains in our background before characterizing the auditory phenotype of +/*dfw*^{i5}. Still, an examination of auditory sensitivity in +/*dfw*^{i5} mice

negative for both *ahl* and *ahl8* alleles showed a progression of the phenotype by backcross generation (Figure 2.7).

The +/*dfw*^{i5} mice in generations N3, N4 and N5 all have a similar phenotype with statistically significant hearing loss at most frequencies compared to controls and are not statistically different from one another (Table 2.1). However, a shift in sensitivity occurs in N6 with thresholds at 22.6 kHz improving compared to N5. By N10, +/*dfw*^{i5} appear to be much more similar to other known heterozygous PMCA2 null mutants with dramatic hearing loss at high frequencies, but relatively normal thresholds at low- and mid-frequencies when tested at five weeks. Between N6 and N10, thresholds significantly improved at 5.6 and 16 kHz in a two-way ANOVA. Taken together, the generational progression of the +/*dfw*^{i5} auditory phenotype suggests that at least one other, unknown, gene or modifier may contribute to hearing loss in DBA or B6 strains, and was crossed out of our line between N5 and N10. If multiple genes were present at N5, then mice in N6 may have lost at least one gene but still maintain another locus contributing to the phenotype. Alternately, the intermediate phenotype in N6 may reflect heterozygosity at the unknown locus, although this cannot be confirmed without a thorough analysis of the genomic sequence of all the mice involved in this study.

The proposed unknown locus possesses a modifier function in respect to heterozygosity at *Atp2b2* since wild-type controls do not show a progression of phenotype by generation (not shown). To assess if the unknown locus was directly affecting regulation of PMCA2 or *Atp2b2*, protein and RNA levels were quantified from mice in N3-N6, when the modifier gene could be present, and N10 (Figure 2.8). PMCA2 expression is unchanged between the early and late generational groups (Figure 2.8A), with heterozygotes expressing 65.15% and 63.31% of control expression, respectively. Protein levels represent averaged data for seven +/*dfw*^{i5} mice

in N3-N6 and five +/*dfw*^{i5} mice in N10. Similarly, there is no difference in total *Atp2b2* expression between mice of each generational group (Figure 2.8B and 2.8C) or how much of the total RNA is transcribed from the mutant allele (Figure 2.8D, see Chapter 3.2 for a description of the allelic discrimination method). Thus, the proposed modifier function of the unknown locus does not appear to affect PMCA2 expression directly and may involve another hearing loss gene.

2.4. Discussion

A thorough characterization of a new PMCA2 mutant allele, *dfw*^{i5}, emphasizes the large effect PMCA2 gene dosage can have on physiological function. Here, we report that *dfw*^{i5} is a null PMCA2 allele and that +/*dfw*^{i5} have impaired auditory transduction but no discernible motor or vestibular abnormalities. That an impairment on the rotarod behavioral task has been previously reported in similar null heterozygous mutants, +/*dfw*^{2J} and +/*dfw*^{3J} (McCullough & Tempel, 2004), suggests mice haploinsufficient for PMCA2 may sit at the cusp of vestibular impairment. Presumably, these mice have approximately 50% calcium clearance activity relative to controls and that this represents the critical amount of PMCA2 necessary for normal vestibular behavior. Just a small reduction in PMCA2 activity to 30% in *dfw*/*dfw* leaves these mice with an overt vestibular phenotype. Another step-wise decrease in PMCA2 seen in *dfw*^{i5}/*dfw*^{i5} and *dfw*^{2J}/*dfw*^{2J} animals noticeably worsens the impairment, implying that we can estimate from 0% to 50% activity as a range where PMCA2 function is physiologically important for vestibular behavior. It would, however, be interesting to assess the vestibular function of *dfw* and *dfw*^{i5} mice with a more sensitive measure, such as the vestibular ocular

reflex (VOR), to better resolve how decreased expression of PMCA2 may affect the vestibular system and to separate vestibular from motor components.

In contrast, the 30% activity in *dfw*/*dfw* is not sufficient for any detectible auditory brainstem responses. While responses are present in +/dfw^{i5}, sensitivity is still greatly affected, particularly at high-frequencies. At the highest frequencies tested, 32 and 40 kHz, +/dfw^{i5} mice have lost about 40-45 dB SPL in sensitivity compared to wild-type, which is equivalent to the estimated contribution of outer hair cells as the cochlear amplifier (Ryan & McGee, 1977; Prosen *et al.*, 1978; Stebbins *et al.*, 1979). Paired with the anatomical data for +/dfw^{i5} cochleae, we can conclude that, at 5 weeks of age, many stereocilia bundles of the high-frequency hair cells at the base of the cochlea are present but are not functioning normally. This supports what has been previously reported in loss of function PMCA2 mutants (Spiden *et al.*, 2008; Bortolozzi *et al.*, 2010) and can be extended to null PMCA2 mutations. Studies that have examined the anatomy of dfw^{2J} mutants have focused only on homozygous mutants and were qualitative in nature (Street *et al.*, 1998; Wood *et al.*, 2004). Here we provide a quantitative measure of hair cell counts and a complete report of hair cell morphology across the entire sensory epithelium for both heterozygous and homozygous PMCA2 null mice.

Undoubtedly, the presence of stereocilia in the sensory epithelium even when transduction is greatly affected indicates that there is a lag, which may be considerable, between loss of hair cell function and complete hair cell death evidenced by loss of stereocilia bundles. Of note, relatively normal stereocilia bundles on the surface of the organ of Corti have been reported even in mice with non-functioning or abnormal hair cell bodies (Bock & Steel, 1983). This is also demonstrated by the presence of OHC and IHC stereocilia in homozygous mutant dfw^{i5}/dfw^{i5} cochleae, which are profoundly deaf and may never have coordinated hair cell

activity. Interestingly, although none of the hair cells (from the apex to the base) in the homozygous mutant are ever thought to be functional, there is still a bias toward hair cell loss at the base of the cochlea in these mice. This has been seen in other PMCA2 mutants (Spiden *et al.*, 2008; Bortolozzi *et al.*, 2010) and may reflect the intrinsic properties of the OHCs at this location. Supporting this idea, OHCs at the base of the cochlea are predicted to have a higher MET channel conductance resulting in a greater influx of calcium into the stereocilia bundles (Beurg *et al.*, 2010). Recent work suggests that the density of PMCA2 expression in the stereocilia along the tonotopic axis is unchanged (Chen *et al.*, 2012) ruling out the possibility that increased PMCA2 activity in basal hair cells could help compensate for the additional calcium current. It seems likely that this would be exacerbated in PMCA2 mutant mice and that hair cells at the base of the cochlea would have a higher propensity for calcium overload. In combination, while dfw^{i5}/dfw^{i5} mice are completely deaf due to sensorineural hearing loss and a lack of coordinated transduction, conduction of auditory stimuli into the inner ear remains intact. Therefore, hair cells at the base may be more susceptible to mechanical damage or metabolic overload due to the high frequency movements of the basilar membrane at this location.

One subtle feature of the $+/dfw^{i5}$ auditory phenotype is the small, but significant, loss of sensitivity at 5.6 kHz, the lowest frequency tested. High-frequency hearing loss is the most common type of sensorineural hearing loss seen in both humans and mice and possible mechanisms for this loss discussed above involve metabolic stress on the OHCs. Low-frequency loss, on the other hand, is much less common and the mechanism for loss at low frequencies is not well understood. In this study, one clue comes from the interaction of the *ahl* allele in modifying the severity of hearing loss in $+/dfw^{i5}$. The SNP used to screen for the

presence of the *ahl* allele, *Cdh23*^{G753A}, alters splicing and causes skipping of exon 7 in the majority of the transcript (Noben-Trauth *et al.*, 2003). Extracellular tip links are formed by the interaction of cadherin 23 and protocadherin 15, and calcium is essential for the structural rigidity of cadherin 23 in the tip link (Sotomayor *et al.*, 2010). Because PMCA2 is the primary mechanism for extrusion of calcium into the endolymph immediately surrounding the stereocilia bundles, it is plausible that decreased calcium clearance activity could also affect the structural integrity of the tip link. In the most extreme case, mutants lacking PMCA2 were found to have a detectably lower endolymphatic calcium concentration (Wood *et al.*, 2004). Could it be possible that the decreased expression of PMCA2 in +/*dfw*^{i5} lowers the calcium concentration in the extracellular microdomain immediately surrounding the stereocilia bundle?

A closer look at the modifying interaction of *ahl* within +/*dfw*^{i5} individuals reveals that low frequency hearing in the mouse is greatly impacted by the presence of even one mutated *Cdh23* allele. Although the highest frequencies in +/*dfw*^{i5} are already severely affected, thresholds at 32 and 40 kHz do not worsen in combination with the *ahl* allele. In contrast, low frequencies are significantly elevated with each copy of the *ahl* allele, and the only mouse with both affected copies at the *ahl* locus had higher thresholds in the low- to mid-frequency range than at high frequencies. This result shows that the interaction between *Atp2b2* and *Cdh23* may be much stronger than previously appreciated, and suggests that a reduction in PMCA2 expression can be critical for transduction at low frequencies. The sensitivity of the interaction between *Atp2b2* and *Cdh23* at low frequencies may be due, in part, to the morphology of the stereocilia at this location. Low-frequency hair cells at the apex of the cochlea have long stereocilia and coordinated movements of the bundle may be particularly sensitive to changes in the structural integrity of the tip link. Similarly, in humans homozygous for a mutation in

CDH23, only one copy of a PMCA2 mutant allele is necessary to extend hearing loss to low frequencies (Schultz et al., 2005) suggesting that the mechanism of hearing impairment via the interaction of *ATP2B2* and *CDH23* is not species specific.

It is possible that the decrease in PMCA2 expression in +/*dfw*^{i5}, independently affects transduction at 5.6 kHz via a more structural mechanism by affecting the rigidity of the tip link. If a reduction of PMCA2 expression to 50% is sufficient to lower the calcium concentration in the endolymph surrounding the stereocilia bundle, and as a result weaken the structural rigidity of tip-links containing cadherin 23, we might notice morphological abnormalities of the stereocilia at this location. Scanning EM images taken at the apex of +/*dfw*^{i5} show that the stereocilia bundles, particularly of inner hair cells, appear to be slightly disorganized compared to control cochleae. However, a higher resolution study of stereocilia bundle morphology across the tonotopic axis in PMCA2 mutants would be necessary to determine if PMCA2 activity can directly affect tip link structure.

	5.6 kHz	8 kHz	11.3 kHz	16 kHz	22.6 kHz	32 kHz	40 kHz
+/+ vs N3 +/-	*	n.s.	n.s.	***	***	***	***
+/+ vs N4 +/-	***	**	n.s.	***	***	***	***
+/+ vs N5 +/-	***	*	*	***	***	***	***
+/+ vs N6 +/-	***	n.s.	n.s.	***	***	***	***
+/+ vs N10 +/-	*	n.s.	n.s.	n.s.	***	***	***
N4 vs N5 (+/+)	n.s.	n.s.	n.s.	n.s.	n.s.	n.s.	n.s.
N5 vs N6 (+/+)	n.s.	n.s.	n.s.	n.s.	n.s.	n.s.	n.s.
N6 vs N10 (+/+)	n.s.	n.s.	n.s.	n.s.	n.s.	n.s.	n.s.
N3 vs N4 (+/-)	n.s.	n.s.	n.s.	n.s.	n.s.	n.s.	n.s.
N4 vs N5 (+/-)	n.s.	n.s.	n.s.	n.s.	n.s.	n.s.	n.s.
N5 vs N6 (+/-)	n.s.	n.s.	n.s.	n.s.	**	n.s.	n.s.
N6 vs N10 (+/-)	**	n.s.	n.s.	***	n.s.	n.s.	n.s.

Table 2.1. Statistical differences between generations of +/*dfw*^{i5} and controls. A comparison of heterozygotes at each generation compared to controls shows loss at most frequencies for mice in N3 (n=3), N4 (n=6) and N5 (n=5). Thresholds improve at 22.6 kHz in N6 heterozygotes (n=9) at again at 5.6 and 16 kHz in N10 heterozygotes (n=13). There is no progression of phenotype in wild-type controls of each generation (there were no N3 wild-type littermates negative at *ahl* to include in this comparison; n=5 at N4; n=4 at N5; n=3 at N6; n=14 at N10).

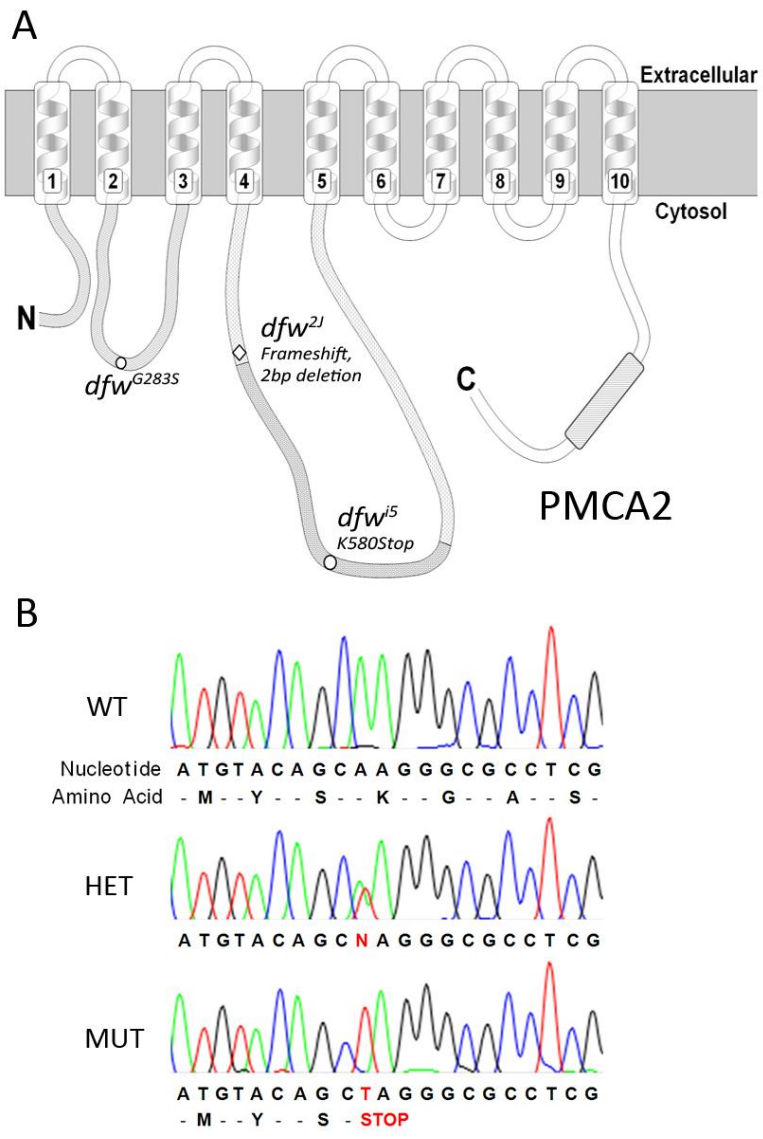

Figure 2.1. Relative location and sequence of the *dfw*^{i5} SNP. (*A)* Schematic representation of PMCA2 protein structure. Membrane-spanning domains are numbered 1-10 and the relative locations of the *deafwaddler* mutations are shown. The *dfw* and *dfw*^{i5} point mutations are indicated by open circles while the *dfw*^{2J} frameshift is represented by an open diamond. (*B)* Electropherogram of genomic sequence from wild-type (top) as well as heterozygous (middle) and homozygous (bottom) *dfw*^{i5} mutants showing the A to T point mutation resulting in a pre-mature stop codon.

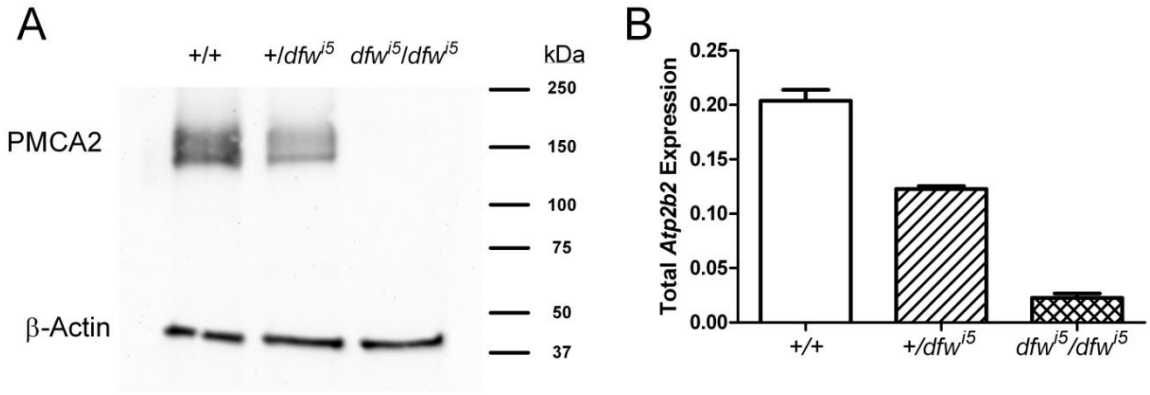

Figure 2.2. Expression of PMCA2 and *Atp2b2* is reduced in brainstem of *dfw*^{i5} mutant mice. *(A)* A representative western blot using an N-terminal antibody to PMCA2 shows reduced expression in +/*dfw*^{i5} and no detectible expression in *dfw*^{i5}/*dfw*^{i5} mice. *(B)* Total RNA expression is also decreased significantly in +/*dfw*^{i5} and *dfw*^{i5}/*dfw*^{i5} mice. Error bars represent SEM.

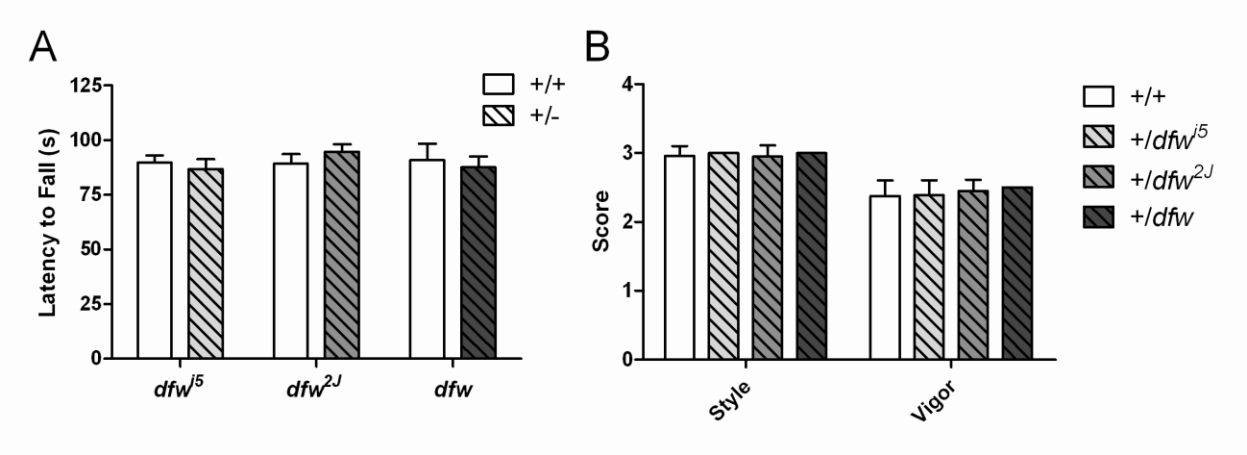

Figure 2.3. Mice heterozygous for *deafwaddler* alleles perform equally well as wild-type in rotarod and swim tests. *(A)* Average latency to fall in rotarod tests are shown for heterozygous (hashed bars) and wild-type (white bars) littermates of each strain. *(B)* Each mouse was assessed for their ability to swim by scoring for swimming style and vigor on a 3-point scale (see methods). Error bars represent SEM.

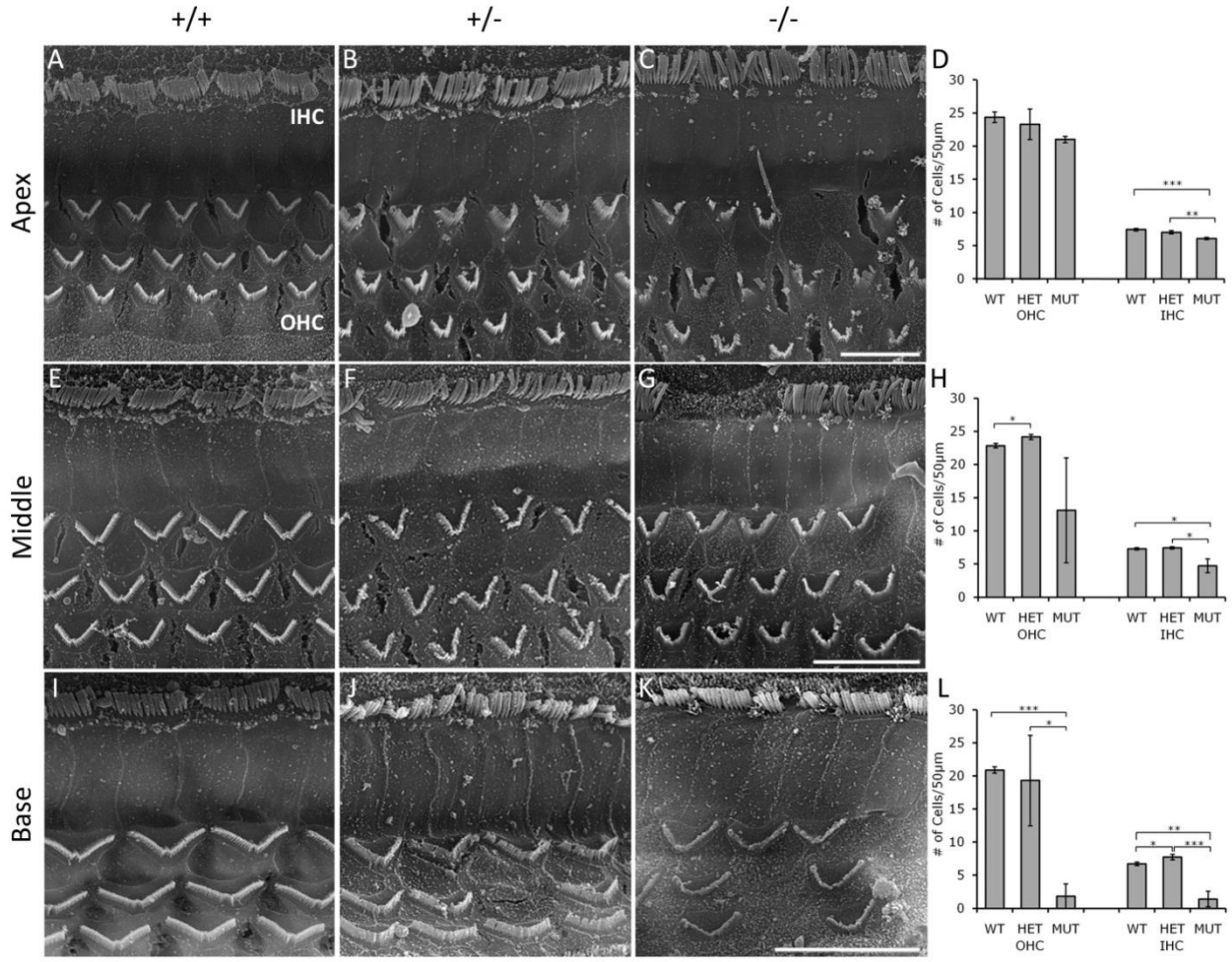

Figure 2.4. Scanning electron microscopy of *dfw*^{i5} animals. Representative images of inner (IHC) and outer hair cells (OHC) are shown for apical (A-C) middle (E-G) and basal (I-K) regions of the cochlea. Wild-type hair cells (A,E,I) are highly organized, +/*dfw*^{i5} hair cells (B,F,J) are occasionally disorganized or abnormal while *dfw*^{i5}/*dfw*^{i5} hair cells (C,G,K) are often disorganized, fused, stubby or missing. The image shown for the base of *dfw*^{i5}/*dfw*^{i5} is not representative of hair cell number, and a patch was chosen to reflect the morphology of mutant hair cells at this location. Scale bars = 10 µm for each row. *(D,H,L)* Cell counts for apical (D), middle (H) and basal (L) cochlear regions for outer and inner hair cells (n=3 for each genotype). Cells were counted according to the presence of any stereocilia despite the shape or organization of the stereocilia bundle. Very minimal loss was seen in hair cell counts at the apex in mutant mice. Loss was more dramatic in the middle turn of *dfw*^{i5}/*dfw*^{i5} and was progressively dramatic at the base with large regions of missing hair cells. In the base of +/*dfw*^{i5}, hair cell loss was variable with some cochleae missing a significant percentage of cells and others mostly intact (reflected by the large error bars). *p<0.05, **p<0.01, ***p<0.001 in two-way, unpaired t-test. Error bars represent standard deviation.

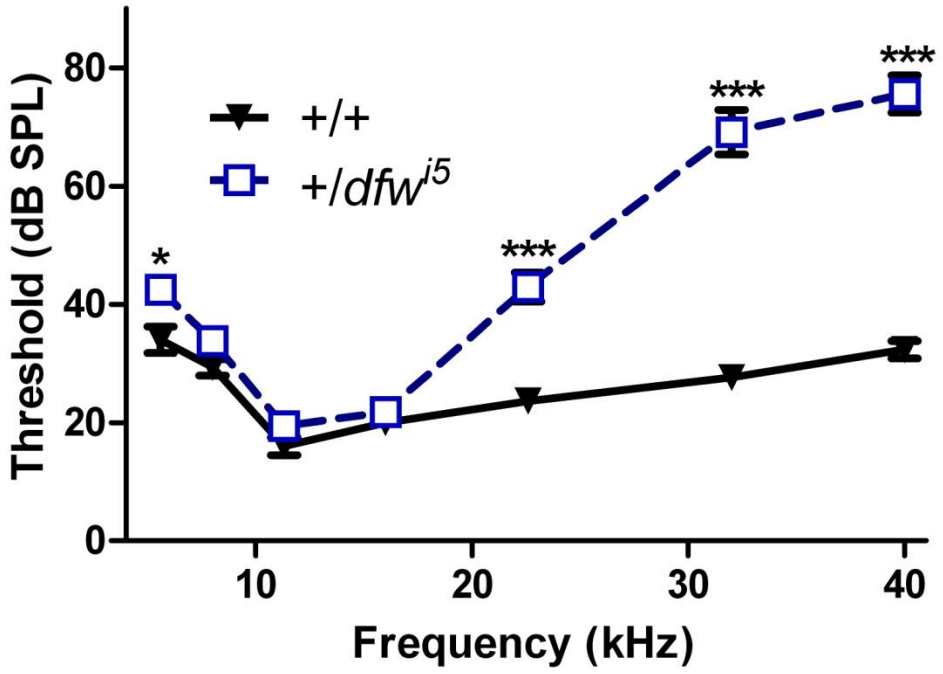

Figure 2.5. +/*dfw*^{i5} has hearing loss relative to wild-type controls. Mice heterozygous for the *dfw*^{i5} allele have significant hearing loss when compared to littermates at 5.6, 22.6, 32 and 40 kHz. *p<0.05, **p<0.01 and ***p<0.001 in a two-way ANOVA with Bonferonni post-hoc comparisons. Error bars represent SEM.

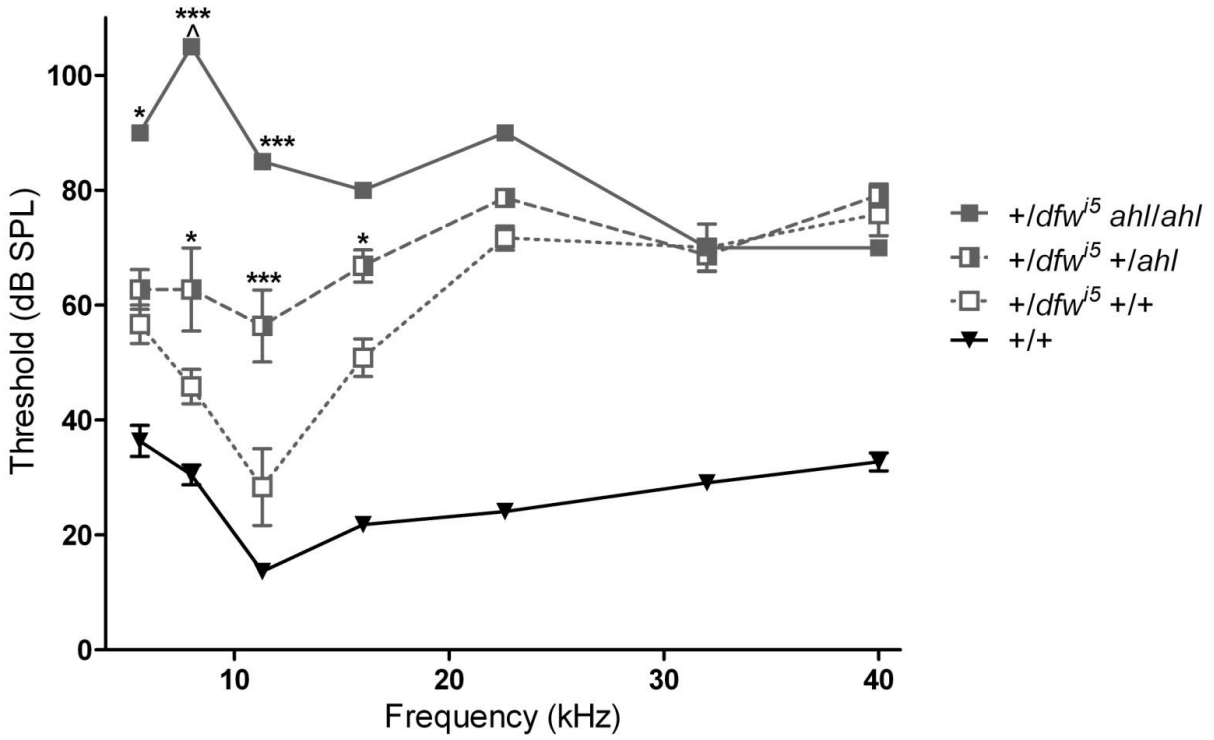

Figure 2.6. The *dfw*^{i5} allele strongly interacts with the *ahl* locus. Variability of ABR thresholds in early generations of +/*dfw*^{i5} mice segregated with the presence of the *Cdh23*^{G753A} allele at the *ahl* locus. Mice negative for the *Cdh23*^{753A} allele had the best sensitivity of +/*dfw*^{i5} animals (open squares, n=16), while +/*dfw*^{i5} mice also heterozygous for the *Cdh23*^{753A} allele have increased thresholds (half-filled squared, n=11) and one +/*dfw*^{i5} mouse homozygous for the *Cdh23*^{G753A} allele had severely elevated thresholds (filled squares, n=1). Average wild-type (solid line) thresholds are shown for reference. ^ indicates no threshold was detectable at this frequency. Error bars represent SEM. *p<0.05 and ***p<0.001 in a two-way ANOVA relative to +/*dfw*^{i5} animals without the presence of the *ahl* allele.

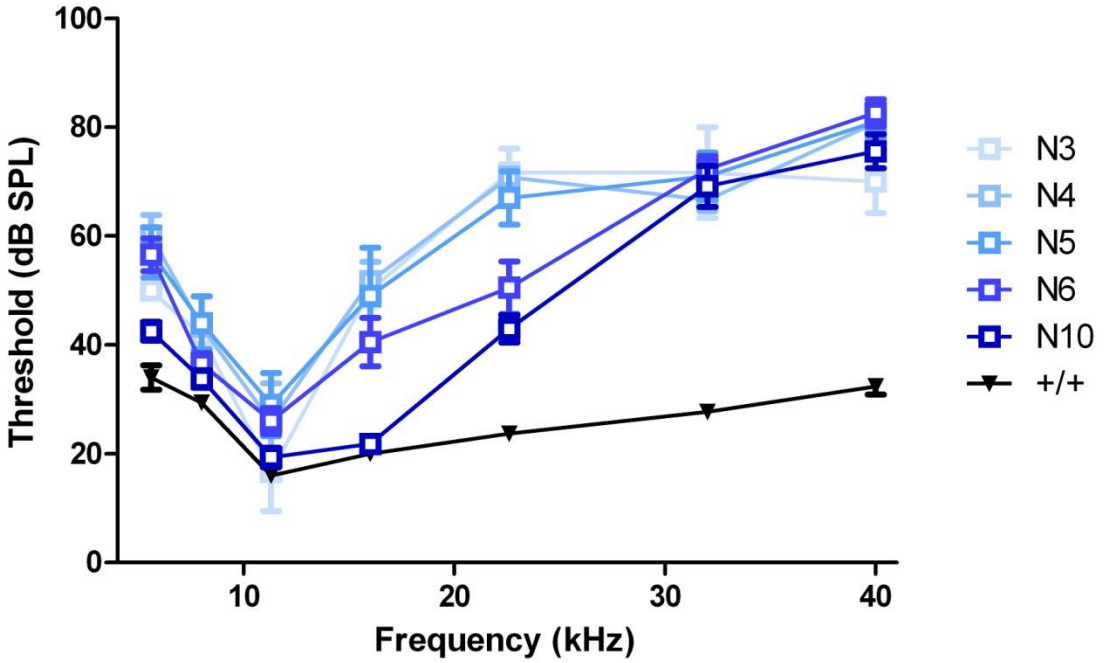

Figure 2.7. Progression of +/*dfw*^{i5} phenotype by backcross generation. Auditory sensitivity in +/*dfw*^{i5} was relatively stable from generations N3 to N5. A shift in sensitivity occurred in N6 and again in N10, where auditory sensitivity and expression levels were characterized. Error bars represent SEM.

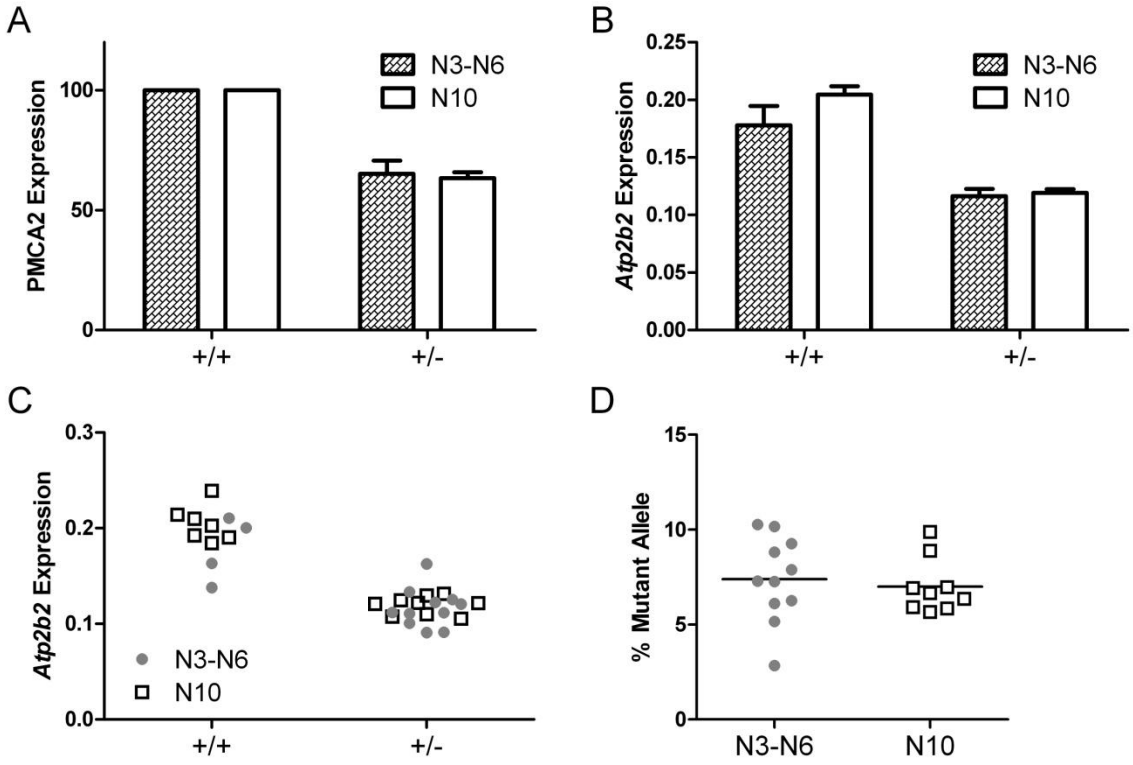

Figure 2.8. Protein and RNA expression levels in +/*dfw*^{i5} brainstem are not affected by generation. *(A)* PMCA2 expression is reduced to 65.15% and 63.31% of controls in N3-N6 and N10 mice, respectively. *(B-C)* Total *Atp2b2* is expressed at the same level in each generation group and is represented as group averages (B) and for each individual sample (C). *(D)* The percentage of mutant allele expressed in +/*dfw*^{i5} does not change between N3-N6 and N10. Error bars represent SEM.

Chapter 3

Ancestral Haplotype Affects Gene Expression and Auditory Transduction in *Deafwaddler* Mice

Summary

Here we examine PMCA2s quantitative role in auditory transduction by comparing a new PMCA2 mutant allele, *dfw*^{i5}, to two other mutants, *dfw* and *dfw*^{2J}. The *dfw* allele is partially functional while both *dfw*^{2J} and *dfw*^{i5} are null alleles. Homozygous mutants from each strain are deaf, while heterozygous mutants each display a distinctive auditory phenotype determined by auditory brainstem responses (ABRs) ranging from mild in +/*dfw* to most severe in +/*dfw*^{i5}. Despite a difference in auditory phenotype of two haploinsufficient strains, +/*dfw*^{i5} and +/*dfw*^{2J}, western blot and quantitative real-time PCR analyses show no differences in the expression of PMCA2 protein or total *Atp2b2* mRNA. There is however a small, but highly significant increase in the mutant transcript present in +/*dfw*^{i5} relative to +/*dfw*^{2J}, that is associated with ancestral haplotype at the *Atp2b2* locus. Correlations between sensitivity at 32 and 40 kHz and mutant allele expression within +/*dfw*^{i5} individuals, are statistically significant and suggest that the mutant allele may directly contribute to the worsened phenotype in these mice.

3.1. Introduction

Upon sound-evoked deflection of stereocilia bundles present on hair cells of the inner ear, both K^+ and Ca^{2+} enter through the tips of stereocilia via the mechanoelectric transduction channels at this location (Lumpkin & Hudspeth, 1995). This Ca^{2+} must be rapidly cleared for fast, efficient and recurrent auditory transduction. The main player involved in Ca^{2+} clearance in the stereocilia is PMCA2 (Yamoah *et al.*, 1998; Dumont *et al.*, 2001; Hill *et al.*, 2006). It has been well established that PMCA2 is crucial for auditory transduction (Kozel *et al.*, 1998; Street *et al.*, 1998; Yamoah *et al.*, 1998; Takahashi & Kitamura, 1999; Kozel *et al.*, 2002; McCullough & Tempel, 2004). PMCA2 is encoded by the *Atp2b2* gene and several mutations in this gene have been characterized, leading to varying degrees of hearing loss (Kozel *et al.*, 1998; Street *et al.*, 1998; Takahashi & Kitamura, 1999; McCullough & Tempel, 2004; Schultz *et al.*, 2005; Ficarella *et al.*, 2007; McCullough *et al.*, 2007; Spiden *et al.*, 2008; Bortolozzi *et al.*, 2010). The first naturally occurring mutation characterized in PMCA2 (or any PMCA) was the *deafwaddler*, $Atp2b2^{G283S}$, point mutation (Street *et al.*, 1998). Also referred to as *dfw*, mutant mice are deaf and display significant balance problems as the name indicates. Biochemical assays have estimated that the *dfw* mutation reduces Ca^{2+} transport by PMCA2 to 30% of control (Penheiter *et al.*, 2001). Therefore, it is assumed that *dfw/dfw* mutant mice also maintain about 30% PMCA2 pump function *in vivo* and that this level of function is not sufficient for auditory transduction. Mice homozygous for PMCA2 mutations resulting in null alleles (*Atp2b2*-KO, dfw^{2J}, dfw^{3J}) have no PMCA2 function, are deaf, and display very severe motor and vestibular defects (Kozel *et al.*, 1998; McCullough & Tempel, 2004). Mice heterozygous for loss-of-function PMCA2 mutant alleles display various auditory phenotypes ranging from relatively normal sensitivity in +/*dfw* (McCullough & Tempel, 2004) to

substantial, progressive hearing loss as seen in +/*Oblivion* (Spiden *et al.*, 2008) and +/*Tommy* (Bortolozzi *et al.*, 2010).

Alterations in PMCA2 which affect auditory function in humans have also been reported. A human mutation similar, but not identical, to the *dfw* mutation is caused by a substitution of a glycine residue to a serine residue ten amino acids away from the homologous site of the *dfw* point mutation (Ficarella *et al.*, 2007). Another point mutation discovered in the human population lies in the ATP-binding pocket of PMCA2 (Schultz *et al.*, 2005). Both of these human point mutations occur as heterozygous alleles in the population and only result in hearing loss in individuals who possess an additional mutation in another hearing loss gene such as *CDH23* (Schultz *et al.*, 2005; Ficarella *et al.*, 2007). Hence, independent characterizations of mouse and human mutations in PMCA2 confer a wide range of auditory phenotypes. However, a more quantitative comparison of how small changes in PMCA2 activity can affect auditory sensitivity has yet to be examined. By directly comparing a newly characterized *deafwaddler* allele, dfw^{i5}, to the *dfw* and dfw^{2J} alleles, this study furthers our understanding of the quantitative role of PMCA2 in auditory transduction in young adult mice.

3.2 Methods

Animals

Four alleles of *deafwaddler* mice were compared in this study. The $Atp2b2^{dfw}$ allele arose spontaneously in C3H/HeJ mice (Lane, 1987) and was obtained by our lab in 1989 from The Jackson Lab (JAX). The $Atp2b2^{dfw2J}$ allele arose spontaneously in CBy.A/J-$Ttc7^{fsn}$ at JAX and was obtained in 1997 (Street *et al.*, 1998). Both strains have been backcrossed to good hearing CBA/CaJ for more than 20 generations in the Tempel lab resulting in the congenic strains

CBACa.C3-*Atp2b2*^{dfw} (referred to here as *dfw*) and CBACa.Cby-*Atp2b2*^{dfw2J} (referred to as *dfw*^{2J}). The *Atp2b2*^{dfwi5} allele arose in a mutagenesis screen wherein DBA/2J mice were exposed to N-ethyl-N-nitrosourea (ENU) then crossed to C57BL/6J and screened for motor disorders at the Ernest Gallo Clinic and Research Center (Speca *et al.*, 2006). Originally identified as Line 70, the mutant was transferred to us from San Francisco and renamed *dfw*^{i5} (kind gift of A. Peterson). All of the *dfw*^{i5} mice used for ABR testing and molecular expression analysis have been backcrossed into CBA/CaJ for at least 10 generations and do not carry the *ahl* allele, designated as incipient congenic CBACa.D2(B6)-*Atp2b2*^{dfwi5}. The *Atp2b2*^{3J} allele (herein referred to as *dfw*^{3J}) arose in the C57BLKS/J-*m*+/+*Lepr*^{db} colony at JAX and was characterized by our lab after 5-7 generational backcrosses into CBA/CaJ (McCullough & Tempel, 2004). Our lab no longer maintains a colony of *dfw*^{3J} mice which are currently cryopreserved at JAX in a C57BL/6J-related background. It was not feasible to recover these mice and backcross them into CBA/CaJ for multiple generations for inter-strain comparison in this study. All strains were maintained in a backcross to CBA/CaJ obtained from JAX and replaced every 3-4 generations to retain a stock that is isogenic with CBA/CaJ at JAX. Animals were maintained on a 12 hour light/dark cycle and kept in an environment with minimal exposure to noise. All procedures were approved by the University of Washington Institutional Animal Care and Use Committee (IACUC).

Auditory Testing

All mice were tested for auditory sensitivity using ABRs at five weeks of age across frequencies ranging from 5.6 kHz to 40 kHz. The procedure was the same as described in Chapter 2. Briefly, mice were anesthetized, put into a sound proof box on a heating pad and

secured with a bite plate. A series of 350 tones (3ms long with a 1ms rise/fall $\cos^2$ function) were administered and brain responses were recorded. Brainwaves were recorded for 15ms following the initiation of each tone with 75ms spacing between repetitions (13.3 Hz). Threshold was determined to be the lowest intensity sound (dB SPL) which evoked a recognizable and reproducible brainwave (at least 2 out of 3 trials).

Expression Analysis

For all molecular expression assays, tissue was collected from mice between five and six weeks of age. The Western blotting protocol was the same as described in Chapter 2. Freshly dissected brain tissue was flash frozen on dry ice and stored at -80^{o}C until further use. Tissue was equilibrated for 30 minutes at -20^{o}C and then homogenized in cold lysis buffer. Protein concentrations of each sample to be compared on the same blot were processed in parallel and were determined using a BCA assay (Pierce) and a NanoDrop Spectrophotometer ND-1000 (NanoDrop Technologies Inc.). For each sample, 5 µg aliquots were prepared by mixing with sample buffer [62.5 mM Tris-HCl pH 6.8, 5 mM EGTA, 25% glycerol, 2% SDS, 0.01% bromophenol blue, and 350 mM DTT (added fresh)] and denaturing for 10 minutes at 50^{o}C. These samples were then stored overnight at -20^{o}C and loaded onto a 4-20% gradient polyacrilamide RGEL (BioRad) the next day. Separated proteins were then transferred to a nitrocellulose membrane (BioRad). Primary and secondary antibody concentrations were 1:15,000 for β-actin (monoclonal, anti-mouse, Sigma) and 1:7,500 for PMCA2 (N-terminal, polyclonal, anti-rabbit, Affinity BioReagents). The ECL Plus kit (GE Healthcare) was used to generate the chemiluminescent signal which was visualized immediately using a Fotodyne Luminary/FX instrument (Fotodyne Inc.). Quantification of protein bands was done on non-

manipulated images taken using PC Image software (Fotodyne Inc.) and analyzed using ImageJ (NIH). PMCA2 expression in each lane was normalized to β-actin expression. Heterozygous and homozygous expression levels were determined as a percentage of wild-type littermate expression for each blot. The image shown in this chapter was inverted to look like a conventional blot developed using film.

For RNA expression analysis, fresh brainstem or cochlear tissue was stored in RNA*later* (Qiagen), equilibrated for 24 hours at 4^{o}C to allow the solution to penetrate the tissue, and transferred to -20^{o}C for later use. RNA was isolated using the RNeasy Plus Universal Mini Kit (Qiagen) according to the manufacturer's protocol. Samples were homogenized with a POLYTRON PT 1200 rotor-starter homogenizer and total RNA from each sample (2 µg total RNA for brainstem and about 1 µg total RNA for whole cochleae) was reverse-transcribed into complimentary DNA (cDNA) using SMARTScribe Reverse Transcriptase (Clontech) and random hexamer primers (Applied Biosystems). These samples were used for quantitative PCR (qPCR) analysis using SYBR green master mix (BioRad) and primers designed for total-, *α*- and *β-Atp2b2* (PMCA2), *Gm15082* (linc82) and *Gm15083* (linc83) as well as for reference genes *Actb* (β-actin) and *Sdha* (succinate dehydrogenase, subunit A). Forward and reverse primer sequences are the same as in Chapter 2, with additional primer sets as follows: *α-Atp2b2,* 5'-CGGAGTGTGGACTGACAGCA-3' and 5'-GGTTACATCAGAGGCGCCAG-3'; *β-Atp2b2*, 5'-GCTGGCGATTGCCTTAGC-3' and 5'-GAGGAGTGTCCCCAGGAGTG-3'; *Gm15082*, 5'-CAGGCAATGGTAGTTACCCTGTA-3' and 5'-GAAAGCCACTCAGGGAAGTG-3'; *Gm15083,* 5'-CTCATGCTCCTGCTGTGAAG-3' and 5'-GGTTCACCAACTCCCTGAAG-3'. The qPCR reactions were done on a BioRad iCycler with iQ5 software. Data for each sample is an average

of at least three runs where technical replicates had a relative standard deviation (RSD) of less than 3% for each primer set.

Whole cochlear samples were dissected by quickly removing both cochleae from the temporal bone and perfusing each with RNA*later* by poking a hole at the apex and perfusing through the oval window. After perfusion, cochleae were trimmed of as much excess bone, debris, vasculature and neuronal tissue as possible while keeping the whole cochlea intact. In particular, the semi-circular canals were removed and vestibular epithelia cleared leaving only tissue past the round and oval windows. Additionally, as much of the spiral ganglia was removed as possible without disrupting the integrity of the modiolus.

Allelic Discrimination

Allele specific TaqMan probes (Applied Biosystems) were designed to distinguish between wild-type and mutant cDNAs in +/*dfw*^{i5}, +/*dfw*^{2J} and +/*dfw*^{3J} samples. cDNAs for +/*dfw*^{i5} and +/*dfw*^{2J} were prepared as described above and were the same samples used for expression analyses. Since we no longer maintain a colony of *dfw*^{3J} mice, we used RNAs that had been isolated and stored at -80^{o}C since the original characterization of this allele in our lab (McCullough & Tempel, 2004). These RNAs had been isolated from whole brain tissue and were still of very high quality (A260/280 ratios greater than 2.0 for all samples). cDNAs were generated from one +/+, four +/*dfw*^{3J} and three *dfw*^{3J}/*dfw*^{3J} RNAs in addition to three +/*dfw*^{2J} and two *dfw*^{2J}/*dfw*^{2J} RNAs that were isolated and stored with the *dfw*^{3J} samples so that they could be used for direct comparison. Genotypes were verified using probes specific for the causal mutations. These *dfw*^{2J} and *dfw*^{3J} samples are designated by a (B) in the results section. Taqman probes used for each strain spanned an exon/exon junction to ensure that only cDNA

would be amplified and to eliminate the possibility of gDNA amplification in these samples. For *dfw*^{i5}, the causal mutation occurs near the end of an exon, and could be used for allelic discrimination. Both *dfw*^{2J} and *dfw*^{3J} deletions occur in the middle of an exon and could not be used for cDNA specific allelic discrimination. Instead, an ancestral mutation carried by both of these alleles (resulting in a change of amino acid 731 from a D to E) was used as a surrogate for allelic discrimination since a cDNA specific probe could be designed to this mutation. This probe was also used to distinguish between CBA/CaJ and C57BL/6J alleles in hybrid mice. To control for differential amplification efficiency between primer/probe sets as well as differential sensitivity of the camera for alternately labeled dyes (VIC and FAM), three standards, each containing a 1:1 mixture of wild-type and mutant alleles, were run with each assay and data were normalized to these standards. To generate mutation-specific PCR standards, primers were designed to amplify cDNA from one mutant and one wild-type mouse spanning the region of interest (or one CBA and one B6 mouse in the case of the aa731 probe). High concentrations of these products were purified to ensure accurate concentration readings and were mixed in a 1:1 ratio as the cDNA standard. Three independent mixtures of these amplification products were made and then serially diluted such that the threshold cycles of the standards during quantification were similar to those of the cDNA samples. All three standards for each probe were run in duplicate for each assay, averaged, and sample data for each strain was normalized to its standard. At least one wild-type and one mutant cDNA sample from each strain were also run as positive controls. Allelic differentiation data represents at least three runs of each heterozygous cDNA sample where the %RSD was less than 3% for technical replicates.

3.3. Results

3.3.1. *A comparison of auditory sensitivity in deafwaddler mutants*

ABR sensitivity was assessed in heterozygous deafwaddler mutants for the *dfw*, *dfw*^{2J} and *dfw*^{i5} alleles to directly compare relative reductions in PMCA2 function to auditory sensitivity (see Table 3.1 for a comparison of alleles used in this study). The *dfw* allele has been well characterized over the past 15 years (Street *et al.*, 1998; Penheiter *et al.*, 2001; Ficarella *et al.*, 2007) and was the first identified mutation in PMCA2 (Street *et al.*, 1998). The *dfw* mutation results in the substitution of a guanine residue to a serine in the actuator domain of PMCA2 and is estimated to reduce the calcium clearance activity of PMCA2 to 30% (Penheiter *et al.*, 2001). Because it has been thoroughly studied, it is a useful benchmark for comparison in this experiment. The *dfw*^{2J} (Street *et al.*, 1998) and *dfw*^{i5} alleles each encode premature stop codons and are null alleles. The *dfw*^{2J} allele is also often used to study PMCA2 function (Noben-Trauth *et al.*, 1997; Zheng & Johnson, 2001; McCullough & Tempel, 2004; Jones *et al.*, 2005; Kurnellas *et al.*, 2005; Duncan *et al.*, 2006; VanHouten *et al.*, 2010), particularly in the context of an interaction with *ahl* (see Chapter 2), and has been considered a standard for a PMCA2 null allele. Here we directly compare a new null allele, *dfw*^{i5}, to these known *deafwaddler* mutants. Another null allele, *dfw*^{3J}, could not be included in many of the experiments for this study because we no longer maintain a colony of this strain (see Methods, "*Animals*").

Because homozygous mutants for each of the alleles used in this experiment are deaf via ABR (data not shown), the auditory phenotypes of heterozygous mutants were the focus of this study. Auditory testing was carried out using ABRs at 5.6, 8, 11.3, 16, 22.6, 32 and 40 kHz of five-week-old mice (Figure 3.1). Thresholds from wild-type littermate controls of each strain were not statistically different (Figure 3.2), and are grouped for clarity (Figure 3.1A, black

inverted triangles). Furthermore, there were no differences between male and female animals tested within a group (Figure 3.2) so both genders were used in the analysis. A two-way ANOVA comparing each heterozygous strain and grouped wild-type controls showed a significant main effect of strain, frequency and interaction between strain and frequency (Figure 3.2A, $p<0.0001$ for each source of variation). Post-hoc comparisons show significant differences between the heterozygous strains at 22.6 kHz, 32 kHz and 40 kHz (Table 3.2). At 40 kHz, +/*dfw*^{i5} and +/*dfw*^{2J} are not statistically different. Further analysis of statistical differences at each frequency was carried out using a two-way ANOVA between heterozygous mice of each strain and their (non-grouped) wild-type littermates (Figure 3.2B-D). Mice heterozygous for the partially functional *dfw* allele demonstrated only a mild hearing loss at high frequencies (Figure 3.2B, gray triangles, n=7) that was statistically significant at 32 kHz and 40 kHz compared to wild-type littermates (n=4). The +/*dfw*^{2J} mice also had significant hearing loss at 32 and 40 kHz as well as loss at 5.6 and 22.6 kHz (Figure 3.2C, red circles, n=18) relative to their littermates (n=8). Surprisingly, +/*dfw*^{i5} animals had a more severe phenotype than that of +/*dfw*^{2J} with higher ABR thresholds at 22.6 and 32 kHz (Figure 3.2D, blue squares, n=17), in addition to loss at 5.6 and 40 kHz compared to wild-type (n=15). Individual traces from heterozygous animals are shown on the right panel of Figure 3.2B-D. Several +/*dfw* mice have thresholds similar to controls across the entire frequency range while only a couple of +/*dfw*^{2J} and +/*dfw*^{i5} individuals have auditory thresholds similar to wild-type littermates across the entire range. Statistical comparisons are detailed in Table 3.2.

3.3.2. *PMCA2 protein expression analysis*

Although *dfw*^{2J} and *dfw*^{i5} are both null alleles, +/*dfw*^{2J} and +/*dfw*^{i5} have different auditory phenotypes necessitating a quantitative comparison of PMCA2 expression in each of these strains. Protein blots of brainstem tissue from several mice of each strain were assessed for PMCA2 expression (Figure 3.3). As expected, using an N-terminal antibody to PMCA2, no visible truncation product (nor full-length protein) was detected in either *dfw*^{2J}/*dfw*^{2J} or *dfw*^{i5}/*dfw*^{i5} mice (Figure 3.3A). Reduced PMCA2 expression is seen in +/*dfw*^{2J} and +/*dfw*^{i5} mice compared to wild-type littermates (Figure 3.3A and B). PMCA2 expression in each genotype of these strains was quantified from a total of at least seven blots using brainstem tissue from different animals (Figure 3.3B). A two-way ANOVA indicated a significant effect of genotype ($p<0.0001$) but no significant strain effect or interaction between strain and genotype, emphasizing the reduction of PMCA2 expression in heterozygous individuals and lack of PMCA2 expression in homozygous mutants. There is no detectable PMCA2 expression difference in the brainstem of +/*dfw*^{2J} and +/*dfw*^{i5} mice (Figure 3.3B, 62.5% of controls in +/*dfw*^{2J} compared to 62.9% of controls in +/*dfw*^{i5}).

3.3.3. *Atp2b2 mRNA transcript expression analysis*

Because the nature and origin of the *dfw*^{2J} (frameshift mutation, originally from a substrain of BALB/cByJ) and *dfw*^{i5} (nonsense mutation, originally on a DBA/2J background) alleles are different, we hypothesized that the phenotypic difference between the strains might be attributed to altered transcript regulation or expression. The *Atp2b2* transcript in the central nervous system is generated from two independent transcriptional start sites, α and β, with each contributing significantly to overall transcript production (Silverstein & Tempel, 2006).

Accordingly, we quantified total *Atp2b2*, *α-Atp2b2*, and *β-Atp2b2* expression in +/*dfw*^{i5} and +/*dfw*^{2J} animals and wild-type littermates. Total RNA was isolated from brainstem of 5-6 week-old mice and expression levels of each transcript type were quantified (Figure 3.4A). In brainstem, *α-Atp2b2* is expressed at about ½ the level of *β-Atp2b2* (Figure 3.5A and B). Total, *α*- and *β-Atp2b2* expression was reduced in +/*dfw*^{i5} (n=9) and +/*dfw*^{2J} (n=8) to 60.2, 62.5 and 56.8% of controls (n=7) and to 58.6, 59.4 and 54.4% of controls (n=7), respectively. Total-*Atp2b2* expression is greatly reduced to 11.0% in *dfw*^{i5}/*dfw*^{i5} and to 7.2% in *dfw*^{2J}/*dfw*^{2J} (n=2 for each strain) compared to wild-type littermates (data not shown). A two-way ANOVA shows an overall effect of genotype ($p<0.0001$) but no strain effect. An unpaired, two-tailed t-test showed significant differences between genotypes within a strain for all transcript types ($p<0.001$ for each strain).

Even though *α-Atp2b2* is the lesser of the two transcript types in brainstem (Figure 3.5), normalizing expression to wild-type controls for each transcript shows consistently higher levels of *α-Atp2b2* than *β-Atp2b2* in heterozygous individuals of each strain (Figure 3.4B and Figure 3.5B). The preferential expression of *α-Atp2b2* over *β-Atp2b2* is significant in a two-tailed, paired t-test for each strain ($p<0.05$). Quantitation of transcript expression in brainstem allows for a direct comparison of *Atp2b2* to PMCA2 expression. In both heterozygous strains, the reduction in RNA resembles the reduction in protein, with *α-Atp2b2* levels most closely mirroring PMCA2 expression (62.5% *α-Atp2b2* vs. 62.9% PMCA2 in +/*dfw*^{i5} and 59.4% *α-Atp2b2* vs. 62.5% PMCA2 in +/*dfw*^{2J}). In addition, we asked if RNA and protein expression correlated within +/*dfw*^{i5} individuals (Figure 3.4C). Interestingly, a significant correlation was seen between PMCA2 expression and *α-Atp2b2* but not with *β-Atp2b2*, suggesting that

α-Atp2b2 may be particularly important for PMCA2 expression in these animals. Correlation fits and significance between PMCA2 expression and each type are described in Table 3.3.

In addition to brainstem, RNA was also isolated from whole cochlea of +/+ and +/- individuals of each strain to better approximate expression in auditory hair cells which almost exclusively express the *α-Atp2b2* transcript type (Silverstein & Tempel, 2006). Whole cochlear preps include a heterogeneous population of cell types that includes auditory hair cells, but also spiral ganglia which contain a considerable amount of PMCA2 (see Methods for a description of whole cochlear dissections). Nonetheless, the ratio of *α-Atp2b2* to *β-Atp2b2* expression in these preps improved from 1:2 in brainstem to over 1:1 in whole cochlea (Figure 3.5). Again, a significant reduction in the expression of each transcript type was detected in +/dfw^{i5} (n=9) and +/dfw^{2J} (n=8) mice compared to wild-type littermates (Figure 3.6A). Total, *α-* and *β-Atp2b2* transcripts were expressed at 61.1, 65.7 and 56.3% of controls (n=5) and at 62.0, 65.4 and 53.4% of controls (n=7) in +/dfw^{i5} and +/dfw^{2J}, respectively. The preferential expression of *α-Atp2b2* over *β-Atp2b2* in heterozygous individuals was even more apparent in the cochlea (Figure 3.6) and was significant in a two-way, paired t-test ($p<0.01$ in +/dfw^{i5} and $p<0.001$ in +/dfw^{2J}). Thus, it appears that a specific up-regulation of *α-Atp2b2* occurs in these heterozygous mutants as an attempt to compensate for the reduction in PMCA2.

3.3.4. *Ancestral variation between deafwaddler null mutants*

The dfw^{i5} and dfw^{2J} mutations arose on alleles of different genetic backgrounds, DBA/2J (DBA) and BALB/cByJ (BALB/c), respectively. We set out to determine if ancestral background differences may contribute to the disparity in phenotypes between +/dfw^{i5} and +/dfw^{2J} even though these strains have been backcrossed into our wild-type CBA/CaJ (CBA)

background for 10 or more generations. We postulated that variations may be particularly likely to remain in the region immediately surrounding *Atp2b2*, the gene selected for when genotyping.

SNP identification using the Mouse Genome Informatics database (Bult *et al.*, 2008) was used as a starting point to compare ancestral variation between DBA, BALB/c and C57BL/6J (B6, the reference sequence) within and near the *Atp2b2* gene on Chr. 6. Because CBA variation has not been detailed in this region, SNPs were identified between the other two strains and B6, and then sequenced in CBA genomic DNA. We were particularly interested in genetic variations in the proximal promoter region of the hair-cell, *α-Atp2b2*, transcript and those causing amino acid changes in PMCA2. Using the MGI database, we identified one non-synonymous coding mutation causing a glutamic acid (E) in B6 to aspartic acid (D) substitution at residue 731 in PMCA2 of DBA. We sequenced genomic DNA (gDNA) from DBA and CBA, and found that the variation is present in both strains. Of interest, BALB/c has the B6 variant (E), and sequencing of dfw^{i5}/dfw^{i5} and dfw^{2J}/dfw^{2J} gDNA showed that the aspartic acid (D) was carried with the dfw^{i5} allele while the glutamic acid (E) has been carried with the dfw^{2J} allele (Table 3.4).

Further sequence analysis of the proximal promoter up to 3,200 bp upstream of the *α-Atp2b2* transcriptional start site revealed several single nucleotide variations carried by both CBA and DBA strains relative to B6 reference sequence (Table 3.4). Of note, published variations for BALB/c are identical to B6 in this region. Sequencing of dfw^{i5}/dfw^{i5} and dfw^{2J}/dfw^{2J} gDNA confirmed the presence of five SNPs in the proximal promoter region of *Atp2b2* between dfw^{i5} and dfw^{2J} mutant alleles. Since CBA and DBA are ancestrally identical in this region, the dfw^{i5} promoter can be treated as if it is the same as a wild-type littermate.

However, the *dfw*^{2J} allele has carried BALB/c ancestral variations (identical to B6) in the proximal promoter of *Atp2b2* making this promoter unique from the CBA (wild-type) and *dfw*^{i5} promoters (Figure 3.7).

3.3.5. *Allelic Discrimination Reveals Differential Ancestral Regulation*

Although no significant difference in overall transcript expression between the strains was immediately apparent, provided with knowledge of ancestral variation carried by the mutant alleles, we chose to examine further the possibility of a difference in RNA regulation by designing allele specific probes to distinguish between wild-type/*dfw*^{i5} and wild-type/*dfw*^{2J} cDNA (see Methods). Thus, we were able to compare the relative amount of mutant transcript contributing to total *Atp2b2* expression in these heterozygous strains. The percentage of mutant transcript in brainstem tissue from each heterozygous strain is shown in Figure 3.8A, with +/*dfw*^{i5} expressing nearly 3X the amount of mutant transcript than +/*dfw*^{2J} (6.9% compared to 2.4%, respectively, $p<0.001$).

To see if this difference could be attributed to ancestral haplotype in other *deafwaddler* alleles, we also assessed mutant allele expression in +/*dfw*^{3J}. The *dfw*^{3J} mutation originated in a B6 sub-strain and is a 4-bp deletion in the third coding exon of *Atp2b2*. When characterized in parallel (McCullough & Tempel, 2004), +/*dfw*^{2J} and +/*dfw*^{3J} were found to have indistinguishable auditory phenotypes. Given the similarity in phenotype between +/*dfw*^{2J} and +/*dfw*^{3J} as well as the similarity between ancestral haplotype at the *Atp2b2* locus between BALB/c and B6, we predicted that +/*dfw*^{3J} would express the same amount of mutant allele as +/*dfw*^{2J}. Whole brain RNAs from the original characterization of the +/*dfw*^{3J} mutant in our lab (one set containing four +/*dfw*^{3J} RNAs with controls and the other set, processed in parallel,

containing three analogous +/*dfw*^{2J} RNAs with controls) were converted into cDNA and tested (Figure 3.8A). These samples show no difference in mutant allele expression between +/*dfw*^{2J} and +/*dfw*^{3J} (2.4% and 2.6%, respectively). [The "(B)" designation is meant to indicate that they should only be directly compared to one another.] A greater percentage of mutant allele was also seen in whole cochlear preps of +/*dfw*^{i5} mice compared to +/*dfw*^{2J} (Figure 3.8B, $p<0.001$). Additionally, in both strains the percentage of mutant allele increased between brainstem and cochlea to 11.4% in +/*dfw*^{i5} and to 7.2% in +/*dfw*^{2J}, demonstrating a significant overall effect of tissue type ($p<0.0001$).

In order to differentiate between: 1) an effect of the causal mutations on the *dfw*^{i5} and *dfw*^{2J} alleles and, 2) an effect of ancestral variation, we assessed if the two mutant haplotypes have a functional consequence on *Atp2b2* expression independent of the null mutations. To do so, we crossed a CBA mouse (promoter haplotype 1) with a B6 mouse (promoter haplotype 2) to create a hybrid with one allele of each promoter haplotype (like +/*dfw*^{2J}) but lacking a null mutation. If each haplotype is regulated in the same way, the alleles should be expressed at equivalent levels. Using the same allelic discrimination probe used for +/*dfw*^{2J} and +/*dfw*^{3J} (see Methods), we were able to assay the relative expression of CBA and B6 alleles in these F1 hybrid mice (n=5). Consistent with higher expression of the *dfw*^{i5} allele over the *dfw*^{2J} allele, the CBA transcript was found to be expressed at about twice the level of the B6 transcript (66.1% vs. 33.9%, respectively) (Figure 3.8C). Using a two-tailed, one-sample t-test with a theoretical mean of 50%, the alleles were determined to be differentially expressed ($p<0.0005$). This indicates that the difference in promoter haplotype functionally affects the regulation of the CBA and B6 alleles, and therefore the *dfw*^{i5} and *dfw*^{2J} mutant alleles.

We also asked if it is possible that a difference in intrinsic stability of the *dfw*^{i5} and *dfw*^{2J} transcripts could contribute to the notable expression difference. A computer-run simulation of RNA secondary structure (Gruber *et al.*, 2008) predicts the minimum free energy for CBA, *dfw*^{i5} and *dfw*^{2J} transcripts to be -2677.14 kcal/mol, -2677.34 kcal/mol and -2668.17 kcal/mol, respectively (Figure 3.9A-C). These data indicate that the lower energy (and therefore more stable) secondary structures are formed by the CBA and *dfw*^{i5} transcripts with only a minimal difference between the two. Conversely, the predicted secondary structure of the *dfw*^{2J} transcript seems to be disrupted compared to CBA and there is a loss of 9.97 kcal/mol in free energy, which is approximately the hydrogen bonding energy in 2 base pairings (using the average GC content of the wild-type transcript). Free energies and predicted secondary structures were also calculated for *dfw*^{3J} and B6 transcripts (Figure 3.9D and E). Remarkably, the predicted structure of the *dfw*^{2J}, the *dfw*^{3J} and the B6 transcripts closely resemble one another, suggesting that the SNPs in the B6 haplotype may affect RNA structure more so than the *dfw*^{2J} and *dfw*^{3J} deletions. However, these predicted changes in stability cannot fully account for the expression differences we report for these transcripts.

3.3.6. *Molecular Correlations to Phenotype*

Since there was no detectable difference in protein expression between +/*dfw*^{i5} and +/*dfw*^{2J} animals in the brainstem, we wondered if the mutant *dfw*^{i5} transcript could directly affect auditory sensitivity. We looked to see how much of the phenotypic variation within +/*dfw*^{i5} individuals could be accounted for by expression differences in mutant-*Atp2b2* in cochlea and brainstem. Only frequencies that were significantly different from controls (5.6, 22.6, 32 and 40 kHz) were included in this analysis. The cohorts used for each tissue type were

not identical, but they each contained the same amount of variation at the frequencies of interest (Figure 3.10). Of note, each cohort contained an individual that had relatively intact transduction at high frequencies, but these were different animals. Comparisons of RNA and protein expression to sensitivity at each frequency in +/*dfw*^{i5} (n=6) are described in Table 3.5 and notable comparisons are presented in Figure 3.11. The only significant correlation that exists in this tissue type is between *α-Atp2b2* expression and sensitivity at 22.6 kHz (p=0.029) where animals with the highest level of expression have the best thresholds. Mutant transcript expression in the brainstem does not correlate to sensitivity.

In the cochlea, wild-type *Atp2b2* expression does not correlate to sensitivity at any frequency. Conversely, increasing amounts of mutant-*Atp2b2* in +/*dfw*^{i5} (n=7) correlate to higher ABR thresholds at 32 and 40 kHz (Figure 3.12), but not at 5.6 and 22.6 kHz (Table 3.6). Applying the percentage of mutant transcript to the expression of *α*- and *β-Atp2b2* in the cochlea strengthens the correlation to mutant *α-Atp2b2* but not to mutant *β-Atp2b2* which is no longer statistically significant (see Table 3.6). Moreover, that the strongest correlation to phenotype is at 32 kHz, the frequency where +/*dfw*^{i5} most significantly differs from +/*dfw*^{2J}, implicates mutant transcript expression as a contributing factor in the phenotypic difference between the strains. These results imply that mutant-*Atp2b2* might directly interfere with auditory sensitivity in the cochlea and, in particular, may interfere with transduction in high-frequency hair cells of the inner ear.

3.3.7. *Other considerations*

While it is intriguing to attribute the phenotype of +/*dfw*^{i5} to increased mutant transcript expression in the cochlea, we acknowledge that other mechanisms likely contribute to impaired

transduction in *dfw*^{i5} and other *deafwaddler* mutants. We would predict that mutant transcript expression could also explain the variation in sensitivity at high frequencies within +/*dfw*^{2J}. However, if mutant transcript expression was the only contributor to loss of sensitivity at these frequencies in +/*dfw*^{i5} and +/*dfw*^{2J}, then we would expect to see a substantial overlap in mutant transcript expression that would be more consistent with the overlap in thresholds at these frequencies. It is possible that another regulatory feature of the genome could be affected by the difference in ancestral haplotype surrounding *Atp2b2*.

The *Atp2b2* gene is over 300 kb long with several large intronic regions (Figure 3.13A). It has become increasingly apparent that intronic and intergenic regions of the genome can serve important regulatory and functional roles in mammalian organisms (Consortium *et al.*, 2012). Here we confirm the presence of 5 SNPs in the proximal promoter of *Atp2b2* between the *dfw*^{i5} and *dfw*^{2J} haplotypes, but there are over 300 reported SNPs between the haplotypes in the region spanning *Atp2b2*, and all but three are intronic or proximal to the 5' or 3' end of the gene. Since the mutant transcripts for these alleles are mostly degraded, and are never made into protein, one could argue that a SNP in an intron has the potential to have a greater impact on *Atp2b2* regulation or PMCA2 expression than a variation in the coding sequence. We noticed that two uncharacterized non-coding RNA genes, *Gm15082* (linc82) and *Gm15083* (linc83), sit complementary to the 5' end of *Atp2b2* (Figure 3.13A, purple arrows).

Expression of these RNAs was confirmed in the brainstem and cochlea of wild-type mice (Figure 3.13B and C). The linc82 RNA is primarily expressed in the brainstem with minimal expression in the cochlea, and linc83 is primarily expressed in the cochlea with negligible expression in the brainstem (Figure 3.13B). Abundance relative to total *Atp2b2* expression is also shown for each lincRNA and tissue type (Figure 3.13C). Quantification of lincRNA

expression in these tissues reveals that linc82 is unchanged in +/+ and +/- mice from each strain, but linc83 expression in the cochlea of +/*dfw*^{2J} is significantly higher than in controls (Figure 3.14). This result is consistent with a difference in haplotype between wild-type and mutant alleles in +/*dfw*^{2J} but not in +/*dfw*^{i5}. While we do not know the function of these non-coding RNAs, this serves as proof of principle that other regulatory elements in the genome may be affected by differences in haplotype at the *Atp2b2* locus.

3.4. Discussion

This study compares a new *deafwaddler* null allele, *dfw*^{i5}, to two previously characterized mutants, +/*dfw* and +/*dfw*^{2J}, to examine the degree to which PMCA2 function quantitatively affects auditory transduction. As a reflection of the importance of PMCA2 to auditory transduction, haploinsufficiency in +/*dfw*^{2J} has been previously reported to affect auditory function (McCullough & Tempel, 2004) but not to the extent as we report here for +/*dfw*^{i5}. Western protein blots confirm that both *dfw*^{2J} and *dfw*^{i5} alleles are functional nulls with no full-length or truncated PMCA2 protein detectable in either strain. Heterozygous animals from each strain express slightly over half of wild-type PMCA2 levels without any detectable truncation products. Consequently, it was not immediately apparent what causes the phenotypic difference between +/*dfw*^{2J} and +/*dfw*^{i5}.

Analysis of *Atp2b2* transcript expression in these strains at 6 weeks of age is complex since it can be generated from two independent transcriptional start sites, and both wild-type and mutant mRNA can contribute to the total expressed transcript in +/*dfw*^{2J} and +/*dfw*^{i5} mice. Total transcript expression in +/*dfw*^{2J} and +/*dfw*^{i5} is about 60% of controls, suggesting that a large degree of non-sense mediated RNA degradation is occurring in neuronal tissue from these

heterozygous strains (Losson & Lacroute, 1979; Zetoune *et al.*, 2008). The only notable difference between *Atp2b2* expression in +/*dfw*^{2J} and +/*dfw*^{i5} is the discernible increase in mutant-*Atp2b2* seen in +/*dfw*^{i5}. The high statistical significance this result ($p<0.0001$ for the overall strain effect) suggests that mutant-*Atp2b2* may be the primary contributor to the phenotypic disparity between +/*dfw*^{2J} and +/*dfw*^{i5}.

Our data support a correlation between ancestral haplotype at *Atp2b2* and expression of mutant allele in three +/*dfw*^{null} mice. Although the *dfw*^{i5} mutation was generated on a DBA allele, CBA (the wild-type background) and DBA have the same ancestry surrounding *Atp2b2*. This means that, excluding the causal mutation, the wild-type and mutant alleles in +/*dfw*^{i5} mice are identical. However, we identified five ancestral SNP variations carried from the BALB/c background onto the *dfw*^{2J} promoter, causing it to differ from the wild-type and *dfw*^{i5} alleles. The variants on the *dfw*^{2J} promoter permit differential regulation of the mutant and wild-type alleles in +/*dfw*^{2J}. Allelic discrimination in CBA/B6 hybrid mice, with one of each promoter haplotype, shows that the CBA allele is expressed preferentially over the B6 allele, suggesting that regulatory features of the CBA haplotype confer stronger expression. If the wild-type and *dfw*^{i5} haplotypes result in stronger expression of *Atp2b2* than the *dfw*^{2J} haplotype, this could account for the difference in expression levels of the mutant alleles in +/*dfw*^{2J} and +/*dfw*^{i5} mice.

Taking this hypothesis one step further, predicted transcription factor binding sites (Quandt *et al.*, 1995) were determined for *dfw*^{i5} and *dfw*^{2J} alleles containing the five genetic variations in the proximal promoter of *Atp2b2*. While each variation altered the predicted binding of one or more transcription factors, possibly the most interesting SNP is 1957 bp upstream from the transcriptional start site and lies in the core consensus sequence for the homeodomain protein family of transcription factors. These transcription factors are predicted

to bind to the *dfw*^{i5} promoter but not to the *dfw*^{2J} promoter at this location. Homeodomain-containing proteins such as Brn3.1 (known as POU4F3 in humans) are known to be expressed in the inner ear and affect auditory function in adult mice (Keithley *et al.*, 1999). Loss of binding by such a transcription factor may contribute to the differential expression of *dfw*^{i5} and *dfw*^{2J} transcripts.

Alternatively, the degradation, rather than the production, of mutant transcripts might differ between the strains. Non-sense mediated decay may be more efficient for the *dfw*^{2J} transcript than the *dfw*^{i5} transcript. Recognition of a premature stop codon by the exon junction complex (EJC) usually occurs only when the codon is more than 50 nucleotides upstream of the exon-exon splice site (Nagy & Maquat, 1998; Isken *et al.*, 2008; Le Hir & Seraphin, 2008). In the *dfw*^{2J} allele, the premature stop codon is located just over 100 nucleotides upstream from the next exon splice site, while in the *dfw*^{i5} allele, the premature stop codon is only 26 nucleotides upstream of the nearest exon splice site. It is clear from our data that non-sense mediated decay occurs robustly for both transcripts, although the site (nuclear or cytoplasmic) or mechanism (with or without association with the EJC and with or without ribosomal association) may be different (Maquat, 2004; 2005) and could result in differential degradation efficiency. However, the differential *Atp2b2* regulation seen in CBA/B6 hybrids suggests that the production of mutant transcript is the main source of the expression difference since neither transcript in the hybrids is degraded.

Higher levels of mutant transcript are detected in both brainstem and cochlear tissue of +/*dfw*^{i5} compared to +/*dfw*^{2J}, indicating the regulatory mechanism that contributes to the difference is not tissue-type specific. Increased levels of mutant transcript seen in both strains in the cochlea compared to brainstem imply, however, that mutant allele production or

degradation mechanisms may be tissue specific. In regard to RNA expression, the main difference between brainstem and cochlea is the increased usage of the *α-Atp2b2* transcriptional start site over the *β-Atp2b2* transcriptional start site (see Figure 3.8 and Silverstein & Tempel, 2006). Distinguishing between expression levels of each transcript type reveals that heterozygotes in each strain preferentially express *α-Atp2b2* over *β-Atp2b2* in comparison to their wild-type counterparts, suggesting that *α-Atp2b2* expression is critical for auditory transduction and compensation. This is supported also by the evidence that auditory hair cells overwhelmingly express *α-Atp2b2* over any other transcript type (Silverstein & Tempel, 2006). It is possible that the transcription factors needed for expression of *α-Atp2b2* are different from those that transcribe *β-Atp2b2* and are expressed differentially in these cell-types. As a result, the *α-Atp2b2* promoter may be stronger than the *β-Atp2b2* promoter making it energetically favorable to express and up-regulate *α-Atp2b2* in cell types that are highly dependent on PMCA2 activity for auditory transduction. The mature *α-Atp2b2* transcript might also be more stable than the mature *β-Atp2b2* transcript. If promoter strength and/or inherent stability are differential characteristics of the *α-* and *β-* transcripts, higher levels of mutant transcript might be generated from the *α-Atp2b2* start site, resulting in higher mutant allele expression in the cochlea.

Mechanisms to recognize and degrade mutant transcript may also be less effective in the cochlea than in the brainstem since the efficiency of non-sense mediated decay in mouse can be tissue dependent (Zetoune *et al.*, 2008). A significant change in non-sense mediated decay efficiency might be reflected by a difference in total *Atp2b2* expression in these tissues. Total *Atp2b2* is reduced to an average of 60.2 and 58.6% in +/*dfw*^{i5} and +/*dfw*^{2J} brainstem, respectively, and to 61.1 and 62.0% in +/*dfw*^{i5} and +/*dfw*^{2J} cochlea, respectively. While total

expression levels are marginally higher in the cochlea, the difference does not seem to fully account for the magnitude of the increase in mutant allele expression, especially for +/*dfw*^{i5}. Thus, the rise in mutant transcript expression in the cochlea of heterozygous mice could be a byproduct of increased *α-Atp2b2* abundance.

How mutant transcript might lead to decreased auditory sensitivity is another matter. We report a negative correlation between mutant transcript expression and ABR sensitivity in +/*dfw*^{i5}, indicating that mutant transcript can directly affect auditory transduction. Moreover, this correlation only exists with mutant transcript expressed in the cochlea and not in the brainstem. That this trend appears to be tissue specific suggests the mutant transcript may interfere with transduction by affecting a cell type that is unique to the cochlea. The only cell types expressing PMCA2 in our cochlear prep are auditory hair cells and spiral ganglion neurons (Furuta *et al.*, 1998; Wood *et al.*, 2004). While we cannot rule out the spiral ganglia, the properties of these cells are presumably more similar to those expressing PMCA2 in the brainstem. Given the specialized morphology and mechanoelectric transduction properties of auditory hair cells, they are an appropriate candidate cell type that could be directly affected by mutant-*Atp2b2* expression.

Preferential expression of *α-Atp2b2* is apparent in both +/*dfw*^{i5} and +/*dfw*^{2J} cochlea. Because the *dfw*^{i5} and wild-type alleles have indistinguishable promoters, the cellular energy dedicated to up-regulating wild-type *α-Atp2b2* will also generate a significant amount of mutant transcript in the process. This may be exacerbated in auditory hair cells that predominately express *α-Atp2b2*. It is possible that the additional *dfw*^{i5} transcript in auditory hair cells acts as a "molecular sink" by tying up translational machinery necessary for up-regulation of the functional, wild-type allele. Recent examples of "decoy RNAs" have been described (Wang &

Chang, 2011) and can bind a variety of RNA binding proteins including transcription factors or other regulatory elements (Martianov *et al.*, 2007; Baek *et al.*, 2008; Bartel, 2009; Hung *et al.*, 2011). In the context of auditory hair cells, density has been attributed to polyribosome complexes and rough endoplasmic reticulum localized near the cuticular plate in hair cells toward the base of the stereocilia (Hirose *et al.*, 2004; Grati *et al.*, 2006). The relatively fast turnover of PMCA2 in the stereocilia of about 5-7 hours (Grati *et al.*, 2006) might require the utilization of these polyribosome complexes for rapid generation and subsequent transport of PMCA2 into the stereocilia membrane. Although PMCA2 is expressed at relatively low levels compared to other stereocilia proteins such as β-actin, it is it is the second most abundant transmembrane protein detected in the stereocilia (Shin *et al.*, 2007) suggesting the rough endoplasmic reticulum near the cuticular plate may generate a substantial amount of PMCA2 delivered into the stereocilia bundle. If *Atp2b2* transcript is stabilized and translated by polyribosome complexes toward the base of the stereocilia, the presence of additional dfw^{i5} transcript in $+/dfw^{i5}$ animals may interfere with translation of the wild-type PMCA2, causing a worsened auditory phenotype relative to $+/dfw^{2J}$.

The dfw^{i5} transcript might also indirectly affect transduction in high frequency hair cells by adding to their metabolic load. The cellular energy required to recognize and degrade the mature dfw^{i5} transcript might create an additional insult to these cells which already have to function very efficiently to clear calcium and respond to high frequency stimuli. That mutant allele expression only correlates to worsened sensitivity at the highest frequencies tested (32 and 40 kHz) supports this mechanism. We suspect that this mechanism is not unique to $+/dfw^{i5}$, and might generalize to $+/dfw^{2J}$ to account for the variability also seen at these frequencies in this strain. Of all $+/dfw^{i5}$ mice tested in a variety of experiments, 4 of 28 (14%) had "good"

thresholds at high frequencies (50 dB SPL or below). This was also true for +/*dfw*^{2J} individuals with 2 of 18 (11%) retaining "good" thresholds at high frequencies. We hypothesize that these +/*dfw*^{2J} individuals would also express the least mutant *Atp2b2*.

To summarize, mutant transcript expression in +/*dfw*^{i5} is significantly higher than in +/*dfw*^{2J} and may be caused by differential promoter regulation on these alleles, as evidenced by unique ancestral haplotypes in this region. We propose that the phenotypic consequence of additional mutant transcript in +/*dfw*^{i5}, either directly or indirectly, is a worsening of auditory sensitivity relative to +/*dfw*^{2J}. Alternatively, another regulatory element surrounding *Atp2b2* might be affected by haplotype differences in this region and lead to the phenotypic difference between the strains. As proof of principle, the non-coding RNA generated from the *Gm15083* gene in cochlea of +/*dfw*^{2J} is differentially expressed, and might contribute to the phenotype in these mice.

Lastly, we have identified variations in the proximal promoter of the *dfw*^{2J} allele and have shown decreased expression of B6 *Atp2b2* associated with this haplotype, which has implications in the interaction with *Cdh23*. The critical dependence of outer hair cells on PMCA2 function is exemplified in Chapter 2 by the interaction of the *ahl* locus in +/*dfw*^{i5} animals (Figure 2.6). In this study, we demonstrate that *Atp2b2* is differentially regulated in B6 than in CBA. As discussed in more detail in Chapter 2, B6 mice are carriers of the *ahl* allele, which is associated with exon skipping in *Cdh23* and has been attributed to cause age-related hearing loss in these mice (Noben-Trauth *et al.*, 2003). Recently, however, it was shown that isolated homozygosity at the *ahl* locus (B6-like at this location) in an otherwise CBA background (denoted CBA.B6-*ahl*) does not duplicate the early-onset hearing loss seen in B6 controls (Kane *et al.*, 2012). In fact, the complementary congenic mice (CBA-like at *ahl* in an

otherwise B6 background, denoted B6.CBA-*ahl*+) had a worse phenotype than did CBA.B6-*ahl* at 8 kHz by 15 months of age. These results demonstrate that another affected gene is needed in combination with homozygosity at *ahl* to produce the hearing loss phenotype seen in B6. Moreover, the intermediate phenotype is seen only at lower frequencies in the CBA.B6-*ahl* and B6.CBA-*ahl*+ congenic strains. Our result demonstrating the strength of the interaction of the *ahl* allele with *Atp2b2* at low frequencies (Figure 2.6), and the differential regulation of *Atp2b2* expression in CBA/B6 hybrid mice (Figure 3.7C), suggests *Atp2b2* is a viable candidate. We propose *Atp2b2* is a prospective candidate gene that contributes to age-related hearing loss in B6 via decreased expression of *Atp2b2* transcript and consequently PMCA2 (relative to CBA) as a result of promoter haplotype at this location.

Allele	Mutation type (Effect)	+/- Auditory Phenotype	PMCA2 Expression*	PMCA2 Pump Efficiency*	Summed Function*
dfw	G283S (expressed)	Mild	100%	30%[2]	30%
dfw^{2J}	2bp deletion (null)	Moderate	0%	-	0%
dfw^{3J}	4bp deletion (null)[1]	Moderate	0%	-	0%
dfw^{i5}	K580Stop (null)	Moderate	0%	-	0%

Table 3.1. Summary of *deafwaddler* alleles. Four different *deafwaddler* alleles are compared, each with a unique mutation in PMCA2. Phenotypes are given for heterozygous mutants for each allele and described relative to wild-type controls. The +/*dfw* mice have mild loss at high frequencies while the other three strains have more severe loss at high frequencies and some loss at low and mid-range frequencies (See Figure 3.1). Expression, efficiency and function are estimates for the mutant allele only. Summed function is the combination of PMCA2 expression and efficiency. Hypothetically, an additional 50% could be added to this value to estimate total calcium clearance activity of a heterozygote for each allele. *Represents estimated values.

[1.] McCollough & Tempel, 2004. [2.] Penheiter *et al*. 2001.

	+/*dfw*	+/*dfw*^{2J}	+/*dfw*^{i5}
+/+	32.0**; 40.0***	5.6*, 22.6**, 32.0***, 40.0***	5.6*, 22.6***, 32.0***, 40.0***
+/*dfw*	N/A	22.6**, 32.0***, 40.0***	22.6***, 32.0***, 40.0***
+/*dfw*^{2J}	N/A	N/A	22.6*, 32.0***

Table 3.2. Statistical differences between auditory phenotypes of strains at 5 weeks. *p<0.05, **p<0.01, ***p<0.001

	Total *Atp2b2*	WT-*Atp2b2*	MUT-*Atp2b2*	Alpha	Beta	A/B Ratio
PMCA2	0.29 (0.17)	0.31 (0.15)	0.14 (0.35)	*0.60 (0.025)	0.032 (0.67)	0.19 (0.28)

Table 3.3. Correlation between PMCA2 (protein) and *Atp2b2* (RNA) expression in +/*dfw*^{i5} brainstem. Values shown are the correlation constant, r^2, and p-value indicating if the slope of the linear regression is significantly non-zero. Correlations, r^2 (p-value), which are significant are indicated with an asterisk.

Genotype	p1 (-2188)	p2 (-1957)	p3 (-1593)	p4 (-1588)	p5 (-1192)	AA731
CBA and DBA*	A	A	C	T	A	T (D)
BALB/c* and B6*	T	G	T	C	G	G (E)
WT	A	A	C	T	A	T (D)
dfw^{i5}	A	A	C	T	A	T (D)
dfw^{2J}	T	G	T	C	G	G (E)

Table 3.4. SNPs detected in the proximal promoter of *Atp2b2*. SNPs are designated as p1-p5 and positions (in nucleotides) upstream of the *α*-, hair-cell transcriptional start site are indicated in parentheses. A coding SNP changing the predicted residue at position 731 is also indicated and the resulting residue is in parentheses. Strains marked with an asterisk (*) were not sequenced, and SNPs shown are those published on the MGI Database (Eppig *et al.*, 2012). CBA (WT), *dfw*^{i5} and *dfw*^{2J} polymorphisms were identified by sequencing. The wild-type and *dfw*^{i5} transcripts show ancestry identical to CBA/CaJ and DBA/2J in this region while the *dfw*^{2J} transcript retains BALB/cByJ ancestry. Reference, C57BL/6J, is also similar to BALB/cByJ in this region.

	5.6 kHz	22.6 kHz	32 kHz	40 kHz
PMCA2	0.0012 (0.95)	0.56 (0.089)	0.057 (0.65)	0.16 (0.44)
Total RNA	0.045 (0.69)	0.20 (0.38)	0.012 (0.84)	0.025 (0.77)
Total WT	0.018 (0.80)	0.27 (0.29)	0.030 (0.74)	0.061 (0.64)
Total MUT	0.20 (0.37)	0.0079 (0.87)	0.044 (0.69)	0.080 (0.59)
Alpha	0.072 (0.61)	*0.74 (0.029)	0.14 (0.47)	0.25 (0.31)
Beta	0.0073 (0.87)	0.0038 (0.91)	0.23 (0.34)	0.15 (0.45)
A/B Ratio	0.056 (0.65)	0.35 (0.22)	0.52 (0.11)	0.49 (0.12)

Table 3.5. Correlation between ABR thresholds and molecular data for PMCA2 and *Atp2b2* expression in +/*dfw*^{i5} brainstem. Values shown are the correlation constant, r^2, and p-value indicating if the slope of the linear regression is significantly non-zero. Correlations, r^2 (p-value), which are significant are indicated with an asterisk.

	5.6 kHz	22.6 kHz	32 kHz	40 kHz
Total RNA	0.039 (0.71)	0.018 (0.77)	0.067 (0.57)	0.12 (0.44)
Total WT	0.021 (0.78)	0.037 (0.68)	0.024 (0.74)	0.066 (0.58)
Total MUT	0.21 (0.36)	0.11 (0.48)	*0.74 (0.013)	*0.69 (0.020)
Alpha	0.0031 (0.92)	0.0012 (0.94)	0.12 (0.45)	0.21 (0.30)
WT Alpha	0.011 (0.84)	0.014 (0.80)	0.043 (0.66)	0.11 (0.47)
MUT Alpha	0.077 (0.59)	0.24 (0.27)	*0.95 (0.0002)	*0.88 (0.0019)
Beta	0.0030 (0.92)	0.22 (0.29)	0.051 (0.63)	0.0017 (0.93)
WT Beta	0.011 (0.84)	0.26 (0.24)	0.10 (0.48)	0.019 (0.77)
MUT Beta	0.22 (0.35)	0.022 (0.75)	0.41 (0.12)	0.47 (0.09)
%MUT Allele	0.12 (0.50)	0.31 (0.19)	*0.61 (0.039)	0.44 (0.11)
A/B Ratio	0.00031 (0.97)	0.17 (0.35)	0.34 (0.17)	0.23 (0.28)

Table 3.6. Correlation between ABR thresholds and molecular data for PMCA2 and *Atp2b2* expression in +/*dfw*^{i5} cochlea. Values shown are the correlation constant, r^2, and p-value indicating if the slope of the linear regression is significantly non-zero. Correlations, r^2 (p-value), which are significant are indicated with an asterisk.

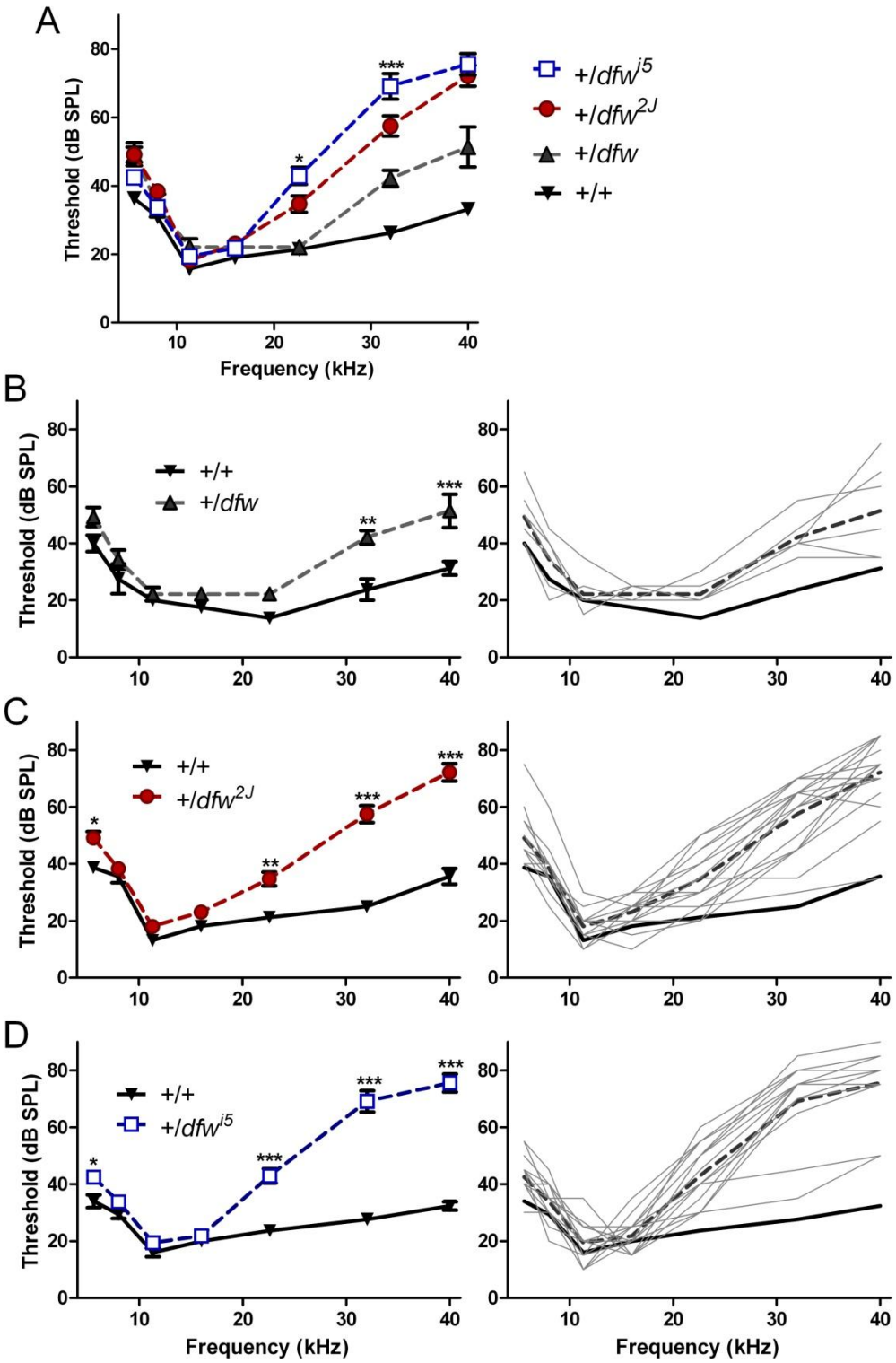

Figure 3.1. Auditory characterization of *deafwaddler* alleles at 5 weeks. *(A)* Average ABR thresholds for heterozygous mice of each strain (dashed lines) plotted with grouped wild-type littermates (solid

line). +/*dfw*^{i5} (blue open squares) and +/*dfw*^{2J} (red circles) have significant hearing loss at several frequencies while +/*dfw* (closed triangles) has only mild hearing loss compared to wild-type controls (solid inverted triangles) at high frequencies. +/*dfw*^{i5} is statistically different from +/*dfw*^{2J} at 22.6 and 32 kHz. Error bars represent SEM. *(B-D)* Plots of averaged ABR thresholds of mice from each strain (left) and heterozygous individuals of each strain (right). The average of the individual traces is shown as a thick dashed line and the wild-type average (solid black line) is shown for reference. Significantly different frequencies between heterozygotes and wild-type littermates of each strain are indicated in the left panel of B-D. For all panels, *p<0.05, **p<0.01, ***p<0.001 in a two-way ANOVA. See Table 3.1 for detailed statistics.

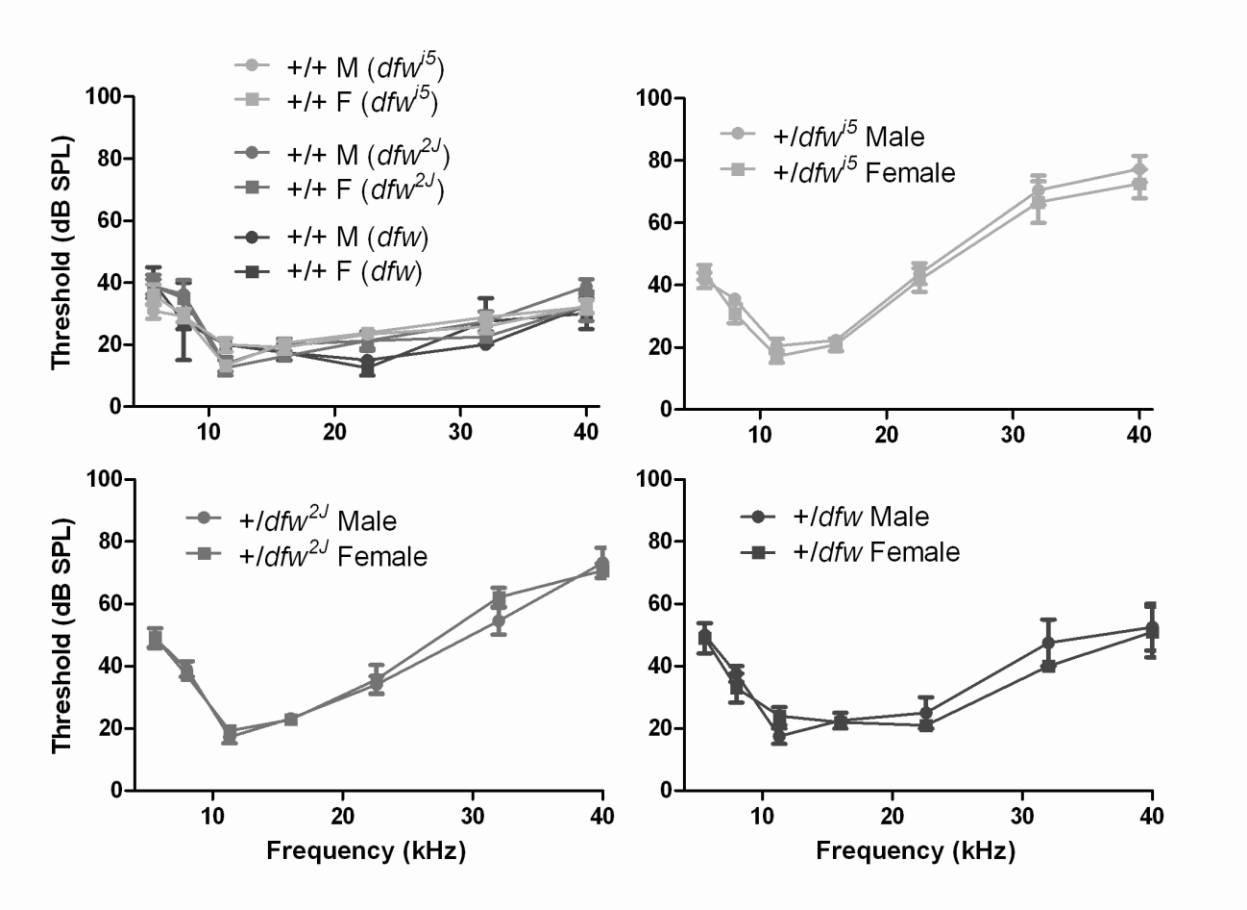

Figure 3.2. Gender does not affect ABR thresholds in *deafwaddler* mice used in this study. Threshold data was averaged for male (M) and female (F) mice of wild-type littermates for each strain (top, left) and heterozygous individuals for +/*dfw*^{j5} (top, right), +/*dfw*^{2J} (bottom, left) and +/*dfw* (bottom, right). No statistical differences were found between male and female groups for any strain or genotype using a two-way ANOVA. Error bars represent SEM.

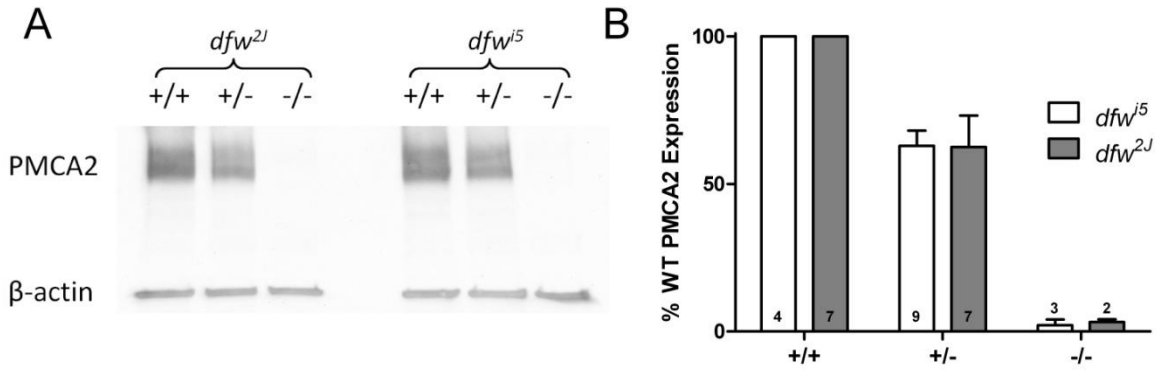

Figure 3.3. PMCA2 expression in *dfw*^{2J} and *dfw*^{i5} mutants is reduced. *(A)* Representative Western blot of mouse brainstem tissue stained for PMCA2 (slightly under 150 kDa marker) and β-actin (slightly above 37 kDa marker). *(B)* Quantification of PMCA2 band intensity from at least seven Western blots of brainstem tissue containing different combinations of wild-type and heterozygous individuals for *dfw*^{i5} (white bars) and *dfw*^{2J} (gray bars). The total number of unique individuals of each genotype included in averaged data (or that were used for normalization in the case of wild-type littermates) is indicated at the bottom of the graph. Error bars represent SEM. There is a strong overall effect of genotype ($p<0.0001$) but no significant strain effect.

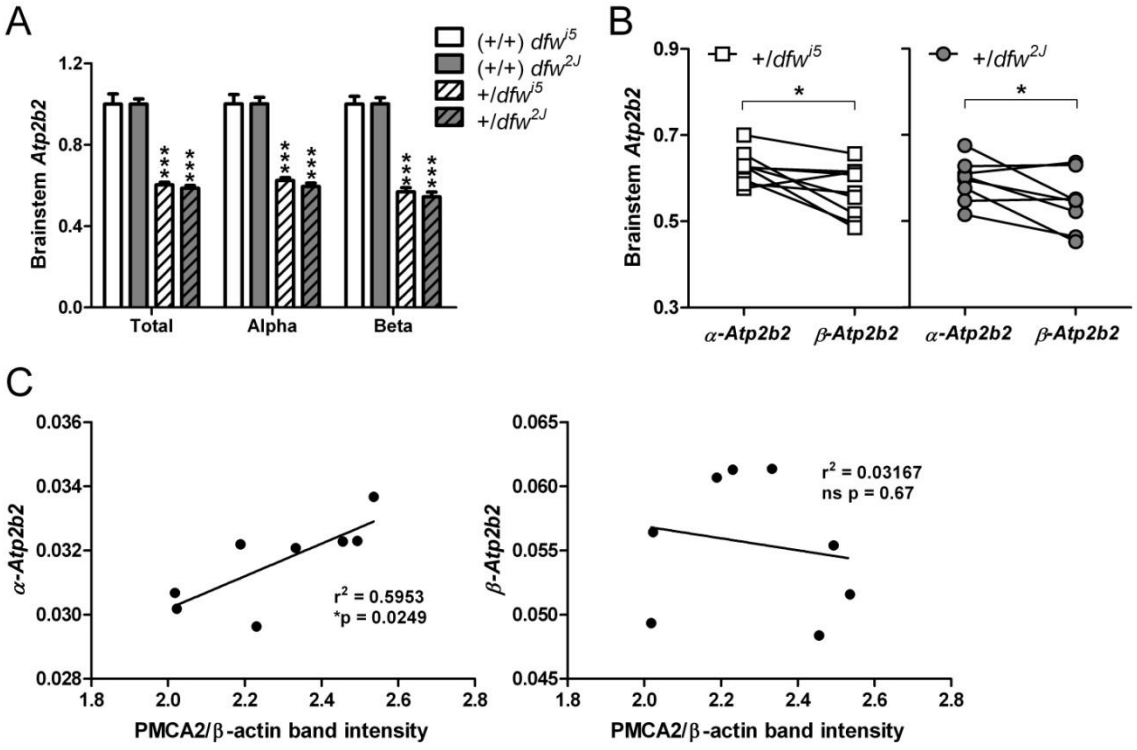

Figure 3.4. *Atp2b2* expression in +/*dfw*^{2J} and +/*dfw*^{i5} is reduced in brainstem. *(A)* Brainstem RNA of individual mice was converted to cDNA and quantified for total-, *α*- and *β-Atp2b2* relative to reference genes for *β*-actin and SDHA. Quantities were then normalized to wild-type expression for each transcript type. ***p<0.001 in a two-way, unpaired t-test between wild-type and heterozygous expression of each transcript type for each strain. Error bars represent SEM. *(B)* Normalized expression in heterozygous individuals demonstrates preferential expression of *α-Atp2b2* over *β-Atp2b2* in brainstem tissue of both strains. *p<0.05 in a two-way, paired t-test. *(C) α-Atp2b2* (left), but not *β-Atp2b2* (right), expression in +/*dfw*^{i5} individuals correlates to PMCA2 intensity.

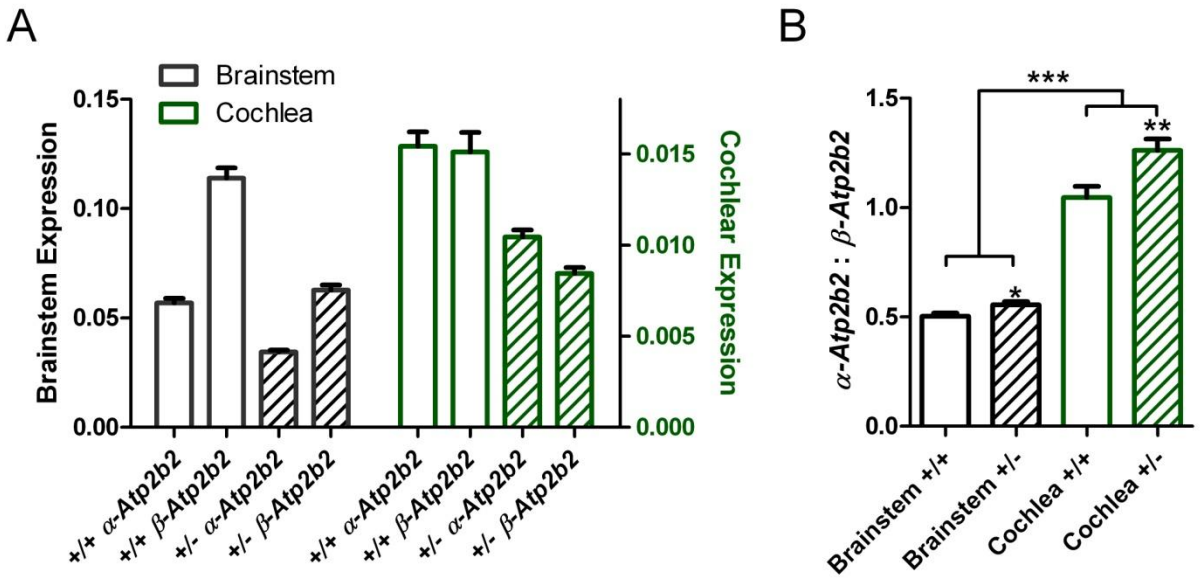

Figure 3.5. *Atp2b2* transcript usage in brainstem and cochlear preps. *(A)* Expression of *α-Atp2b2* and *β-Atp2b2* in brainstem and cochlea of wild-type and heterozygous mice. Data from dfw^{i5} and dfw^{2J} strains was grouped for clarity. *β-Atp2b2* is expressed about two-fold higher than *α-Atp2b2* in brainstem and the transcripts are expressed at roughly equivalent levels in whole cochlea. *(B)* The same data as shown in (A) plotted as a ratio of *α-Atp2b2* to *β-Atp2b2* emphasizes the increase in relative abundance of *α-Atp2b2* in cochlea as well as the increase in *α-Atp2b2* expression in heterozygous mice compared to controls. *p<0.05, **p<0.01, ***p<0.001 in a one-way ANOVA with Bonferonni post-hoc comparisons. Error bars represent SEM.

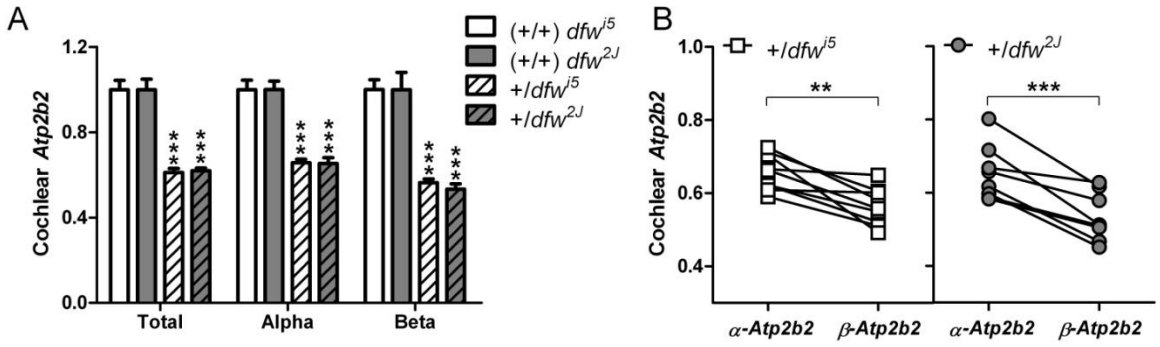

Figure 3.6. *Atp2b2* expression in +/*dfw*^{2J} and +/*dfw*^{i5} is reduced in whole cochlea. *(A)* Cochlear samples from individual mice also show a significant reduction in total-, *α*- and *β-Atp2b2* relative to reference genes for *β*-actin and SDHA. ***p<0.001 in a two-way, unpaired t-test between wild-type and heterozygous expression of each transcript type for each strain. Error bars represent SEM. *(B)* Normalized expression in heterozygous individuals demonstrates preferential expression of *α-Atp2b2* over *β-Atp2b2* in cochlear tissue of both strains. **p<0.01 and ***p<0.001 in a two-way, paired t-test.

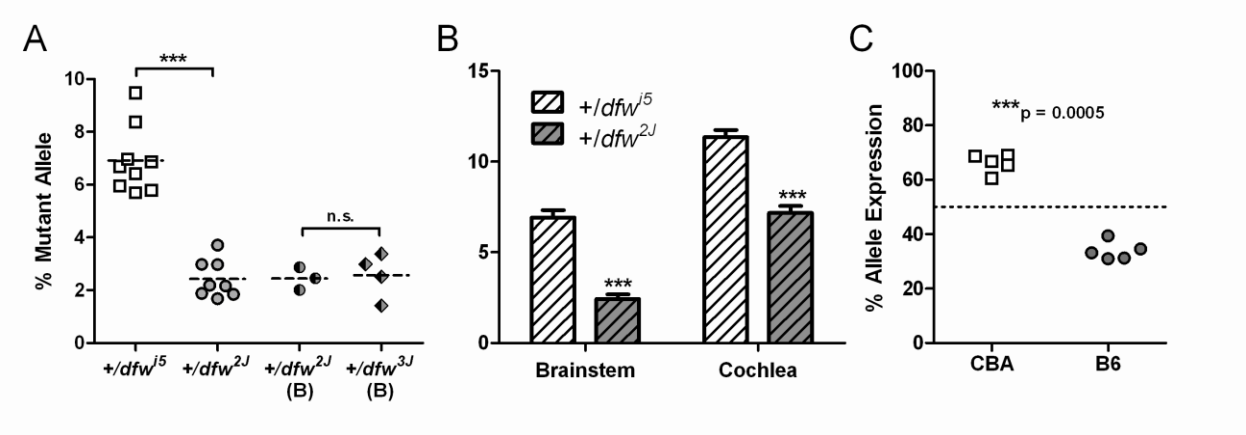

Figure 3.7. The percentage of mutant *Atp2b2* differs between +/*dfw*^{i5} and +/*dfw*^{2J}. *(A-B)* Heterozygous cDNAs used for brainstem and cochlear *Atp2b2* quantification were further analyzed with allele specific probes. ***p<0.001 in a two-way, unpaired t-test. *(A)* +/*dfw*^{i5} expresses significantly higher mutant *Atp2b2* than +/*dfw*^{2J} in brainstem. Whole brain RNAs from a different prep, "B", show no differences in mutant allele expression between two strains, +/*dfw*^{2J} and +/*dfw*^{3J}, with the same haplotype at the proximal *Atp2b2* locus. *(B)* The same data shown +/*dfw*^{i5} and +/*dfw*^{2J} in brainstem (A) plotted with cochlear data for each strain. +/*dfw*^{i5} expresses a significantly higher amount of mutant *Atp2b2* than +/*dfw*^{2J} in multiple tissues, with the percentage increasing for both strains in whole cochlea. Error bars represent SEM. *(C)* Allelic discrimination brainstem of CBA/B6 hybrid mice shows that *Atp2b2* from the CBA allele is expressed at about twice the level as *Atp2b2* from the B6 allele. ***p<0.0005 in a two tailed, one sample t-test with a hypothetical mean of 50%.

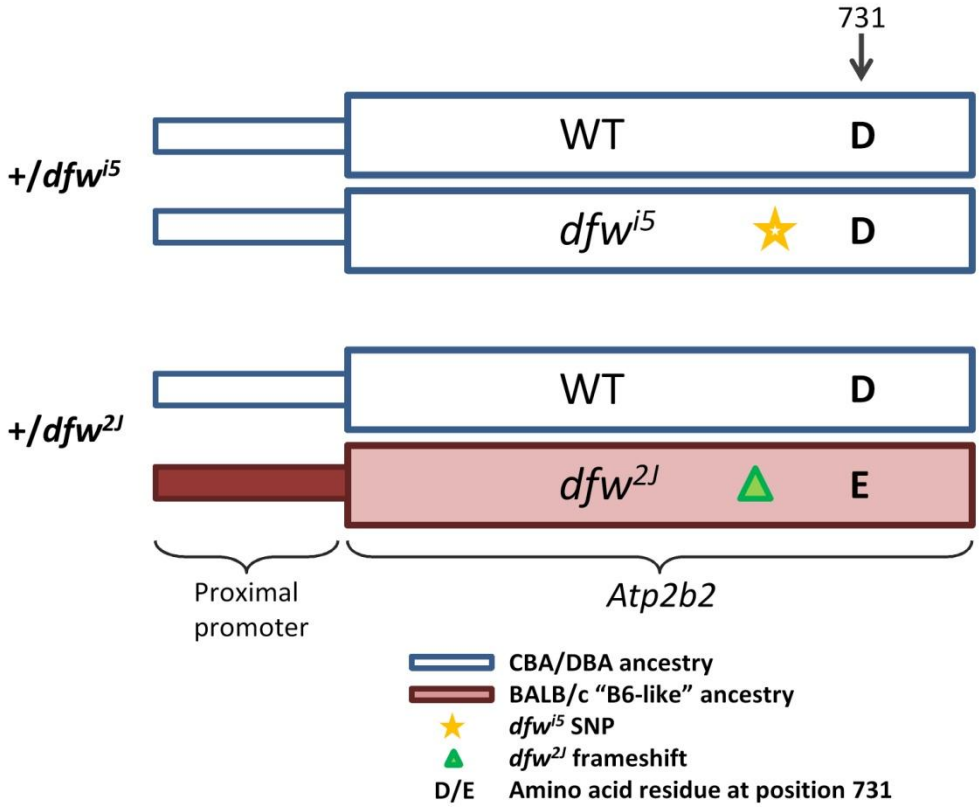

Figure 3.8. Ancestral variation carried on *dfw*^{2J} and *dfw*^{i5} alleles make mutant promoters unique. Schematic of the ancestral lineage in the region of *Atp2b2* for +/*dfw*^{i5} and +/*dfw*^{2J} mice. For detailed information on SNPs in the proximal promoter, see Table 3.2.

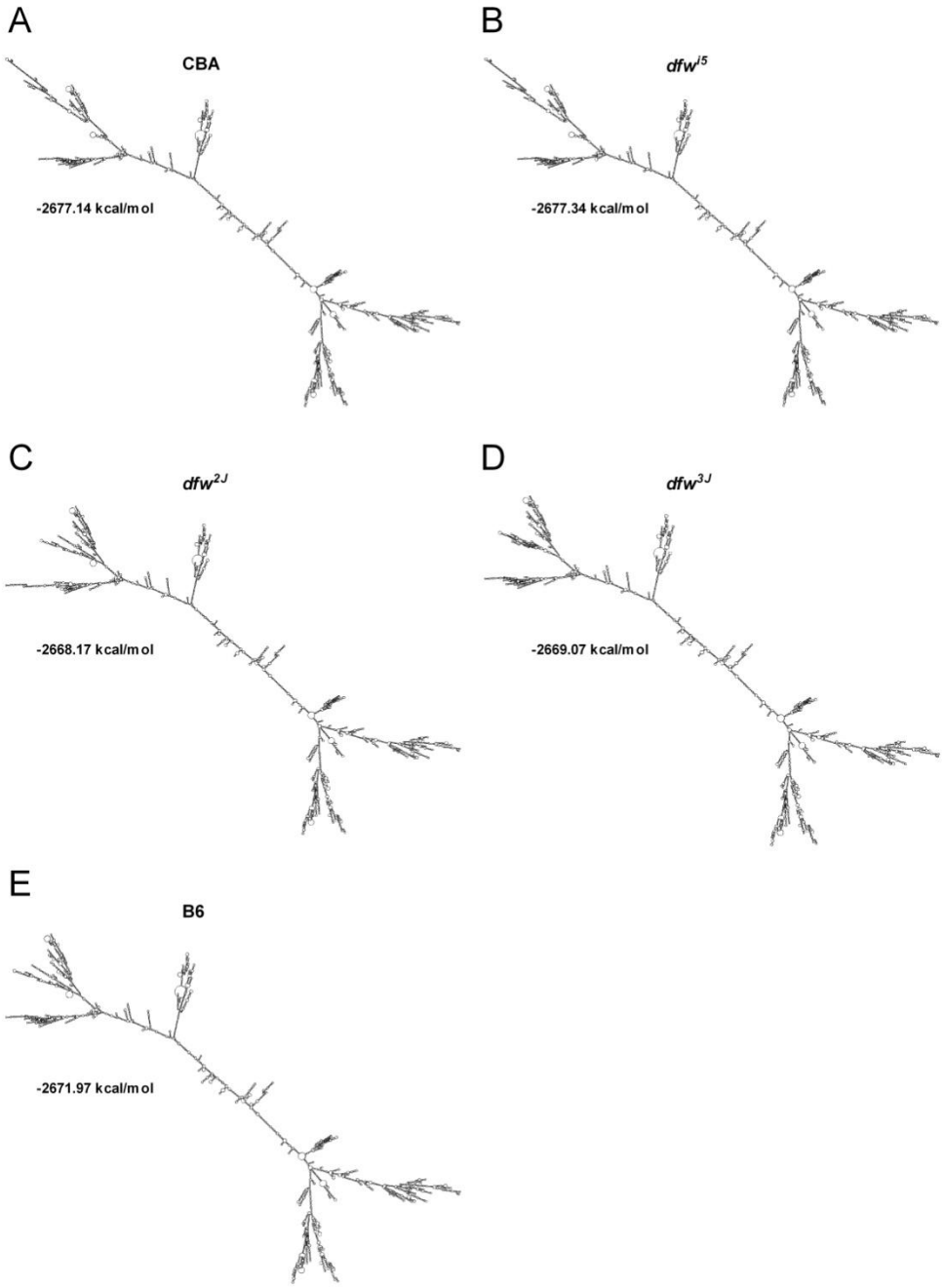

Figure 3.9. Variations in the *α-Atp2b2* transcript cause small changes to the secondary structures for *deafwaddler* alleles. Predicted minimum free energies (MFE) and resulting structures are shown for the *α-Atp2b2* transcripts of CBA (A), dfw^{i5} (B), dfw^{2J} (C), dfw^{3J} (D) and B6 (E). All reported variations were included in input sequences in addition to the mutations of interest. Branching in the upper left portion of the MFE structures is most affected by the variations. The CBA and dfw^{i5} alleles are predicted to be the most stable, followed by B6, and then the dfw^{2J} and dfw^{3J} alleles containing base-pair deletions.

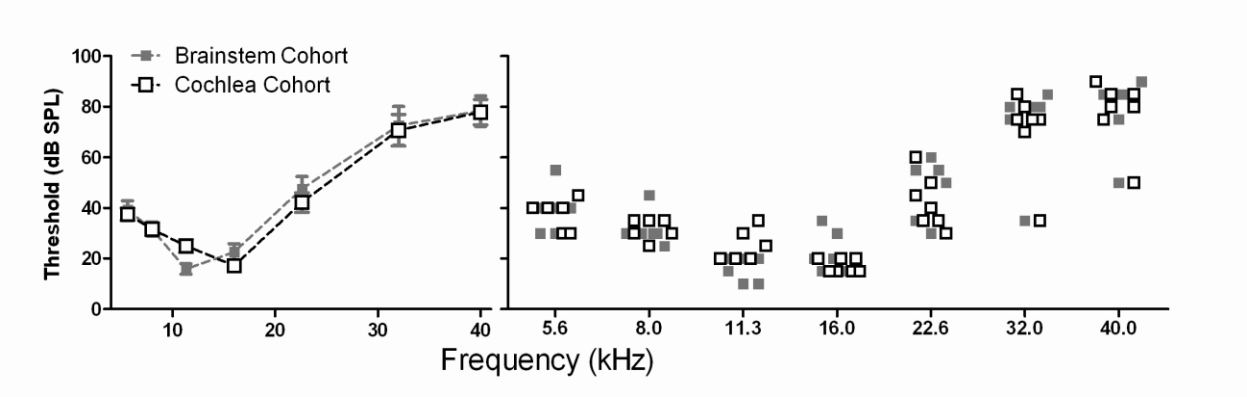

Figure 3.10. Cohort comparison for sets of samples used to correlate sensitivity to expression in brainstem and cochlea. The cohorts used for correlations in each tissue type contained three common and four (cochlea) or three (brainstem) unique individuals. A two-way ANOVA shows no cohort effect and F-tests at 5.6, 22.6, 32 and 40 kHz show no significant differences in the variance of each group. The individual in each cohort with the best thresholds at high frequencies was not common to both cohorts.

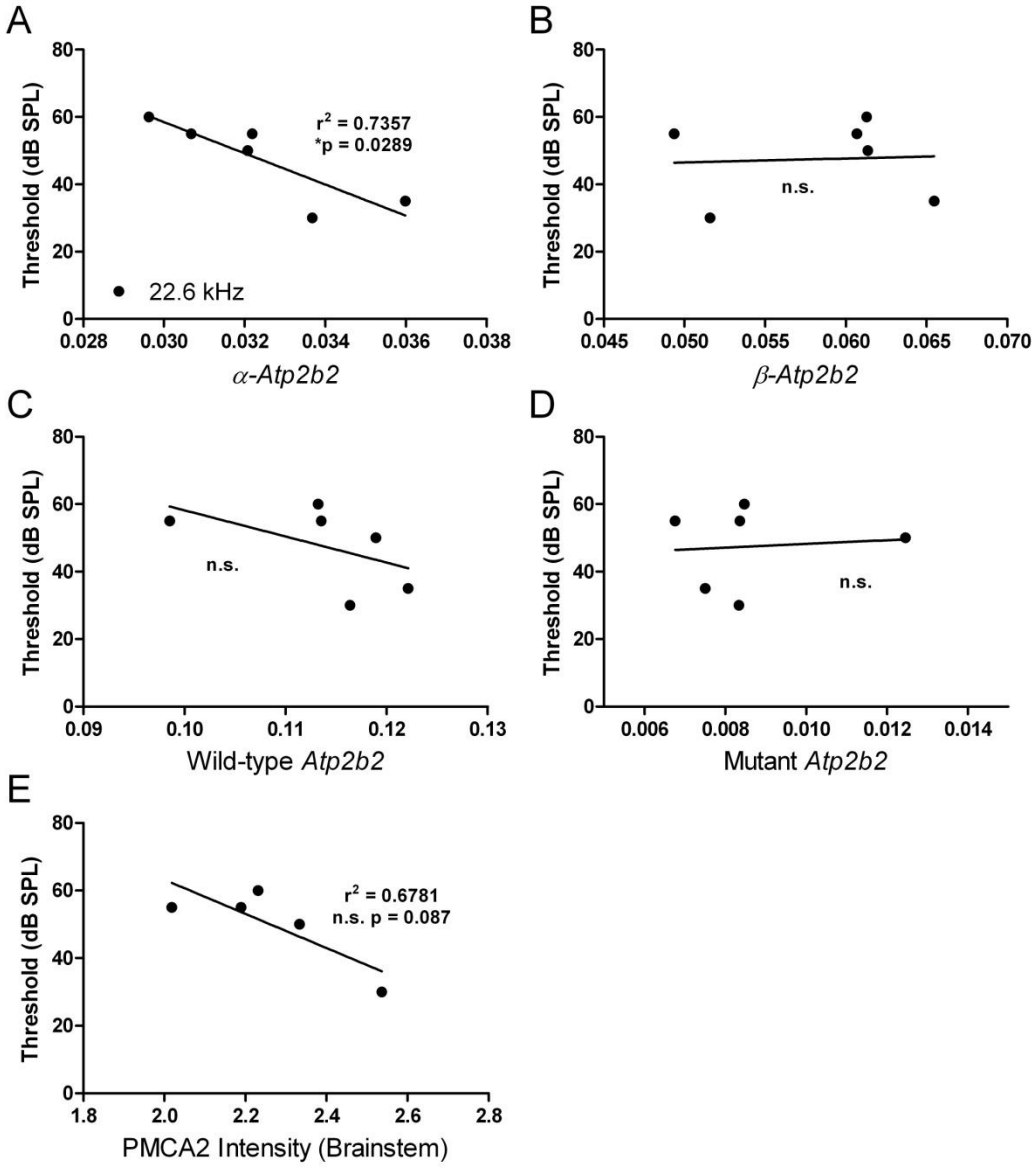

Figure 3.11. Molecular correlations to phenotype in brainstem of +/*dfw*^{i5}. Expression levels of *Atp2b2* and PMCA2 for individual +/*dfw*^{i5} mice were correlated to ABR sensitivity at several frequencies. For a complete statistical analysis of correlations analyzed, see Table 3.5. *(A-B)* ABR threshold at 22.6 kHz correlates to expression of *α-Atp2b2* but not to *β-Atp2b2*, with individuals expressing the most *α-Atp2b2* having the best sensitivity at this frequency. *(C)* Total transcript levels adjusted for mutant allele expression (resulting in wild-type *Atp2b2*) do not significantly correlate to threshold. *(D)* Estimated PMCA2 expression in brainstem slightly correlates to threshold at 22.6 kHz, with the trend approaching statistical significance.

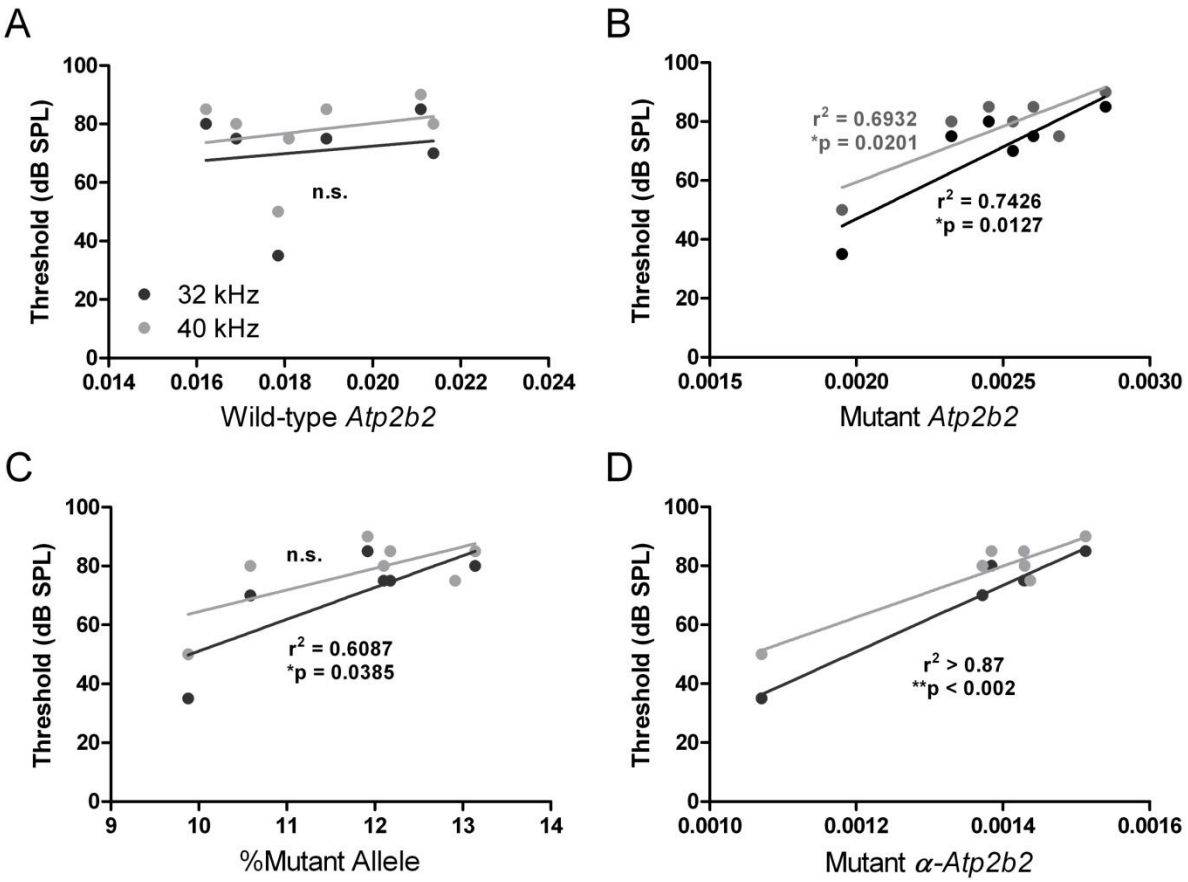

Figure 3.12. Mutant *Atp2b2* expression correlates to auditory phenotype in cochlea of +/*dfw*^{i5}. Thresholds at frequencies significantly different from wild-type controls were examined for correlations to *Atp2b2* expression within +/*dfw*^{i5} individuals. *(A-D)* A significant correlation exists between mutant *Atp2b2* (B) in cochlea of +/*dfw*^{i5} and auditory sensitivity at 32 and 40 kHz. There is no correlation to wild-type *Atp2b2* (A) in the cochlea. Individuals expressing the most mutant *Atp2b2* in cochlea have the highest thresholds, or worst sensitivity, at these frequencies. The correlation is weakened when thresholds are compared to the percentage of mutant allele (C) and strengthened when the percentage of mutant allele is applied to the proportion of *α-Atp2b2* present in the cochlea (D).

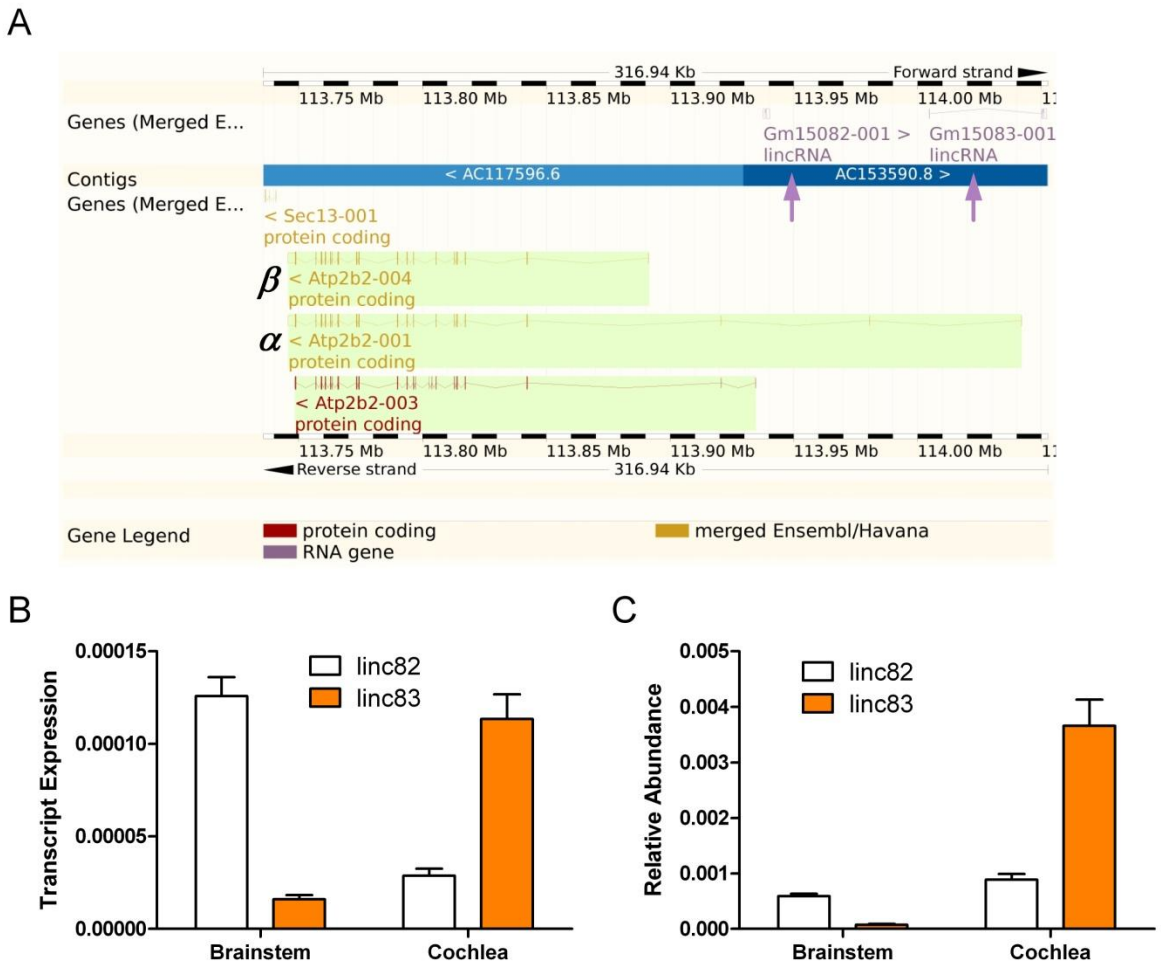

Figure 3.13. Two lincRNA genes sit complementary to *Atp2b2* and are expressed in the brainstem and cochlea of wild-type mice. *(A)* A schematic[1] shows the location of *Atp2b2* on chromosome 6. The *Atp2b2* gene is transcribed from the reverse strand while two predicted long non-coding RNA genes sit complementary to the 5' region of *Atp2b2* on the forward strand of chromosome 6 (indicated by purple arrows). *Gm15083* (or linc83) spans the *α-Atp2b2* translational start and *Gm15082* (linc82) sits upstream of the *β-Atp2b2* transcriptional start site. *(B-C)* LincRNA genes are expressed in a tissue specific manner in wild-type mice with linc82 expression predominating in the brainstem and linc83 expression predominating in the cochlea. Graphs represent absolute expression levels (B) and abundance relative to total *Atp2b2* expression (C). Error bars represent SEM.

[1.] Schematic modified from www.ensembl.org.

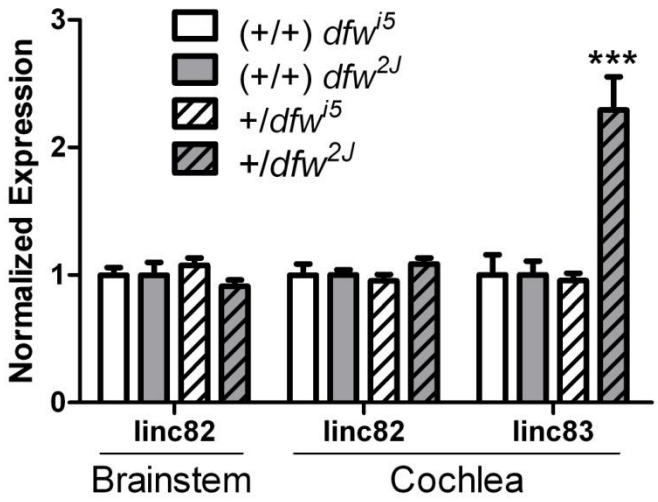

Figure 3.14. Expression of long non-coding RNA *Gm15083* is significantly higher in +/*dfw*^{2J}. Expression levels of linc82 are equivalent between wild-type and heterozygous mice of each strain. Linc83 expression in the cochlea of +/*dfw*^{2J} is significantly higher than wild-type controls whereas expression in +/*dfw*^{i5} is the same as in wild-type littermates. Quantified levels of linc83 in the brainstem are at the limit of detection and were not included in this analysis. ***$p<0.001$ in a one-way ANOVA. Error bars represent SEM.

Chapter 4

Maturation of Auditory Sensitivity in +/*dfw*^{i5} Correlates to Up-regulation of PMCA2

Summary

To date, studies characterizing the effect of PMCA2 mutant mice have centered on the auditory phenotype of late adolescent and adult mice. In this study, we examine the effect of PMCA2 haploinsufficiency in +/*dfw*^{i5} during the maturation of the auditory brainstem response from P16 into adulthood. Sensitivity in wild-type mice improves between P16 and 3 weeks of age, when it becomes quite stable through adolescence. Here we report a frequency-dependent loss of sensitivity and subsequent recovery of thresholds in +/*dfw*^{i5} between P16 and adulthood. We show that *α-Atp2b2* levels increase in wild-type and heterozygous cochleae between P16 and 5 weeks, with levels in +/*dfw*^{i5} increasing more significantly than in their wild-type counterparts. These increases reported for the *α-Atp2b2* transcript type during this stage in development emphasize the favored usage of this transcript for mature auditory transduction. PMCA2 up-regulation was also detected in the brainstem of +/*dfw*^{i5} and implicates that compensation by the wild-type allele is a mechanism by which these mice recover sensitivity at some frequencies between 3 weeks and adulthood.

4.1. Introduction

Auditory transduction relies on the development of a complex set of cell types to transform the mechanical movements of the basilar membrane into an electrical signal that can be interpreted by the brain. The organ of Corti, the auditory sensory epithelium of the cochlea, is made of a range of stereotypically defined cell types including non-sensory cells, inner and outer hair cells as well as a variety of supporting cell types which include Deiters' cells, Hensen's cells and pillar cells that maintain the structural morphology of the epithelium. In combination with the development of specialized cells in the sensory epithelium of the inner ear, are corresponding changes in the expression of proteins and transcription factors that eventually determine the physiological function of a particular cell type (Kelley, 2006).

It has been well established that PMCA2 is required for auditory transduction in the mature mammalian cochlea (Kozel *et al.*, 1998; Street *et al.*, 1998; McCullough & Tempel, 2004). PMCA2 is a neuronal isoform that is expressed in spiral ganglia neurons which innervate the hair cells of the inner ear, and is abundantly expressed in the stereocilia bundles of outer hair cells (Yamoah *et al.*, 1998; Dumont *et al.*, 2001; Wood *et al.*, 2004; Chen *et al.*, 2012). Expression of PMCA2 mRNA (Furuta *et al.*, 1998) and protein is detected as early as P0 in the mammalian cochlea, beginning at the base and appearing by P6 in apical hair cells (Chen *et al.*, 2012). Coordinated auditory responses are not detected in mice until around P12 which is commonly denoted as the "onset of hearing" (Mikaelian & Ruben, 1965). The postnatal onset of auditory transduction in mice affords us the opportunity to study how PMCA2 function might affect sensitivity immediately following the initiation of transduction. In this study, we compare the maturation of ABR thresholds in wild-type and +/dfw^{i5} mice, which encode one

null *Atp2b2* allele, from P16 to 9 weeks of age and correlate changes in sensitivity to expression changes in *Atp2b2* and PMCA2.

4.2. Methods

Animals

The +/*dfw*^{i5} mice and wild-type littermates used in this study ranged in age from P16 to nine weeks of age. All of the *dfw*^{i5} mice have been backcrossed into CBA/CaJ for 10 generations, designated as incipient congenic CBACa.D2(B6)-*Atp2b2*^{dfwi5}. The +/*dfw*^{i5} mice (and littermate controls) used for expression analysis at P16 and P20 were time-mated and assayed exactly four days apart to be as precise as possible at this early developmental stage. Mice are maintained in a backcross to CBA/CaJ which are obtained from JAX and replaced every 3-4 generations to retain a stock that is isogenic with CBA/CaJ at JAX. Animals were kept on a 12 hour light/dark cycle and kept in an environment with minimal exposure to noise. All procedures were approved by the University of Washington Institutional Animal Care and Use Committee (IACUC).

Auditory Testing

All mice were tested for auditory sensitivity using auditory brainstem responses (ABRs) across frequencies ranging from 5.6 kHz to 40 kHz. The procedure was the same as described in Chapters 2 and 3 with a few exceptions. Mice were anesthetized with a mixture of ketamine (130 mg/kg) and xylazine (10 mg/kg) prior to auditory testing, with mice at P16 and three weeks of age dosed at 0.1 mL/gram body weight (gBW) and mice four weeks or older dosed at 0.13 x gBW. The system was calibrated at the beginning of each day of testing to confirm the

equipment was working properly and that the speaker output was within the normal range. To ensure consistency between recordings at early developmental ages, P16 and 3 weeks, the same calibration file was loaded for all ABR testing of these groups. A series of 350 tones at a given frequency and intensity were administered and brain responses were recorded with two electrodes placed subcutaneously at the forebrain and hindbrain. Tones were 3ms long with a 1ms rise/fall $\cos^2$ function and brainwaves were recorded for 15ms following the initiation of each tone at a rate of 13.3 Hz. Threshold at a particular frequency was determined by visual detection as the lowest intensity sound (dB SPL) which evoked a recognizable and reproducible brainwave (at least 2 out of 3 trials).

Expression Analysis

Tissue was collected from +/*dfw*^{i5} mice and wild-type littermates at P16, P20 and five weeks of age for *Atp2b2* and PMCA2 expression analysis. P16 and P20 tissue was collected on the same day as ABR testing in these individuals. Tissue from mice assayed at five weeks (P35-P38) was collected between P38-P48, and is referred to as "5 week" tissue, even if it was collected in the sixth postnatal week.

Atp2b2 Quantification:

For RNA expression analysis, fresh brainstem or cochlear tissue was stored in RNA*later* (Qiagen), equilibrated for 24 hours at 4^{o}C to allow the solution to penetrate the tissue, and transferred to -20^{o}C for later use. The vestibular portion of the inner ear was removed in cochlear dissections in addition to the removal of as much bone, vasculature, debris and neuronal tissue as possible. See Chapter 3 for a longer description of the cochlear dissection method. The protocol for RNA isolation was the same as in Chapters 2 and 3. Briefly, RNA

was isolated using the RNeasy Plus Universal Mini Kit (Qiagen) according to the manufacturer's protocol. Samples were homogenized and total RNA from each sample (2 µg total RNA for brainstem and about 1 µg total RNA for whole cochleae) was reverse-transcribed into complimentary DNA (cDNA). These samples were used for quantitative PCR (qPCR) analysis using SYBR green master mix (BioRad) and primers designed for total-, α- and *β-Atp2b2* (PMCA2), *Atp2b4* (PMCA4), *Gm15082* (linc82) and *Gm15083* (linc83) as well as for reference genes *Actb* (β-actin) and *Sdha* (succinate dehydrogenase, subunit A). Forward and reverse primer sequences for *Atp2b4* are 5'-TCCCAGTGGCTGAGATTGTG-3' and 5'-TCTTCAGATCATTTCCCTGGATTAG-3' and the rest are the same as listed in Chapters 2 and 3. The qPCR reactions were done on a BioRad iCycler with iQ5 software. Data for each sample is an average of at least three runs where technical replicates had a relative standard deviation (RSD) of less than 3% for each primer set.

PMCA2 Quantification:

The Western blotting protocol was the same as described in Chapters 2 and 3 with a few minor exceptions. Protein concentrations of each brainstem sample to be compared on the same blot were processed in parallel and were determined using a BCA assay (Pierce) and a NanoDrop Spectrophotometer ND-1000 (NanoDrop Technologies Inc.). For each sample, 5 µg aliquots were prepared by mixing with sample buffer and denaturing for 10 minutes at 50^{o}C, then storing at -20^{o}C until the next day when they were loaded and separated on a 4-20% polyacrilamide RGEL (BioRad). Separated proteins were then transferred to a nitrocellulose membrane (BioRad). Primary and secondary antibody concentrations were 1:15,000 for β-actin (monoclonal, anti-mouse, Sigma) and 1:7,500 for PMCA2 (N-terminal, polyclonal, anti-rabbit, Affinity BioReagents). The ECL Plus kit (GE Healthcare) was used to generate the

chemiluminescent signal which was visualized immediately using a Fotodyne Luminary/FX instrument (Fotodyne Inc.). Quantification of protein bands was done on non-manipulated images taken using PC Image software (Fotodyne Inc.) and analyzed using ImageJ (NIH). PMCA2 expression in each lane was normalized to β-actin expression. Most blots contained at least one P16, P20 and 5 week heterozygote and gender-matched wild-type littermate. On these blots (referred to as "paired quantification"), each heterozygote was quantified relative to its littermate control. One blot for quantification at each age had several heterozygous and wild-type animals from that time point only (referred to as "grouped quantification"). PMCA2 expression was determined for these blots as the averaged band intensity from all heterozygotes compared to all wild-type controls. Data was combined for graph shown in Figure 4.5, and a comparison of data from each quantification method is shown in Figure 4.6.

Allelic Discrimination:

Allele specific cDNA quantification was done for all +/*dfw*^{i5} samples used in total RNA expression data. See Chapter 3 for a more thorough description of the allelic discrimination method. A cDNA specific Taqman probe (Applied Biosystems) was designed to detect the single nucleotide difference in the mutant and wild-type alleles, one labeled with VIC and the other labeled with FAM. All brainstem and cochlear samples of a particular age were assayed in the same run at and were compared to three independent mixtures of a cDNA standard. To generate the mutation-specific standard for *dfw*^{i5}, primers were designed to amplify cDNA from one *dfw*^{i5}/*dfw*^{i5} and one wild-type mouse. High concentrations of these products were purified to ensure accurate concentration readings and were mixed in a 1:1 ratio as the cDNA standard. Samples and standards were run in technical replicates for each assay and averaged. Wild-type and mutant cDNA samples were also run as positive controls. Allelic differentiation data

represents at least three runs of each heterozygous cDNA sample where the %RSD was less than 3% for technical replicates.

4.3. Results

4.3.1. *Developmental auditory characterization of dfw^{i5}*

Developmental maturation of ABR thresholds in +/*dfw*^{i5} was compared to littermate controls to determine when sensitivity in +/*dfw*^{i5} begins to be affected. Mice begin to hear around post-natal day 12 (P12) and have a mature cochlear potential by P14 (Mikaelian & Ruben, 1965). To ensure we could detect a brainstem response, thresholds were assessed throughout auditory development at P16, 3 weeks (P20 or P21), 4 weeks, 5 weeks, 7 weeks and 9 weeks of age (Figure 4.1). Statistical differences between +/*dfw*^{i5} and wild-type controls are detailed in Table 4.1. While wild-type thresholds improve between P16 and 3 weeks, thresholds in +/*dfw*^{i5} stay the same (5.6, 8 and 11.3 kHz) or are noticeably worse (16 kHz and above) at this stage in auditory development (Table 4.2). Thus, 3 weeks of age marks a critical time point in the development of auditory transduction in wild-type and +/*dfw*^{i5} mice, with overall sensitivity improving in one group and worsening in the other. Thresholds recover at 11.3 and 16 kHz to wild-type levels by 4 weeks of age in +/*dfw*^{i5} and partially improve at 22.6 kHz but not at 32 or 40 kHz. Therefore, the mature auditory phenotype of +/*dfw*^{i5} at 5 weeks of age (Chapters 2 and 3) relies on frequency-dependent recovery of sensitivity in these mice between 3 and 4 weeks of age.

4.3.2. *Atp2b2 regulation in +/dfw^{i5} during the development of auditory transduction*

The frequency-dependent improvement in sensitivity by 4 weeks of age in +/*dfw*^{i5} implies that compensation may occur in these mice. To see if regulatory changes in *Atp2b2* expression occur during this time frame, we looked at total, *α*- and *β-Atp2b2* RNA in the brainstem and cochlea of +/*dfw*^{i5} and controls at P16, P20 and 5 weeks. Expression levels at P16 and 5 weeks should adequately capture a snapshot of expression before and after the critical time point in auditory sensitivity at 3 weeks of age. Total, *α*- and *β-Atp2b2* levels in the brainstem are stable over this time frame with no statistical differences in expression (Figure 4.2A). However, in the cochlea, *α-Atp2b2* expression increases in both wild-type and +/*dfw*^{i5}, with expression at 5 weeks greater than at P16 or at P20 (Figure 4.2B). This increase also translates into an increase in total transcript expression in +/*dfw*^{i5} between P16 and 5 weeks of age. Notably, expression of *β-Atp2b2* is does not change in the cochlea during this time.

An increase in *α-Atp2b2* but not *β-Atp2b2* in the cochlea of both wild-type and heterozygous mice indicates that the *α-Atp2b2* transcript type is particularly important for auditory transduction. Furthermore, preferential expression of *α-Atp2b2* over *β-Atp2b2* was reported in brainstem and cochlear tissue of both +/*dfw*^{i5} and +/*dfw*^{2J} mice at 5-weeks of age (Chapter 3, Figures 3.4 and 3.6). To determine if preferential expression is also seen at earlier stages in development, levels of each transcript type were normalized to controls for each +/*dfw*^{i5} individual and then compared (Figure 4.3). Remarkably, preferential expression of *α-Atp2b2* over *β-Atp2b2* was not seen in P16 or P20 mice in either tissue type, supporting a compensatory change that occurs after 3 weeks of age in +/*dfw*^{i5} mice.

Since mutant *Atp2b2* expression in +/*dfw*^{i5} likely contributes to the auditory phenotype of these mice (Chapter 3), we also checked to see if the percentage of mutant allele expression

changes during auditory development. The same samples used for quantification of *Atp2b2* were assayed for mutant allele expression in brainstem and cochlea of +/*dfw*^{i5} (Figure 4.4). The percentage of mutant allele is stable between P16 and 5 weeks at about 7% expression in the brainstem and about 11% expression in the cochlea (no overall effect of age in a two-way ANOVA). This result indicates that mutant-*Atp2b2* is unlikely to cause the changes in auditory sensitivity during development.

4.3.3. *PMCA2 is up-regulated by 5 weeks in +/dfw*^{i5}

To examine if compensatory changes in *α-Atp2b2* might reflect a change in PMCA2, we also estimated protein expression in the brainstem of +/*dfw*^{i5} and controls at P16, P20 and 5 weeks of age via Western blotting (see Methods). Indeed, PMCA2 expression levels in +/*dfw*^{i5} are up-regulated by 5 weeks of age with respect to wild-type controls for each group (Figure 4.5 and see Figure 4.6 and Table 4.3 for a comparison of the quantification method). These data are surprising since total transcript levels do not increase in the brainstem of these mice, and suggests that preferential expression of *α-Atp2b2* in comparison to *β-Atp2b2*, more so than total *Atp2b2* expression, leads to PMCA2 up-regulation. This is supported by the correlation between *α-Atp2b2* and PMCA2 expression in brainstem of +/*dfw*^{i5} individuals, but not between *β-Atp2b2* and PMCA2 (see Figure 3.4C).

4.3.4. *Other considerations*

Here we propose that increased *α-Atp2b2* expression, leading to an up-regulation of PMCA2, by 5 weeks of age helps to compensate for the auditory deficiency in +/*dfw*^{i5}. However, up-regulation of wild-type PMCA2 in these haploinsufficient mice may not be the

only mechanism for the improvement in sensitivity after 3 weeks of age. Other calcium handling mechanisms, especially in neuronal tissue, may help compensate for the increased calcium load. For example, PMCA4 mRNA is expressed at its highest level in the developing cochlea at P12 (Furuta *et al.*, 1998) and is aberrantly expressed in the stereocilia of P30 dfw^{2J}/dfw^{2J} mice (Wood *et al.*, 2004). For these reasons, we thought PMCA4 might be another candidate for compensation in $+/dfw^{i5}$. However, quantification of cDNA expression in the cochlea shows equivalent expression of PMCA4 transcript in heterozygous mice and controls (Figure 4.7).

To gain insight into the role of the non-coding RNA genes that sit complementary to the *Atp2b2* gene (see Figure 3.13) we also quantified expression of linc82 and linc83 transcripts in the brainstem and cochlea of $+/dfw^{i5}$ mice and controls at P16, P20 and 5 weeks of age (Figure 4.8). Expression levels of linc82 and linc83 in the brainstem, as well as linc82 in the cochlea, are stable over this time course. Conversely, linc83 expression is markedly higher at P16 in the cochlea of both wild-type (CBA) and $+/dfw^{i5}$ mice. Levels decrease at P20 in each genotype, and are lowest at 5 weeks of age. We cannot help but notice that down-regulation of linc83 seems to coincide with the up-regulation of *α-Atp2b2* (compare to Figure 4.2B) and that *Gm15083* (the gene encoding linc83) spans the *α*-promoter for *Atp2b2* (see Figure 3.13A). The linc83 transcript is also highly expressed in the cochlea (compared to the brainstem, see Figure 3.13B) where *α-Atp2b2* is the predominant transcript type (see Figure 3.5). Taken together, these results suggest that linc83 RNA might be involved in regulating *α-Atp2b2* expression and tissue specificity; although a direct study of linc83 function would be necessary to address these hypotheses.

4.4. Discussion

Developmentally, +/*dfw*^{i5} demonstrates a distinct loss of auditory sensitivity at 3 weeks of age with frequency specific recovery by 5 weeks of age. It is possible that subsequent to hearing onset at P10-P14 (Mikaelian & Ruben, 1965), the amount of PMCA2 expressed in these heterozygous nulls is not sufficient for normal auditory transduction. The loss of sensitivity is remarkably similar to that seen in +/*dfw*^{2J} mutants at every frequency (unpublished observation) suggesting that this is not a unique feature of +/*dfw*^{i5}. This may be a critical stage in the development of auditory transduction in these mice. Worsening of thresholds between P16 and 3 weeks may be attributed in part to the presence of PMCA1 mRNA in outer hair cells at P16 which disappears by P21 (Furuta *et al.*, 1998). Expression of compensatory levels of PMCA4 mRNA, as seen in adult *dfw*^{2J}/*dfw*^{2J}, are not detected in the cochlea of +/*dfw*^{i5} at any age, suggesting that another mechanism for compensation occurs in these mice.

Atp2b2 is reported to be stably expressed in mammalian outer hair cells as early as P0 (Furuta *et al.*, 1998). Our data suggests that a specific elevation in *α-Atp2b2* expression in the cochlea (likely from cochlear hair cells) occurs after the onset of hearing in wild-type mice and continues until 5 weeks of age. This increase might be crucial to the maturation and maintenance of auditory transduction into adulthood. Here we show that *α-Atp2b2* and PMCA2 are up-regulated in the cochlea and brainstem of +/*dfw*^{i5}, respectively, and propose that this up-regulation contributes to the recovery of sensitivity at some frequencies by 5 weeks of age. Unfortunately, we were not able to assess PMCA2 expression in the cochlea, or better yet along the tonotopic axis in auditory hair cells, of +/*dfw*^{i5} individuals with high quantitative resolution. Still, given the dependence on *α-Atp2b2* for up-regulation of PMCA2 in the brainstem, we

would hypothesize that the significant increases in *α-Atp2b2* detected in the cochlea also reflect up-regulation of PMCA2 in this tissue in +/*dfw*^{i5}.

This is the first report of a loss in ABR sensitivity followed by frequency-dependent recovery of thresholds in a PMCA2 mutant mouse. A closer examination at each of the frequencies tested lends insight into the mechanism for this loss and subsequent recovery in +/*dfw*^{i5}. At 5.6 and 8 kHz, ABR thresholds do not change dramatically after P16, neither worsening at 3 weeks nor improving thereafter. Why thresholds never improve at 5.6 kHz is a matter of speculation, but indicates that loss of sensitivity at these lowest frequencies in a PMCA2 mutant might be attributed to a different mechanism than hearing loss at higher frequencies in the same animals. In Chapter 2, we discuss the susceptibility of low frequency transduction to the interaction of PMCA2 with *ahl* and postulate that even with wild-type cadherin 23 expression, a reduction of PMCA2 activity to 50% may be sufficient for mild hearing loss at the most apical hair cells of the cochlea due to a destabilization of the tip-link. That thresholds at 8 kHz are virtually normal throughout development suggests this frequency is the most resistant to PMCA2 dysfunction and might represent the tonotopic location where there is a switch between low- and high-frequency mechanisms for hearing loss. Thresholds at 11.3 kHz are indistinguishable from controls at every age but the critical 3 week time point, where maturation of thresholds lags by one week.

At frequencies at and above 16 kHz, the degree of hearing loss at 3 weeks of age is at least 35-45 dB SPL. A 40-50 dB shift is characteristic of a lack in outer hair cell function (Ryan & McGee, 1977; Prosen *et al.*, 1978; Stebbins *et al.*, 1979) and indicates that, at these frequencies, +/*dfw*^{i5} do not provide enough PMCA2 activity at 3 weeks to fully support the signal amplification function attributed to outer hair cells (Brownell *et al.*, 1985; Evans &

Dallos, 1993). At 16 and 22.6 kHz +/*dfw*^{i5} animals are able to fully or partially recover sensitivity throughout adolescence, respectively. These frequencies seem to represent the tonotopic location where transduction is sensitive, and yet the most receptive, to small changes calcium homeostasis due to changes in PMCA2 expression.

Finally, at 32 and 40 kHz, +/*dfw*^{i5} mice maintain the 40-45 dB shift in sensitivity through 9 weeks of age. It is characteristic at these high frequencies to have a significant hearing loss due to a reduction in PMCA2 function (McCullough & Tempel, 2004). Recent work suggests that high-frequency hair cells in PMCA2 mutants may be the most susceptible to calcium overload and subsequent death (see Figures 2.4 and 3.1 in addition to Spiden *et al*., 2006 and Bortolozzi *et al*., 2010) because they have an equivalent density of PMCA2 molecules as low-frequency hair cells (Chen *et al.*, 2012) despite having larger MET channel conductances (Ricci *et al.*, 2003; Beurg *et al.*, 2006). These data support a mechanism involving calcium homeostasis contributes to loss at these frequencies and that neither the PMCA2 expression at 3 weeks of age nor the amount of PMCA2 up-regulation by 5 weeks of age can support function in these cells. The relatively dramatic differences in sensitivity across the tonotopic axis of the mouse cochlea during this developmental stage suggest that Ca^{2+} clearance (and therefore cytosolic Ca^{2+} concentration) is a critical determinant of hair cell function, with a concomitant narrow window for PMCA2 function. This is especially true in stereocilia, which lack other Ca^{2+} clearance mechanisms.

	5.6 kHz	8 kHz	11.3 kHz	16 kHz	22.6 kHz	32 kHz	40 kHz
P16	n.s.	n.s.	n.s.	n.s.	*	**	*
P20	***	n.s.	***	***	***	***	***
4 Weeks	**	n.s.	n.s.	n.s.	***	***	***
5 Weeks	***	n.s.	n.s.	n.s.	***	***	***
7 Weeks	**	n.s.	n.s.	n.s.	n.s.	***	***
9 Weeks	***	**	n.s.	n.s.	n.s.	***	***

Table 4.1. Statistical differences between +/*dfw*^{i5} and controls during auditory development. *p<0.05, **p<0.01 and ***p<0.001 in a Bonferonni post-hoc comparison following a two-way ANOVA (n.s. is not significant).

		5.6 kHz	8 kHz	11.3 kHz	16 kHz	22.6 kHz	32 kHz	40 kHz
+/+	P16 v. 3 wks	***	n.s.	***	*	**	***	***
	P16 v. 5 wks	***	**	***	n.s.	***	***	***
	3 wks v. 5 wks	n.s.	n.s.	n.s.	n.s.	n.s.	n.s.	n.s.
+/*dfw*^{i5}	P16 v. 3 wks	n.s.	n.s.	n.s.	***	*	n.s.	n.s.
	P16 v. 5 wks	n.s.	n.s.	***	n.s.	n.s.	n.s.	n.s.
	3 wks v. 5 wks	n.s.	n.s.	***	***	*	n.s.	n.s.

Table 4.2. Statistical differences of auditory thresholds during development for +/*dfw*^{i5} and controls. *p<0.05, **p<0.01 and ***p<0.001 in a Bonferonni post-hoc comparison following a one-way ANOVA at each frequency for each genotype (n.s. is not significant).

	P16 (+/+)	P16 (+/-)	Blots	P20 (+/+)	P20 (+/-)	Blots	5 Wks (+/+)	5 Wks (+/-)	Blots
Paired	n=5	n=5	5	^n=4	n=5	5	^n=4	n=5	5
Grouped	n=5	n=8	2*	n=4	n=5	1	n=7	n=9	2*

Table 4.3. Comparison of samples used for Western blotting quantitation of PMCA2 during auditory development in +/*dfw*^{i5}. The numbers of samples utilized from unique mice for Western blotting analysis are shown for P16, P20 and 5 week +/*dfw*^{i5} and control brainstem tissue. The total blots used for quantitation of mice from the indicated age and method are also shown. Paired quantitation method: Five blots used for quantitation contained paired, gender-matched littermates of each age (^n=4 for some samples because tissue from the same animal was used for two blots). Grouped quantitation method: Several mice of each genotype and gender from one time point were compared on the same blot. *At P16 and 5 week time points, not all of the samples fit onto one blot, so two gels were run, transferred, incubated, etc. in parallel. These blots were put into the exact same blocking solutions, washes and solutions containing primary and secondary antibodies.

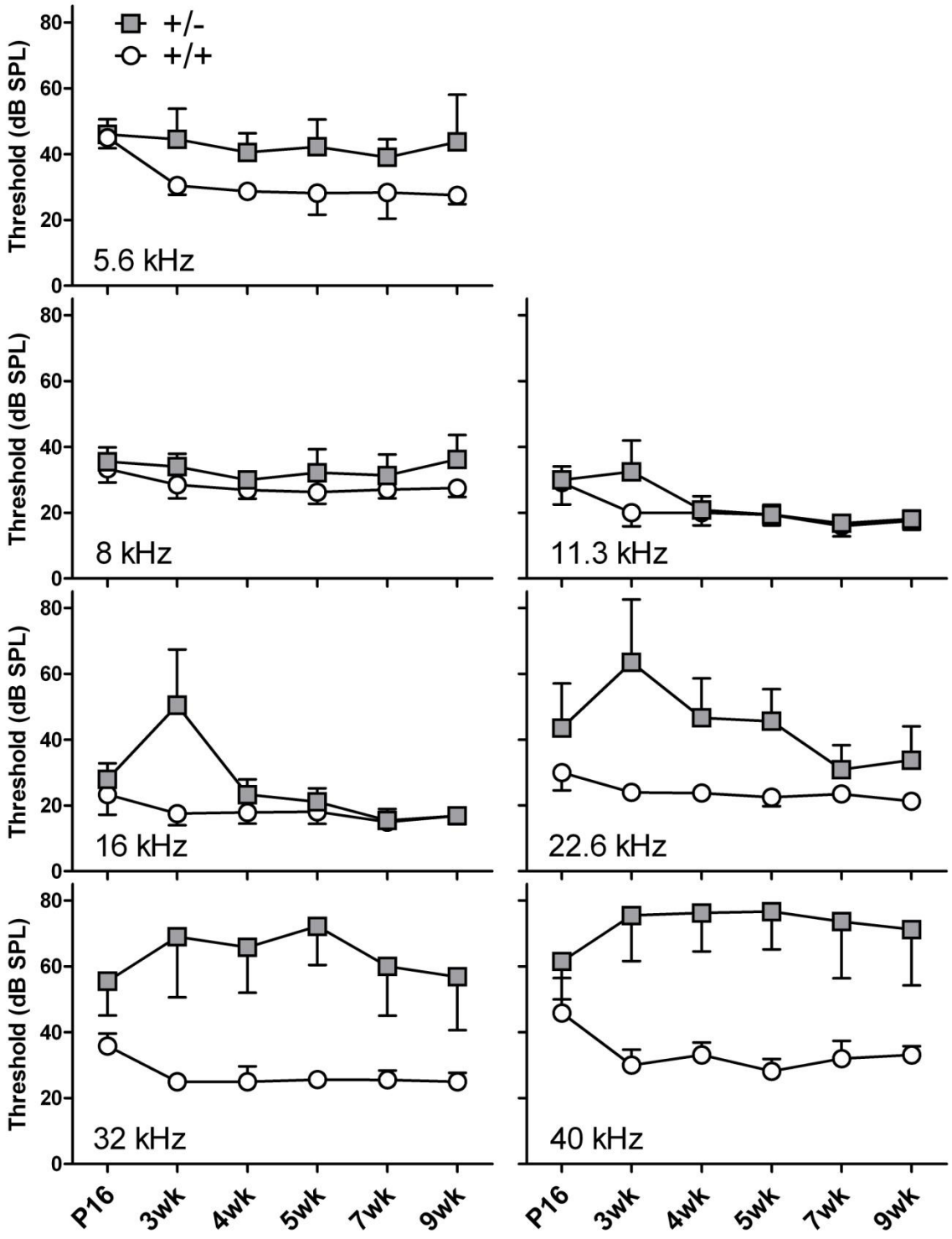

Figure 4.1. Auditory development in +/*dfw*^{i5} and wild-type littermates. ABR sensitivity improves in wild-type controls at all frequencies between P16 and 3 weeks and is mature at each frequency by about 4 weeks of age. In contrast, sensitivity at most frequencies worsens for +/*dfw*^{i5} between P16 and 3

weeks of age, and recovers in a frequency dependent manner through adolescence. See table 4.1 for statistical comparisons between +/*dfw*^{i5} and controls at each frequency and age. Error bars represent standard deviation. The relatively large standard deviations for thresholds of +/*dfw*^{i5} at 11.3, 16 and 22.6 kHz at 3 weeks of age suggests that sensitivity is changing rapidly at this stage of development in these mice. At 32 and 40 kHz, the large standard deviation in +/*dfw*^{i5} throughout adolescence is reflective of an occasional individual with relatively intact sensitivity at these frequencies (see Figure 3.1D and Figure 3.10).

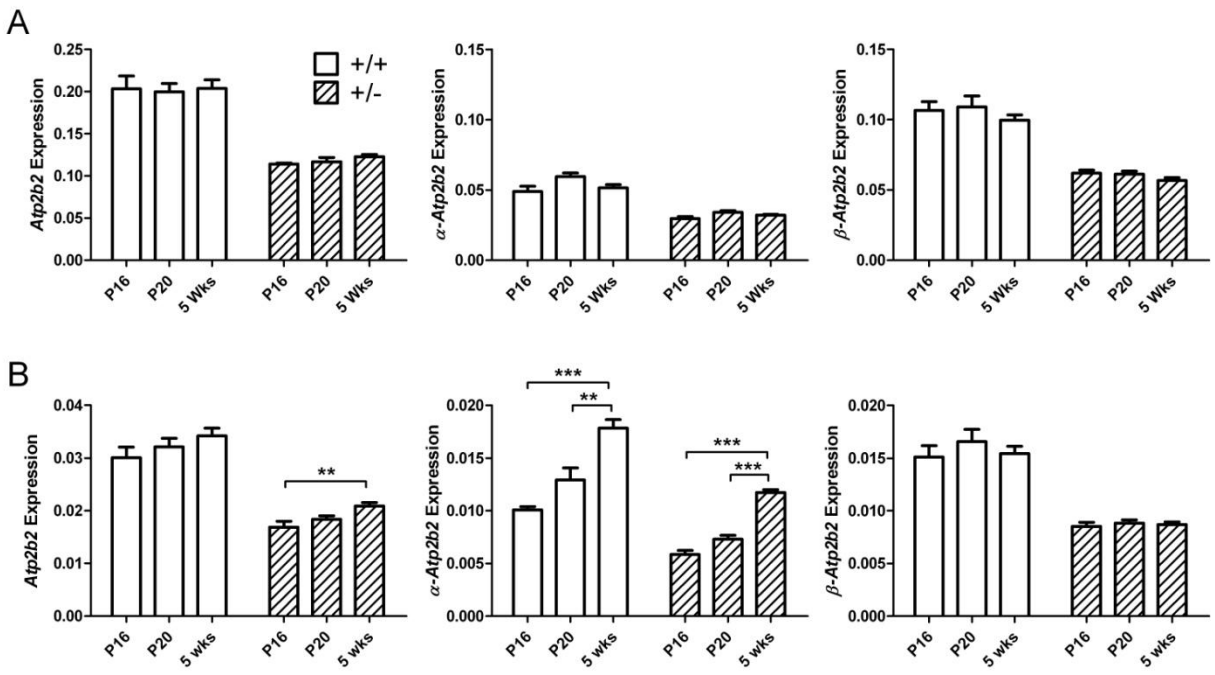

Figure 4.2. *Atp2b2* expression through auditory development. *(A)* Expression does not change for total (left), *α*- (middle) or *β*- (right) *Atp2b2* during auditory development in the brainstem of wild-type or +/*dfw*^{i5} mice. Scale bars are matched for *α*- and *β-Atp2b2* to illustrate the relative abundance of each transcript in the brainstem. *(B)* Total *Atp2b2* expression increases in cochlea of +/*dfw*^{i5} (but not wild-type) mice between P16 and 5 weeks of age (left). Levels of *α-Atp2b2* (middle), but not *β-Atp2b2* (right), increase for both wild-type and heterozygous mice throughout auditory development in the cochlea. Error bars represent SEM.

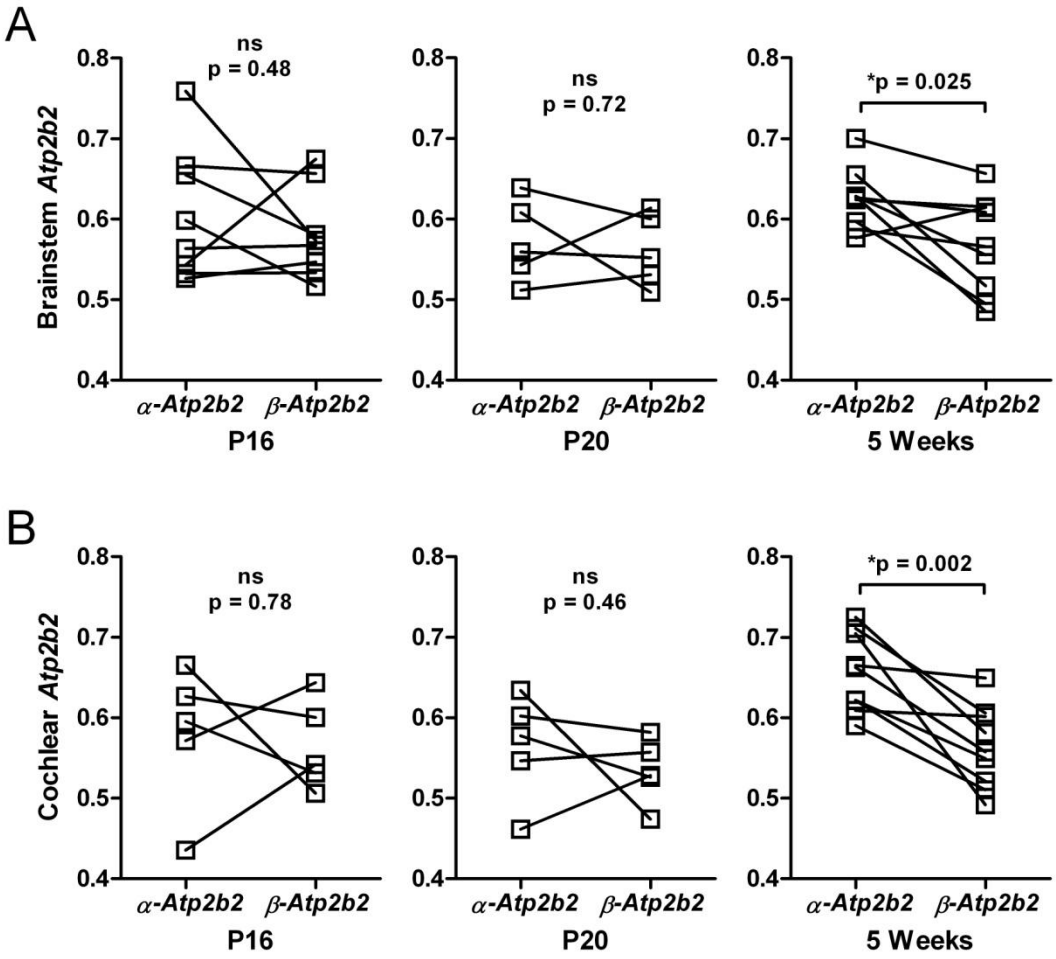

Figure 4.3. *α-Atp2b2* is preferentially up-regulated in +/*dfw*^{i5} by 5 weeks of age. Relative expression of *α-Atp2b2* and *β-Atp2b2* is shown for individual heterozygous mice at each age in brainstem (A) and cochlea (B). Expression levels for both transcripts were normalized to the average wild-type transcript expression at each age. *(A)* Preferential expression of *α-Atp2b2* over *β-Atp2b2* is seen at 5 weeks in brainstem of +/*dfw*^{i5} with almost every individual expressing a greater proportion of *α-Atp2b2* than *β-Atp2b2* compared to controls. *(B)* The preferential up-regulation of *α-Atp2b2* is even more apparent in cochlea of +/*dfw*^{i5} at 5 weeks of age and is not seen at P16 or P20. Significance values shown are from a paired, two-tailed t-test.

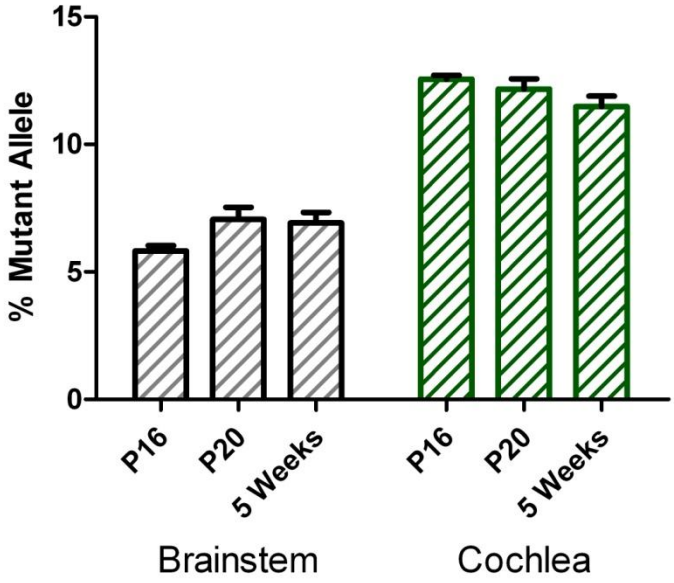

Figure 4.4. The proportion of total *Atp2b2* transcribed from the mutant allele in +/*dfw*^{i5} does not change during auditory development. The percentage of mutant allele in brainstem and cochlea between P16 and 5 weeks stays around 7% and 12% in +/*dfw*^{i5}, respectively. Age was not a significant factor in either tissue type using a one-way ANOVA. Error bars represent SEM.

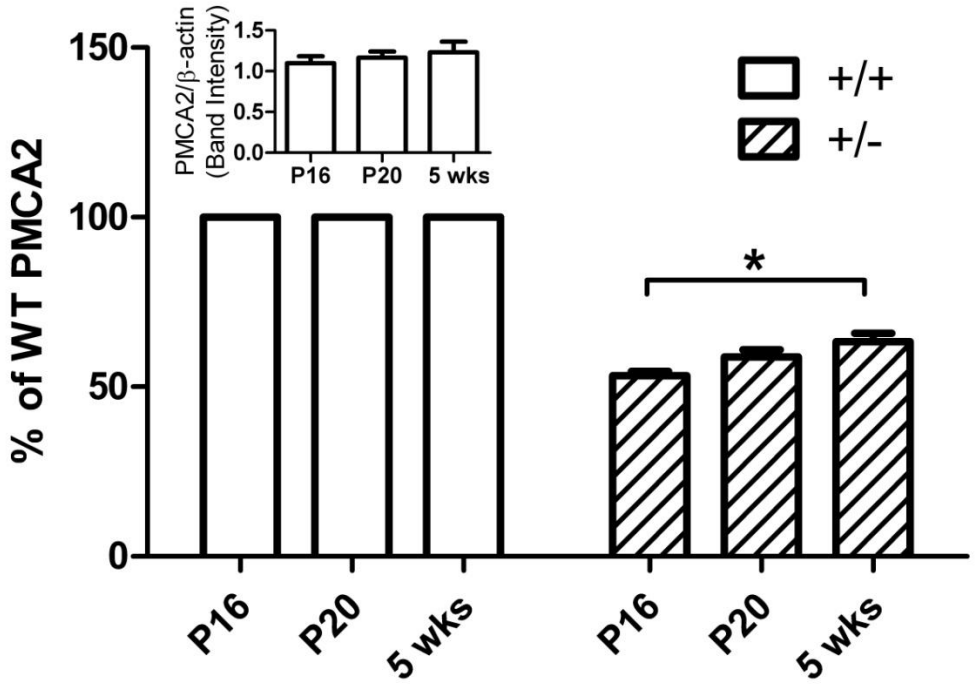

Figure 4.5. PMCA2 expression is up-regulated in +/*dfw*^{i5}. Western blots of brainstem tissue from +/*dfw*^{i5} and wild-type littermates at each age were quantified for PMCA2 expression (see methods). Protein expression increases between P16 and 5 weeks in +/*dfw*^{i5} relative to wild-type controls. (*$p<0.05$) *(Inset)* Wild-type PMCA2 band intensity (normalized to β-actin) across three blots was averaged and is shown to approximate the change in PMCA2 in control brainstem over this time period. Error bars represent SEM.

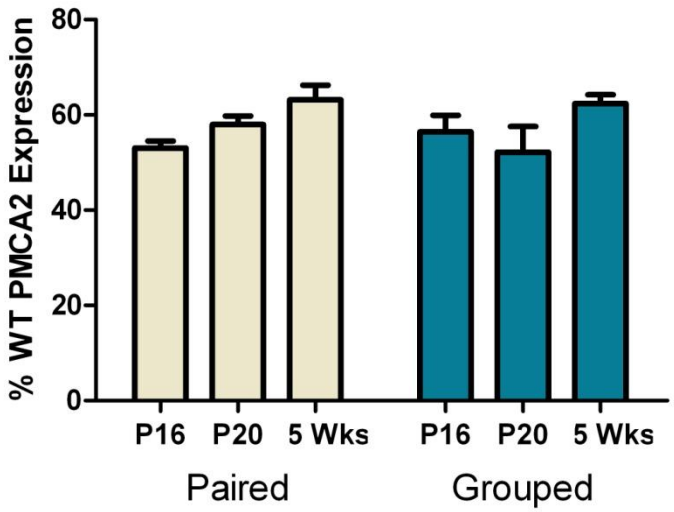

Figure 4.6. Comparison of quantification methods used for PMCA2 expression in brainstem. Averaged data from the two methods used to quantify PMCA2 expression during auditory development in +/*dfw*^{i5} are compared. The paired and grouped methods are described in section 4.2 (Methods) and also in Table 4.3, which shows numbers of mice used for each age and genotype. A two-way ANOVA detects a significant overall effect of age (p=0.021) and no overall effect of quantification method. For simplicity in Figure 4.5, grouped results were averaged into paired data. Error bars represent SEM.

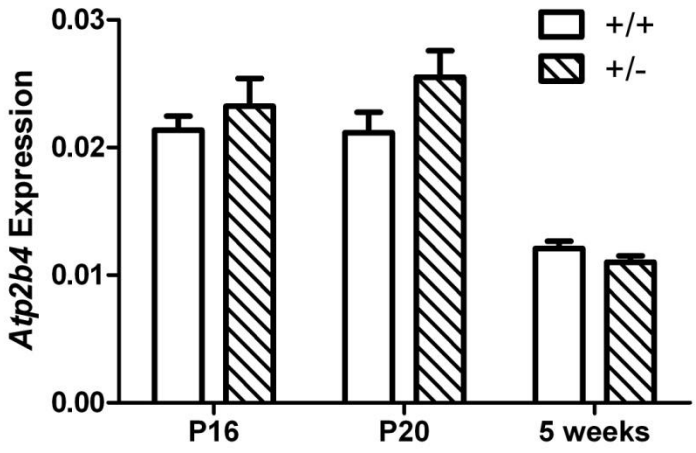

Figure 4.7. Developmental *Atp2b4* (PMCA4) expression in +/*dfw*^{i5} mice. *Atp2b4* levels were quantified in the cochlea of +/*dfw*^{i5} and controls to determine if PMCA4 compensates for PMCA2 deficiency in these mice. There is a significant overall effect of age ($p<0.0001$) indicating that PMCA4 expression decreases by 5 weeks, but no overall effect of genotype in these mice (n.s. $p=0.13$) in a two-way ANOVA. Error bars represent SEM.

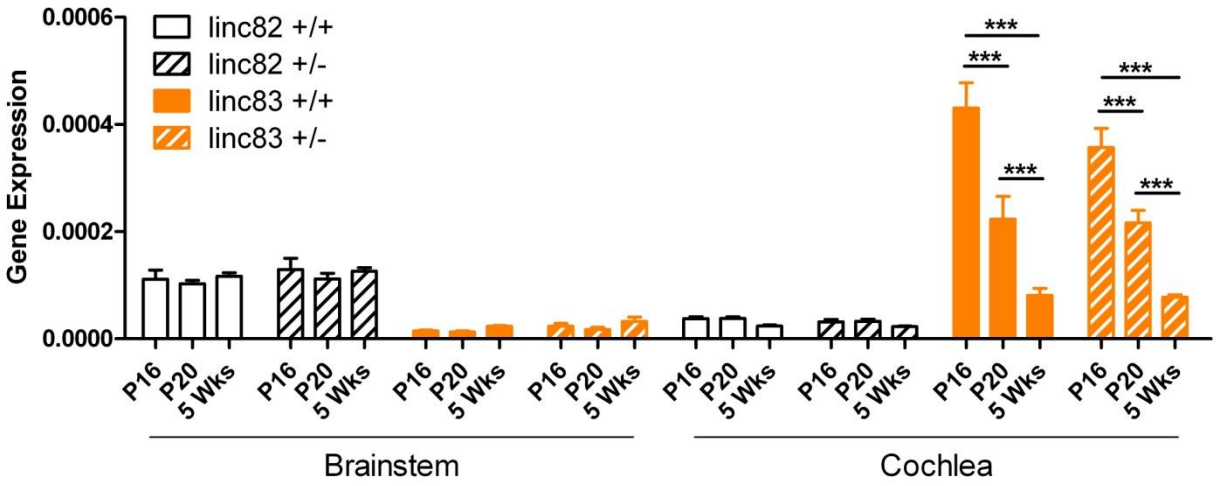

Figure 4.8. *Gm15083* is down-regulated in the cochlea by 5 weeks of age. Levels of *Gm15082* (linc82) and *Gm15083* (linc83) were quantified in the brainstem and cochlea of wild-type and +/*dfw*^{i5} mice during auditory development. Levels of linc82 and linc83 in the brainstem, as well as linc82 in the cochlea, do not change over this time frame and there are no grouped differences between wild-type and heterozygous littermates. For both wild-type and +/*dfw*^{i5}, linc83 expression in the cochlea is significantly down-regulated between P16, P20 and 5 weeks of age. ***p<0.001 in a Bonferonni post-hoc comparison following a two-way ANOVA. Error bars represent SEM.

Chapter 5

Conclusions

The majority of the work in this thesis deals with the characterization of a new *deafwaddler* mutant, *dfw*^{i5}, and the unexpected consequence of this allele on auditory sensitivity. Since the *dfw*^{i5} allele is a PMCA2 null allele like several other characterized PMCA2 mutations to date (*dfw*^{2J}, *dfw*^{3J} and *Atp2b2*^{KO}), it was anticipated that auditory phenotypes of +/*dfw*^{i5} characterized in parallel to that of +/*dfw*^{2J} would be indistinguishable. For certain, an underlying theme of this thesis is the marked physiological and molecular differences that can arise from seemingly benign genetic variation. The scientific community as a whole is just beginning to appreciate how single nucleotide variations in non-coding regions of the mammalian genome can have far reaching consequences on specific gene function, or an entire Chromosomal region, or a regulatory pathway.

Here we present 5 confirmed variants that are present in the proximal *α-Atp2b2* promoter haplotypes of the good-hearing, CBA, and age-related hearing loss, B6, inbred mouse strains. While it is intriguing to suggest that one or more of these nucleotides substantially effects *Atp2b2* regulation as indicated by CBA/B6 hybrid allelic discrimination and *dfw*^{i5} vs. *dfw*^{2J}

mutant transcript abundances, it would be preferable to let these variants serve as a proof of principle that the genetic identities of the CBA and B6 strains are different at this location. It should be noted again that there are over 300 reported SNPs between these two haplotypes at this locus, only three of which are in an *Atp2b2* exon, and only one of which encodes a rather conservative amino acid substitution in the protein from an aspartic acid to a glutamic acid. Of course, that there is a predicted difference in the protein sequence between the inbred strains is of interest, and warrants a comparison of calcium clearance activities of the respective pumps. However, it is possible that any number of the 300 SNPs in the region could modify a regulatory feature of the *Atp2b2* gene. As evidenced by the differential expression of a predicted long non-coding RNA (linc83) in +/dfw^{2J}, it is quite possible that one of these SNPs could alter *Atp2b2* gene regulation via an indirect mechanism. The two long non-coding RNA genes (*Gm15082* and *Gm15083*) that sit complementary to the *Atp2b2* are uncharacterized to date, could very well be involved in gene regulation, and provide a future avenue for research.

Despite the "worsening" of auditory sensitivity in +/dfw^{i5} compared with +/dfw^{2J}, as a result of the genetic variation (compared to our wild-type CBA strain) carried by the mutant allele in +/dfw^{2J}, we believe dfw^{i5} is the truest representative of a null PMCA2 allele in a CBA/CaJ background to date. Therefore, it may be preferable to consider the auditory phenotype of +/dfw^{2J} as a mild "rescue" in sensitivity. We cannot emphasize enough the effect the background of an inbred mouse can have on its physiology. This can be one of the greatest strengths of using inbred mouse strains to model human disease, but can also be a confounding factor unless caution is taken to interpret results with a thorough knowledge of the genetic composition of the strain in question. Background effects are even more important in the study

of a physiological system like auditory transduction that can be extremely sensitive to genetic interactions.

This thesis provides a deeper look into the role of PMCA2 in auditory transduction, and demonstrates that only very small changes in mutant transcript production (in the comparison of +/*dfw*^{i5} and +/*dfw*^{2J}) or *Atp2b2* and PMCA2 expression (in the auditory development of +/*dfw*^{i5}) are needed to modulate auditory sensitivity. Another underlying theme of this thesis is the critical importance of the *α-Atp2b2* transcript for auditory transduction. To our knowledge, this is the first time that expression levels of transcriptional start-site variants of *Atp2b2* have been assessed during development. Certainly, that the *α-Atp2b2* transcript is expressed in auditory hair cells demonstrates it is important for auditory transduction, but why it is preferred over *β-Atp2b2* is unknown. An analysis and comparison of the *α-Atp2b2* and *β-Atp2b2* promoters, as well as a comparison of each of these promoters in CBA and B6, could lend insight into these questions.

Bibliography

Antalffy, G., Mauer, A.S., Paszty, K., Hegedus, L., Padanyi, R., Enyedi, A. & Strehler, E.E. (2012) Plasma membrane calcium pump (PMCA) isoform 4 is targeted to the apical membrane by the w-splice insert from PMCA2. *Cell calcium*, **51**, 171-178.

Assad, J.A., Shepherd, G.M. & Corey, D.P. (1991) Tip-link integrity and mechanical transduction in vertebrate hair cells. *Neuron*, **7**, 985-994.

Baek, D., Villen, J., Shin, C., Camargo, F.D., Gygi, S.P. & Bartel, D.P. (2008) The impact of microRNAs on protein output. *Nature*, **455**, 64-71.

Bartel, D.P. (2009) MicroRNAs: target recognition and regulatory functions. *Cell*, **136**, 215-233.

Beurg, M., Evans, M.G., Hackney, C.M. & Fettiplace, R. (2006) A large-conductance calcium-selective mechanotransducer channel in mammalian cochlear hair cells. *The Journal of neuroscience : the official journal of the Society for Neuroscience*, **26**, 10992-11000.

Beurg, M., Fettiplace, R., Nam, J.H. & Ricci, A.J. (2009) Localization of inner hair cell mechanotransducer channels using high-speed calcium imaging. *Nature neuroscience*, **12**, 553-558.

Beurg, M., Nam, J.H., Chen, Q. & Fettiplace, R. (2010) Calcium balance and mechanotransduction in rat cochlear hair cells. *Journal of neurophysiology*, **104**, 18-34.

Bock, G.R. & Steel, K.P. (1983) Inner ear pathology in the deafness mutant mouse. *Acta Otolaryngol*, **96**, 39-47.

Bortolozzi, M., Brini, M., Parkinson, N., Crispino, G., Scimemi, P., De Siati, R.D., Di Leva, F., Parker, A., Ortolano, S., Arslan, E., Brown, S.D., Carafoli, E. & Mammano, F. (2010) The novel PMCA2 pump mutation Tommy impairs cytosolic calcium clearance in hair cells and links to deafness in mice. *The Journal of biological chemistry*, **285**, 37693-37703.

Brini, M., Coletto, L., Pierobon, N., Kraev, N., Guerini, D. & Carafoli, E. (2003) A comparative functional analysis of plasma membrane Ca2+ pump isoforms in intact cells. *The Journal of biological chemistry*, **278**, 24500-24508.

Brini, M., Marsault, R., Bastianutto, C., Alvarez, J., Pozzan, T. & Rizzuto, R. (1995) Transfected aequorin in the measurement of cytosolic Ca2+ concentration ([Ca2+]c). A critical evaluation. *The Journal of biological chemistry*, **270**, 9896-9903.

Brownell, W.E., Bader, C.R., Bertrand, D. & de Ribaupierre, Y. (1985) Evoked mechanical responses of isolated cochlear outer hair cells. *Science*, **227**, 194-196.

Bult, C.J., Eppig, J.T., Kadin, J.A., Richardson, J.E. & Blake, J.A. (2008) The Mouse Genome Database (MGD): mouse biology and model systems. *Nucleic acids research*, **36**, D724-728.

Burette, A., Rockwood, J.M., Strehler, E.E. & Weinberg, R.J. (2003) Isoform-specific distribution of the plasma membrane Ca2+ ATPase in the rat brain. *The Journal of comparative neurology*, **467**, 464-476.

Carafoli, E. (2002) Calcium signaling: a tale for all seasons. *Proceedings of the National Academy of Sciences of the United States of America*, **99**, 1115-1122.

Caride, A.J., Filoteo, A.G., Penniston, J.T. & Strehler, E.E. (2007) The plasma membrane Ca2+ pump isoform 4a differs from isoform 4b in the mechanism of calmodulin binding and activation kinetics: implications for Ca2+ signaling. *The Journal of biological chemistry*, **282**, 25640-25648.

Chen, Q., Mahendrasingam, S., Tickle, J.A., Hackney, C.M., Furness, D.N. & Fettiplace, R. (2012) The development, distribution and density of the plasma membrane calcium ATPase 2 calcium pump in rat cochlear hair cells. *The European journal of neuroscience*, **36**, 2302-2310.

Clapham, D.E. (2007) Calcium signaling. *Cell*, **131**, 1047-1058.

Consortium, E.P. & Dunham, I. & Kundaje, A. & Aldred, S.F. & Collins, P.J. & Davis, C.A. & Doyle, F. & Epstein, C.B. & Frietze, S. & Harrow, J. & Kaul, R. & Khatun, J. & Lajoie, B.R. & Landt, S.G. & Lee, B.K. & Pauli, F. & Rosenbloom, K.R. & Sabo, P. & Safi, A. & Sanyal, A. & Shoresh, N. & Simon, J.M. & Song, L. & Trinklein, N.D. & Altshuler, R.C. & Birney, E. & Brown, J.B. & Cheng, C. & Djebali, S. & Dong, X. & Dunham, I. & Ernst, J. & Furey, T.S. & Gerstein, M. & Giardine, B. & Greven, M. & Hardison, R.C. & Harris, R.S. & Herrero, J. & Hoffman, M.M. & Iyer, S. & Kelllis, M. & Khatun, J. & Kheradpour, P. & Kundaje, A. & Lassman, T. & Li, Q. & Lin, X. & Marinov, G.K. & Merkel, A. & Mortazavi, A. & Parker, S.C. & Reddy, T.E. & Rozowsky, J. & Schlesinger, F. & Thurman, R.E. & Wang, J. & Ward, L.D. & Whitfield, T.W. & Wilder, S.P. & Wu, W. & Xi, H.S. & Yip, K.Y. & Zhuang, J. & Bernstein, B.E. & Birney, E. & Dunham, I. & Green, E.D. & Gunter, C. & Snyder, M. & Pazin, M.J. & Lowdon, R.F. & Dillon, L.A. & Adams, L.B. & Kelly, C.J. & Zhang, J. & Wexler, J.R. & Green, E.D. & Good, P.J. & Feingold, E.A. & Bernstein, B.E. & Birney, E. & Crawford, G.E. & Dekker, J. & Elinitski, L. & Farnham, P.J. & Gerstein, M. & Giddings, M.C. & Gingeras, T.R. & Green, E.D. & Guigo, R. & Hardison, R.C. & Hubbard, T.J. & Kellis, M. & Kent, W.J. & Lieb, J.D. & Margulies, E.H. & Myers, R.M. & Snyder, M. & Starnatoyannopoulos, J.A. & Tennebaum, S.A. & Weng, Z. & White, K.P. & Wold, B. & Khatun, J. & Yu, Y. & Wrobel, J. & Risk, B.A. & Gunawardena, H.P. & Kuiper, H.C. & Maier, C.W. & Xie, L. & Chen, X. & Giddings, M.C. & Bernstein, B.E. & Epstein, C.B. & Shoresh, N. & Ernst, J. & Kheradpour, P. & Mikkelsen, T.S. & Gillespie, S. & Goren, A. & Ram, O. & Zhang, X. & Wang, L. & Issner, R. & Coyne, M.J. & Durham, T. & Ku, M. & Truong, T. & Ward, L.D. & Altshuler, R.C. & Eaton, M.L. & Kellis, M. & Djebali, S. & Davis, C.A. & Merkel, A. & Dobin, A. & Lassmann, T. & Mortazavi, A. & Tanzer, A. & Lagarde, J. & Lin, W. & Schlesinger, F. & Xue, C. & Marinov, G.K. & Khatun, J. & Williams, B.A. & Zaleski, C. & Rozowsky, J. & Roder, M. & Kokocinski, F. & Abdelhamid, R.F. & Alioto, T. & Antoshechkin, I. & Baer, M.T. & Batut, P. & Bell, I. & Bell, K. & Chakrabortty, S. & Chen, X. & Chrast, J. & Curado, J. & Derrien, T. & Drenkow, J. & Dumais, E. & Dumais, J. & Duttagupta, R. & Fastuca, M. & Fejes-Toth, K. & Ferreira, P. & Foissac, S. & Fullwood, M.J. & Gao, H. & Gonzalez, D. & Gordon, A. & Gunawardena, H.P. & Howald, C. & Jha, S. & Johnson, R. & Kapranov, P. & King, B. & Kingswood, C. & Li, G. & Luo, O.J. & Park, E. & Preall, J.B. & Presaud, K. & Ribeca, P. & Risk, B.A. & Robyr, D. & Ruan, X. & Sammeth, M. & Sandu, K.S. & Schaeffer, L. & See, L.H. & Shahab, A. & Skancke, J. & Suzuki, A.M. & Takahashi, H. & Tilgner, H. & Trout, D. & Walters, N. & Wang, H. & Wrobel, J. & Yu, Y. & Hayashizaki, Y. & Harrow, J. & Gerstein, M. & Hubbard, T.J. & Reymond, A. & Antonarakis, S.E. & Hannon, G.J. & Giddings, M.C. & Ruan, Y. & Wold, B. & Carninci, P. & Guigo, R. & Gingeras, T.R. & Rosenbloom, K.R. & Sloan, C.A. & Learned, K. & Malladi, V.S. & Wong, M.C. & Barber, G.P. & Cline, M.S. & Dreszer, T.R. & Heitner, S.G. & Karolchik, D. & Kent, W.J. & Kirkup, V.M. & Meyer, L.R. & Long, J.C. & Maddren, M. & Raney, B.J. & Furey, T.S. & Song, L. & Grasfeder, L.L. & Giresi, P.G. & Lee, B.K. & Battenhouse, A. & Sheffield, N.C. & Simon, J.M. & Showers, K.A. & Safi, A. & London, D. & Bhinge, A.A. & Shestak, C. & Schaner, M.R. & Kim, S.K. & Zhang, Z.Z. & Mieczkowski, P.A. & Mieczkowska, J.O. & Liu, Z. & McDaniell, R.M. & Ni, Y. & Rashid, N.U. & Kim, M.J. & Adar, S. & Zhang, Z. & Wang, T. & Winter, D. & Keefe,

D. & Birney, E. & Iyer, V.R. & Lieb, J.D. & Crawford, G.E. & Li, G. & Sandhu, K.S. & Zheng, M. & Wang, P. & Luo, O.J. & Shahab, A. & Fullwood, M.J. & Ruan, X. & Ruan, Y. & Myers, R.M. & Pauli, F. & Williams, B.A. & Gertz, J. & Marinov, G.K. & Reddy, T.E. & Vielmetter, J. & Partridge, E.C. & Trout, D. & Varley, K.E. & Gasper, C. & Bansal, A. & Pepke, S. & Jain, P. & Amrhein, H. & Bowling, K.M. & Anaya, M. & Cross, M.K. & King, B. & Muratet, M.A. & Antoshechkin, I. & Newberry, K.M. & McCue, K. & Nesmith, A.S. & Fisher-Aylor, K.I. & Pusey, B. & DeSalvo, G. & Parker, S.L. & Balasubramanian, S. & Davis, N.S. & Meadows, S.K. & Eggleston, T. & Gunter, C. & Newberry, J.S. & Levy, S.E. & Absher, D.M. & Mortazavi, A. & Wong, W.H. & Wold, B. & Blow, M.J. & Visel, A. & Pennachio, L.A. & Elnitski, L. & Margulies, E.H. & Parker, S.C. & Petrykowska, H.M. & Abyzov, A. & Aken, B. & Barrell, D. & Barson, G. & Berry, A. & Bignell, A. & Boychenko, V. & Bussotti, G. & Chrast, J. & Davidson, C. & Derrien, T. & Despacio-Reyes, G. & Diekhans, M. & Ezkurdia, I. & Frankish, A. & Gilbert, J. & Gonzalez, J.M. & Griffiths, E. & Harte, R. & Hendrix, D.A. & Howald, C. & Hunt, T. & Jungreis, I. & Kay, M. & Khurana, E. & Kokocinski, F. & Leng, J. & Lin, M.F. & Loveland, J. & Lu, Z. & Manthravadi, D. & Mariotti, M. & Mudge, J. & Mukherjee, G. & Notredame, C. & Pei, B. & Rodriguez, J.M. & Saunders, G. & Sboner, A. & Searle, S. & Sisu, C. & Snow, C. & Steward, C. & Tanzer, A. & Tapanan, E. & Tress, M.L. & van Baren, M.J. & Walters, N. & Washieti, S. & Wilming, L. & Zadissa, A. & Zhengdong, Z. & Brent, M. & Haussler, D. & Kellis, M. & Valencia, A. & Gerstein, M. & Raymond, A. & Guigo, R. & Harrow, J. & Hubbard, T.J. & Landt, S.G. & Frietze, S. & Abyzov, A. & Addleman, N. & Alexander, R.P. & Auerbach, R.K. & Balasubramanian, S. & Bettinger, K. & Bhardwaj, N. & Boyle, A.P. & Cao, A.R. & Cayting, P. & Charos, A. & Cheng, Y. & Cheng, C. & Eastman, C. & Euskirchen, G. & Fleming, J.D. & Grubert, F. & Habegger, L. & Hariharan, M. & Harmanci, A. & Iyenger, S. & Jin, V.X. & Karczewski, K.J. & Kasowski, M. & Lacroute, P. & Lam, H. & Larnarre-Vincent, N. & Leng, J. & Lian, J. & Lindahl-Allen, M. & Min, R. & Miotto, B. & Monahan, H. & Moqtaderi, Z. & Mu, X.J. & O'Geen, H. & Ouyang, Z. & Patacsil, D. & Pei, B. & Raha, D. & Ramirez, L. & Reed, B. & Rozowsky, J. & Sboner, A. & Shi, M. & Sisu, C. & Slifer, T. & Witt, H. & Wu, L. & Xu, X. & Yan, K.K. & Yang, X. & Yip, K.Y. & Zhang, Z. & Struhl, K. & Weissman, S.M. & Gerstein, M. & Farnham, P.J. & Snyder, M. & Tenebaum, S.A. & Penalva, L.O. & Doyle, F. & Karmakar, S. & Landt, S.G. & Bhanvadia, R.R. & Choudhury, A. & Domanus, M. & Ma, L. & Moran, J. & Patacsil, D. & Slifer, T. & Victorsen, A. & Yang, X. & Snyder, M. & White, K.P. & Auer, T. & Centarin, L. & Eichenlaub, M. & Gruhl, F. & Heerman, S. & Hoeckendorf, B. & Inoue, D. & Kellner, T. & Kirchmaier, S. & Mueller, C. & Reinhardt, R. & Schertel, L. & Schneider, S. & Sinn, R. & Wittbrodt, B. & Wittbrodt, J. & Weng, Z. & Whitfield, T.W. & Wang, J. & Collins, P.J. & Aldred, S.F. & Trinklein, N.D. & Partridge, E.C. & Myers, R.M. & Dekker, J. & Jain, G. & Lajoie, B.R. & Sanyal, A. & Balasundaram, G. & Bates, D.L. & Byron, R. & Canfield, T.K. & Diegel, M.J. & Dunn, D. & Ebersol, A.K. & Ebersol, A.K. & Frum, T. & Garg, K. & Gist, E. & Hansen, R.S. & Boatman, L. & Haugen, E. & Humbert, R. & Jain, G. & Johnson, A.K. & Johnson, E.M. & Kutyavin, T.M. & Lajoie, B.R. & Lee, K. & Lotakis, D. & Maurano, M.T. & Neph, S.J. & Neri, F.V. & Nguyen, E.D. & Qu, H. & Reynolds, A.P. & Roach, V. & Rynes, E. & Sabo, P. & Sanchez, M.E. & Sandstrom, R.S. & Sanyal, A. & Shafer, A.O. & Stergachis, A.B. & Thomas, S. & Thurman, R.E. & Vernot, B. & Vierstra, J. & Vong, S. & Wang, H. &

Weaver, M.A. & Yan, Y. & Zhang, M. & Akey, J.A. & Bender, M. & Dorschner, M.O. & Groudine, M. & MacCoss, M.J. & Navas, P. & Stamatoyannopoulos, G. & Kaul, R. & Dekker, J. & Stamatoyannopoulos, J.A. & Dunham, I. & Beal, K. & Brazma, A. & Flicek, P. & Herrero, J. & Johnson, N. & Keefe, D. & Lukk, M. & Luscombe, N.M. & Sobral, D. & Vaquerizas, J.M. & Wilder, S.P. & Batzoglou, S. & Sidow, A. & Hussami, N. & Kyriazopoulou-Panagiotopoulou, S. & Libbrecht, M.W. & Schaub, M.A. & Kundaje, A. & Hardison, R.C. & Miller, W. & Giardine, B. & Harris, R.S. & Wu, W. & Bickel, P.J. & Banfai, B. & Boley, N.P. & Brown, J.B. & Huang, H. & Li, Q. & Li, J.J. & Noble, W.S. & Bilmes, J.A. & Buske, O.J. & Hoffman, M.M. & Sahu, A.O. & Kharchenko, P.V. & Park, P.J. & Baker, D. & Taylor, J. & Weng, Z. & Iyer, S. & Dong, X. & Greven, M. & Lin, X. & Wang, J. & Xi, H.S. & Zhuang, J. & Gerstein, M. & Alexander, R.P. & Balasubramanian, S. & Cheng, C. & Harmanci, A. & Lochovsky, L. & Min, R. & Mu, X.J. & Rozowsky, J. & Yan, K.K. & Yip, K.Y. & Birney, E. (2012) An integrated encyclopedia of DNA elements in the human genome. *Nature*, **489**, 57-74.

Corey, D.P. & Hudspeth, A.J. (1979) Ionic basis of the receptor potential in a vertebrate hair cell. *Nature*, **281**, 675-677.

Di Palma, F., Holme, R.H., Bryda, E.C., Belyantseva, I.A., Pellegrino, R., Kachar, B., Steel, K.P. & Noben-Trauth, K. (2001) Mutations in Cdh23, encoding a new type of cadherin, cause stereocilia disorganization in waltzer, the mouse model for Usher syndrome type 1D. *Nature genetics*, **27**, 103-107.

Dumont, R.A., Lins, U., Filoteo, A.G., Penniston, J.T., Kachar, B. & Gillespie, P.G. (2001) Plasma membrane Ca2+-ATPase isoform 2a is the PMCA of hair bundles. *The Journal of neuroscience : the official journal of the Society for Neuroscience*, **21**, 5066-5078.

Duncan, J.L., Yang, H., Doan, T., Silverstein, R.S., Murphy, G.J., Nune, G., Liu, X., Copenhagen, D., Tempel, B.L., Rieke, F. & Krizaj, D. (2006) Scotopic visual signaling in the mouse retina is modulated by high-affinity plasma membrane calcium extrusion. *The Journal of neuroscience : the official journal of the Society for Neuroscience*, **26**, 7201-7211.

Eatock, R.A. (2000) Adaptation in hair cells. *Annual review of neuroscience*, **23**, 285-314.

Empson, R.M., Garside, M.L. & Knopfel, T. (2007) Plasma membrane Ca2+ ATPase 2 contributes to short-term synapse plasticity at the parallel fiber to Purkinje neuron synapse. *The Journal of neuroscience : the official journal of the Society for Neuroscience*, **27**, 3753-3758.

Empson, R.M., Turner, P.R., Nagaraja, R.Y., Beesley, P.W. & Knopfel, T. (2010) Reduced expression of the Ca(2+) transporter protein PMCA2 slows Ca(2+) dynamics in mouse cerebellar Purkinje neurones and alters the precision of motor coordination. *The Journal of physiology*, **588**, 907-922.

Eppig, J.T., Blake, J.A., Bult, C.J., Kadin, J.A. & Richardson, J.E. (2012) The Mouse Genome Database (MGD): comprehensive resource for genetics and genomics of the laboratory mouse. *Nucleic acids research*, **40**, D881-886.

Evans, B.N. & Dallos, P. (1993) Stereocilia displacement induced somatic motility of cochlear outer hair cells. *Proceedings of the National Academy of Sciences of the United States of America*, **90**, 8347-8351.

Fernandez-Gonzalez, A., La Spada, A.R., Treadaway, J., Higdon, J.C., Harris, B.S., Sidman, R.L., Morgan, J.I. & Zuo, J. (2002) Purkinje cell degeneration (pcd) phenotypes caused by mutations in the axotomy-induced gene, Nna1. *Science*, **295**, 1904-1906.

Fettiplace, R. & Ricci, A.J. (2003) Adaptation in auditory hair cells. *Current opinion in neurobiology*, **13**, 446-451.

Ficarella, R., Di Leva, F., Bortolozzi, M., Ortolano, S., Donaudy, F., Petrillo, M., Melchionda, S., Lelli, A., Domi, T., Fedrizzi, L., Lim, D., Shull, G.E., Gasparini, P., Brini, M., Mammano, F. & Carafoli, E. (2007) A functional study of plasma-membrane calcium-pump isoform 2 mutants causing digenic deafness. *Proceedings of the National Academy of Sciences of the United States of America*, **104**, 1516-1521.

Furuta, H., Luo, L., Hepler, K. & Ryan, A.F. (1998) Evidence for differential regulation of calcium by outer versus inner hair cells: plasma membrane Ca-ATPase gene expression. *Hearing research*, **123**, 10-26.

Grati, M., Schneider, M.E., Lipkow, K., Strehler, E.E., Wenthold, R.J. & Kachar, B. (2006) Rapid turnover of stereocilia membrane proteins: evidence from the trafficking and mobility of plasma membrane Ca(2+)-ATPase 2. *The Journal of neuroscience : the official journal of the Society for Neuroscience*, **26**, 6386-6395.

Gruber, A.R., Lorenz, R., Bernhart, S.H., Neubock, R. & Hofacker, I.L. (2008) The Vienna RNA websuite. *Nucleic acids research*, **36**, W70-74.

Heim, R., Hug, M., Iwata, T., Strehler, E.E. & Carafoli, E. (1992) Microdiversity of human-plasma-membrane calcium-pump isoform 2 generated by alternative RNA splicing in the N-terminal coding region. *European journal of biochemistry / FEBS*, **205**, 333-340.

Hilfiker, H., Guerini, D. & Carafoli, E. (1994) Cloning and expression of isoform 2 of the human plasma membrane Ca2+ ATPase. Functional properties of the enzyme and its splicing products. *The Journal of biological chemistry*, **269**, 26178-26183.

Hill, J.K., Williams, D.E., LeMasurier, M., Dumont, R.A., Strehler, E.E. & Gillespie, P.G. (2006) Splice-site A choice targets plasma-membrane Ca2+-ATPase isoform 2 to hair bundles. *The Journal of neuroscience : the official journal of the Society for Neuroscience*, **26**, 6172-6180.

Hirose, K., Westrum, L.E., Cunningham, D.E. & Rubel, E.W. (2004) Electron microscopy of degenerative changes in the chick basilar papilla after gentamicin exposure. *The Journal of comparative neurology*, **470**, 164-180.

Howard, J. & Hudspeth, A.J. (1988) Compliance of the hair bundle associated with gating of mechanoelectrical transduction channels in the bullfrog's saccular hair cell. *Neuron*, **1**, 189-199.

Hung, T., Wang, Y., Lin, M.F., Koegel, A.K., Kotake, Y., Grant, G.D., Horlings, H.M., Shah, N., Umbricht, C., Wang, P., Wang, Y., Kong, B., Langerod, A., Borresen-Dale, A.L., Kim, S.K., van de Vijver, M., Sukumar, S., Whitfield, M.L., Kellis, M., Xiong, Y., Wong, D.J. & Chang, H.Y. (2011) Extensive and coordinated transcription of noncoding RNAs within cell-cycle promoters. *Nature genetics*, **43**, 621-629.

Isken, O., Kim, Y.K., Hosoda, N., Mayeur, G.L., Hershey, J.W. & Maquat, L.E. (2008) Upf1 phosphorylation triggers translational repression during nonsense-mediated mRNA decay. *Cell*, **133**, 314-327.

Johnson, K.R., Erway, L.C., Cook, S.A., Willott, J.F. & Zheng, Q.Y. (1997) A major gene affecting age-related hearing loss in C57BL/6J mice. *Hearing research*, **114**, 83-92.

Johnson, K.R., Zheng, Q.Y. & Erway, L.C. (2000) A major gene affecting age-related hearing loss is common to at least ten inbred strains of mice. *Genomics*, **70**, 171-180.

Johnson, K.R., Zheng, Q.Y. & Noben-Trauth, K. (2006) Strain background effects and genetic modifiers of hearing in mice. *Brain research*, **1091**, 79-88.

Jones, S.M., Johnson, K.R., Yu, H., Erway, L.C., Alagramam, K.N., Pollak, N. & Jones, T.A. (2005) A quantitative survey of gravity receptor function in mutant mouse strains. *Journal of the Association for Research in Otolaryngology : JARO*, **6**, 297-310.

Kane, K.L., Longo-Guess, C.M., Gagnon, L.H., Ding, D., Salvi, R.J. & Johnson, K.R. (2012) Genetic background effects on age-related hearing loss associated with Cdh23 variants in mice. *Hearing research*, **283**, 80-88.

Kazmierczak, P., Sakaguchi, H., Tokita, J., Wilson-Kubalek, E.M., Milligan, R.A., Muller, U. & Kachar, B. (2007) Cadherin 23 and protocadherin 15 interact to form tip-link filaments in sensory hair cells. *Nature*, **449**, 87-91.

Keeton, T.P., Burk, S.E. & Shull, G.E. (1993) Alternative splicing of exons encoding the calmodulin-binding domains and C termini of plasma membrane Ca(2+)-ATPase isoforms 1, 2, 3, and 4. *The Journal of biological chemistry*, **268**, 2740-2748.

Keithley, E.M., Erkman, L., Bennett, T., Lou, L. & Ryan, A.F. (1999) Effects of a hair cell transcription factor, Brn-3.1, gene deletion on homozygous and heterozygous mouse cochleas in adulthood and aging. *Hearing research*, **134**, 71-76.

Kelley, M.W. (2006) Regulation of cell fate in the sensory epithelia of the inner ear. *Nature reviews. Neuroscience*, **7**, 837-849.

Kiernan, A.E., Zalzman, M., Fuchs, H., Hrabe de Angelis, M., Balling, R., Steel, K.P. & Avraham, K.B. (1999) Tailchaser (Tlc): a new mouse mutation affecting hair bundle differentiation and hair cell survival. *Journal of neurocytology*, **28**, 969-985.

Kozel, P.J., Davis, R.R., Krieg, E.F., Shull, G.E. & Erway, L.C. (2002) Deficiency in plasma membrane calcium ATPase isoform 2 increases susceptibility to noise-induced hearing loss in mice. *Hearing research*, **164**, 231-239.

Kozel, P.J., Friedman, R.A., Erway, L.C., Yamoah, E.N., Liu, L.H., Riddle, T., Duffy, J.J., Doetschman, T., Miller, M.L., Cardell, E.L. & Shull, G.E. (1998) Balance and hearing deficits in mice with a null mutation in the gene encoding plasma membrane Ca2+-ATPase isoform 2. *The Journal of biological chemistry*, **273**, 18693-18696.

Krizaj, D., Demarco, S.J., Johnson, J., Strehler, E.E. & Copenhagen, D.R. (2002) Cell-specific expression of plasma membrane calcium ATPase isoforms in retinal neurons. *The Journal of comparative neurology*, **451**, 1-21.

Kurnellas, M.P., Lee, A.K., Li, H., Deng, L., Ehrlich, D.J. & Elkabes, S. (2007) Molecular alterations in the cerebellum of the plasma membrane calcium ATPase 2 (PMCA2)-null mouse indicate abnormalities in Purkinje neurons. *Molecular and cellular neurosciences*, **34**, 178-188.

Kurnellas, M.P., Nicot, A., Shull, G.E. & Elkabes, S. (2005) Plasma membrane calcium ATPase deficiency causes neuronal pathology in the spinal cord: a potential mechanism for neurodegeneration in multiple sclerosis and spinal cord injury. *FASEB journal : official publication of the Federation of American Societies for Experimental Biology*, **19**, 298-300.

Lane, P.W. (1987) Deaf waddler (dfw). *Mouse News Lett*, **77**, 129.

Le Hir, H. & Seraphin, B. (2008) EJCs at the heart of translational control. *Cell*, **133**, 213-216.

Losson, R. & Lacroute, F. (1979) Interference of nonsense mutations with eukaryotic messenger RNA stability. *Proceedings of the National Academy of Sciences of the United States of America*, **76**, 5134-5137.

Lumpkin, E.A. & Hudspeth, A.J. (1995) Detection of Ca2+ entry through mechanosensitive channels localizes the site of mechanoelectrical transduction in hair cells. *Proceedings of the National Academy of Sciences of the United States of America*, **92**, 10297-10301.

Lumpkin, E.A. & Hudspeth, A.J. (1998) Regulation of free Ca2+ concentration in hair-cell stereocilia. *The Journal of neuroscience : the official journal of the Society for Neuroscience*, **18**, 6300-6318.

Mammano, F., Bortolozzi, M., Ortolano, S. & Anselmi, F. (2007) Ca2+ signaling in the inner ear. *Physiology*, **22**, 131-144.

Maquat, L.E. (2004) Nonsense-mediated mRNA decay: splicing, translation and mRNP dynamics. *Nature reviews. Molecular cell biology*, **5**, 89-99.

Maquat, L.E. (2005) Nonsense-mediated mRNA decay in mammals. *Journal of cell science*, **118**, 1773-1776.

Marshall, J.F. & Berrios, N. (1979) Movement disorders of aged rats: reversal by dopamine receptor stimulation. *Science*, **206**, 477-479.

Martianov, I., Ramadass, A., Serra Barros, A., Chow, N. & Akoulitchev, A. (2007) Repression of the human dihydrofolate reductase gene by a non-coding interfering transcript. *Nature*, **445**, 666-670.

McCullough, B.J., Adams, J.C., Shilling, D.J., Feeney, M.P., Sie, K.C. & Tempel, B.L. (2007) 3p-- syndrome defines a hearing loss locus in 3p25.3. *Hearing research*, **224**, 51-60.

McCullough, B.J. & Tempel, B.L. (2004) Haplo-insufficiency revealed in deafwaddler mice when tested for hearing loss and ataxia. *Hearing research*, **195**, 90-102.

Mikaelian, D. & Ruben, R.J. (1965) Development of Hearing in the Normal Cba-J Mouse: Correlation of Physiological Observations with Behavioral Responses and with Cochlear Anatomy. *Acta Oto-laryngologica*, **59**, 451-461.

Mullen, R.J., Eicher, E.M. & Sidman, R.L. (1976) Purkinje cell degeneration, a new neurological mutation in the mouse. *Proceedings of the National Academy of Sciences of the United States of America*, **73**, 208-212.

Nagy, E. & Maquat, L.E. (1998) A rule for termination-codon position within intron-containing genes: when nonsense affects RNA abundance. *Trends in biochemical sciences*, **23**, 198-199.

Noben-Trauth, K., Zheng, Q.Y. & Johnson, K.R. (2003) Association of cadherin 23 with polygenic inheritance and genetic modification of sensorineural hearing loss. *Nature genetics*, **35**, 21-23.

Noben-Trauth, K., Zheng, Q.Y., Johnson, K.R. & Nishina, P.M. (1997) mdfw: a deafness susceptibility locus that interacts with deaf waddler (dfw). *Genomics*, **44**, 266-272.

Ohmori, H. (1987) Gating properties of the mechano-electrical transducer channel in the dissociated vestibular hair cell of the chick. *The Journal of physiology*, **387**, 589-609.

Penheiter, A.R., Filoteo, A.G., Croy, C.L. & Penniston, J.T. (2001) Characterization of the deafwaddler mutant of the rat plasma membrane calcium-ATPase 2. *Hearing research*, **162**, 19-28.

Pickles, J.O., Comis, S.D. & Osborne, M.P. (1984) Cross-links between stereocilia in the guinea pig organ of Corti, and their possible relation to sensory transduction. *Hearing research*, **15**, 103-112.

Prosen, C.A., Petersen, M.R., Moody, D.B., Stebbins, W.C. & Hawkins, J.E., Jr. (1978) Permanent threshold shift and cochlear hair cell loss in the kanamycin-treated guinea pig. *Otolaryngology*, **86**, ORL-886-887.

Quandt, K., Frech, K., Karas, H., Wingender, E. & Werner, T. (1995) MatInd and MatInspector: new fast and versatile tools for detection of consensus matches in nucleotide sequence data. *Nucleic acids research*, **23**, 4878-4884.

Renteria, R.C., Strehler, E.E., Copenhagen, D.R. & Krizaj, D. (2005) Ontogeny of plasma membrane Ca2+ ATPase isoforms in the neural retina of the postnatal rat. *Visual neuroscience*, **22**, 263-274.

Ricci, A.J., Crawford, A.C. & Fettiplace, R. (2003) Tonotopic variation in the conductance of the hair cell mechanotransducer channel. *Neuron*, **40**, 983-990.

Ryan, A. & McGee, T.J. (1977) Development of hearing loss in kanamycin treated chinchillas. *The Annals of otology, rhinology, and laryngology*, **86**, 176-182.

Schultz, J.M., Yang, Y., Caride, A.J., Filoteo, A.G., Penheiter, A.R., Lagziel, A., Morell, R.J., Mohiddin, S.A., Fananapazir, L., Madeo, A.C., Penniston, J.T. & Griffith, A.J. (2005) Modification of human hearing loss by plasma-membrane calcium pump PMCA2. *The New England journal of medicine*, **352**, 1557-1564.

Shin, J.B., Longo-Guess, C.M., Gagnon, L.H., Saylor, K.W., Dumont, R.A., Spinelli, K.J., Pagana, J.M., Wilmarth, P.A., David, L.L., Gillespie, P.G. & Johnson, K.R. (2010) The R109H variant of fascin-2, a developmentally regulated actin crosslinker in hair-cell stereocilia, underlies early-onset hearing loss of DBA/2J mice. *The Journal of neuroscience : the official journal of the Society for Neuroscience*, **30**, 9683-9694.

Shin, J.B., Streijger, F., Beynon, A., Peters, T., Gadzala, L., McMillen, D., Bystrom, C., Van der Zee, C.E., Wallimann, T. & Gillespie, P.G. (2007) Hair bundles are specialized for ATP delivery via creatine kinase. *Neuron*, **53**, 371-386.

Siemens, J., Lillo, C., Dumont, R.A., Reynolds, A., Williams, D.S., Gillespie, P.G. & Muller, U. (2004) Cadherin 23 is a component of the tip link in hair-cell stereocilia. *Nature*, **428**, 950-955.

Silverstein, R.S. & Tempel, B.L. (2006) Atp2b2, encoding plasma membrane Ca2+-ATPase type 2, (PMCA2) exhibits tissue-specific first exon usage in hair cells, neurons, and mammary glands of mice. *Neuroscience*, **141**, 245-257.

Sotomayor, M., Weihofen, W.A., Gaudet, R. & Corey, D.P. (2010) Structural determinants of cadherin-23 function in hearing and deafness. *Neuron*, **66**, 85-100.

Speca, D.J., Rabbee, N., Chihara, D., Speed, T.P. & Peterson, A.S. (2006) A genetic screen for behavioral mutations that perturb dopaminergic homeostasis in mice. *Genes, brain, and behavior*, **5**, 19-28.

Spiden, S.L., Bortolozzi, M., Di Leva, F., de Angelis, M.H., Fuchs, H., Lim, D., Ortolano, S., Ingham, N.J., Brini, M., Carafoli, E., Mammano, F. & Steel, K.P. (2008) The novel mouse mutation Oblivion inactivates the PMCA2 pump and causes progressive hearing loss. *PLoS genetics*, **4**, e1000238.

Stahl, W.L., Eakin, T.J., Owens, J.W., Jr., Breininger, J.F., Filuk, P.E. & Anderson, W.R. (1992) Plasma membrane Ca(2+)-ATPase isoforms: distribution of mRNAs in rat brain by in situ hybridization. *Brain research. Molecular brain research*, **16**, 223-231.

Stauffer, T.P., Guerini, D. & Carafoli, E. (1995) Tissue distribution of the four gene products of the plasma membrane Ca2+ pump. A study using specific antibodies. *The Journal of biological chemistry*, **270**, 12184-12190.

Stebbins, W.C., Hawkins, J.E., Jr., Johnson, L.G. & Moody, D.B. (1979) Hearing thresholds with outer and inner hair cell loss. *American journal of otolaryngology*, **1**, 15-27.

Street, V.A., McKee-Johnson, J.W., Fonseca, R.C., Tempel, B.L. & Noben-Trauth, K. (1998) Mutations in a plasma membrane Ca2+-ATPase gene cause deafness in deafwaddler mice. *Nature genetics*, **19**, 390-394.

Strehler, E.E., Strehler-Page, M.A., Vogel, G. & Carafoli, E. (1989) mRNAs for plasma membrane calcium pump isoforms differing in their regulatory domain are generated by alternative splicing that involves two internal donor sites in a single exon. *Proceedings of the National Academy of Sciences of the United States of America*, **86**, 6908-6912.

Takahashi, K. (1999) Evaluation of Inner Ear Histology and Auditory Brainstem Response inWriggle Mouse Sagami. *Acta Oto-laryngologica*, **119**, 767-772.

Takahashi, K. & Kitamura, K. (1999) A point mutation in a plasma membrane Ca(2+)-ATPase gene causes deafness in Wriggle Mouse Sagami. *Biochemical and biophysical research communications*, **261**, 773-778.

VanHouten, J., Sullivan, C., Bazinet, C., Ryoo, T., Camp, R., Rimm, D.L., Chung, G. & Wysolmerski, J. (2010) PMCA2 regulates apoptosis during mammary gland involution and predicts outcome in breast cancer. *Proceedings of the National Academy of Sciences of the United States of America*, **107**, 11405-11410.

Wang, K.C. & Chang, H.Y. (2011) Molecular mechanisms of long noncoding RNAs. *Molecular cell*, **43**, 904-914.

Wood, J.D., Muchinsky, S.J., Filoteo, A.G., Penniston, J.T. & Tempel, B.L. (2004) Low endolymph calcium concentrations in deafwaddler2J mice suggest that PMCA2 contributes to endolymph calcium maintenance. *Journal of the Association for Research in Otolaryngology : JARO*, **5**, 99-110.

Yamoah, E.N., Lumpkin, E.A., Dumont, R.A., Smith, P.J., Hudspeth, A.J. & Gillespie, P.G. (1998) Plasma membrane Ca2+-ATPase extrudes Ca2+ from hair cell stereocilia. *The Journal of neuroscience : the official journal of the Society for Neuroscience*, **18**, 610-624.

Zetoune, A.B., Fontaniere, S., Magnin, D., Anczukow, O., Buisson, M., Zhang, C.X. & Mazoyer, S. (2008) Comparison of nonsense-mediated mRNA decay efficiency in various murine tissues. *BMC genetics*, **9**, 83.

Zheng, Q.Y. & Johnson, K.R. (2001) Hearing loss associated with the modifier of deaf waddler (mdfw) locus corresponds with age-related hearing loss in 12 inbred strains of mice. *Hearing research*, **154**, 45-53.

Vita

Claire Watson was raised in Los Alamos, NM and attended Los Alamos High School. During this time she worked at the Los Alamos National Laboratory in the Biology Division. She attended Trinity University in San Antonio, TX and received a Bachelor of Science degree in Biochemistry with a minor in Mathematics in the spring of 2006. At Trinity, Claire worked with Dr. Steven Bachrach and wrote an honors thesis in computational organic chemistry. She entered into the Department of Pharmacology doctoral program at the University of Washington in the fall of 2006 and earned a Doctor of Philosophy in 2012.